CENTRO DE INVESTIGACIONES EN OPTICA, A.C.

# POLARIMETRY OF LONG-PERIOD FIBER GRATINGS


By

**M. en C. Karla María Salas Alcántara**


Thesis submitted in fulfillment of
the requirements for the degree of

**DOCTOR EN CIENCIAS (ÓPTICA)**

Supervised by

**Dr. Rafael Espinosa Luna**
**Dr. Ismael Torres Gómez**


CENTRO DE INVESTIGACIONES EN ÓPTICA, A.C.

LEÓN, GUANAJUATO, MÉXICO.



AUGUST 2014

Examiners:

Dr. Yury Barmenkov (CIO)
Dr. Olivier Pottiez (CIO)
Dr. David Monzón Hernández (CIO)
Dr. Gelacio Atondo Rubio (UAS)

# Acknowledgments

I would like to express my sincere grateful for two persons: my thesis advisors Dr. Rafael Espinosa Luna and Dr. Ismael Torres Gómez for their constant guidance, support, encouragement and the valuable comments through the course of this research work. Thank you both none of this would have been possible without your help, my total appreciation and gratitude.

To my examiners committee Dr. Yury Barmenkov, Dr. Olivier Pottiez and Dr. David Monzón for their valuable comments which allowed me to improve this thesis and for their knowledge and experience shared that helped me to be formed as a researcher. In the same way I express my gratitude to Dr. Gelacio Atondo for participate as my external examiner and taking the time to review this thesis work.

To Myriam Jiménez for the support in the laboratory and her friendship, thanks for all.

I also would like to express my gratitude to Alfredo Lopez and Reyna Martinez for the support and the encouragement in this adventure.

To my classmates and friends with whom I shared experiences and work time, to all the members of the GIPYS group. To my friends for their interest, support and

mainly for being so comprehensive! RICR, Karely, M, Lupita, Ninfa, Villa, Arely and Delia. To Dr. Mario Rodriguez for share his time, knowledge and his friendship. A special thanks to Laura Aparicio for her continuous and invaluable support and help with many aspects of my life during the seven years that we spent at CIO. Thank you for being a true friend at all times.

I am also grateful to CONACYT for the financial support to realize my doctoral studies.

Finally, I would like to dedicate this thesis to my family the most important people in my life. To my mother, Mrs. Natividad Alcántara and to my father, Mr. Martiniano Salas, for the unconditional support, understanding and the continuous sacrifices which made this possible. To my sisters: Georgina, Ofelia, Maura and Janeth for the support and the encouragement to realize this work. To my brothers: Jacinto and Armando for their support in all ups and downs of this journey.

# Publications

## Journal papers (Refereed)

1. **Karla M. Salas-Alcántara**, Laura Aparicio-Ixta, Ismael Torres-Gómez, Gabriel Ramos-Ortiz, Rafael Espinosa-Luna, Mario Rodríguez, Juan L.Pichardo-Molina, "Modal interferometer based on the transition cladding-modes coupling assisted by a single long-period fiber grating" To be submitted to Photonics Technology Letters, IEEE.

2. O. J. Velarde-Escobar**, Karla M. Salas-Alcántara**, Rafael Espinosa-Luna, G. Atondo Rubio, I Torres-Gómez, "Polarimetric parameters associated to comercial optical fibers", accepted in Revista Mexicana de Física.

3. **Karla M. Salas-Alcántara**, Rafael Espinosa-Luna, I Torres-Gómez, "Determination of the Mueller matrix of UV-inscribed long-period fiber grating", *Appl. Opt.* **53** (2) 269-277 (2013).

4. **Karla M. Salas-Alcántara**, Rafael Espinosa-Luna, I Torres-Gómez. "Polarimetric Mueller-Stokes analysis of photonic crystal fibers with mechanically induced long-period gratings", *Opt. Eng.* **51**(8), 085005(1-8) (2012).

## Conference papers

1. **K. Salas-Alcántara**, I Torres-Gómez, D. Monzón Hernández, A. Martínez Ríos, "Micro-displacement sensor using a Mach-Zehnder interferometer with long-period gratings". VIII Simposio la Óptica en la Industria. Toluca de Lerdo, Estado de México Proceedings of the SPIE (2011).

2. L. García*, I. Torres-Gómez, A. Martínez-Ríos, D. Monzón-Hernández**, K. Salas-Alcántara**, F. Arteaga-Sierra. "Temperature Response of Mechanically-Induced Long-Period Gratings in Photonic Crystal Fiber", Proceedings of the SPIE , WSOF (2010).

# Chapter book

3. Experimental polarimetric properties of long-period fiber gratings, Recent Research Developments in Optics, Vol 8 S.G. Pandali, research singpost, Vol. 8, Pages. 11, **Karla M. Salas-Alcántara**, Rafael Espinosa-Luna and Ismael Torres-Gómez. (2014)

# National congress

4. **K. Salas-Alcántara**, Rafael Espinosa-Luna, I Torres-Gómez**.** "Análisis polarimétrico de Mueller-Stokes de la fibra Óptica empleada por Telmex en sus redes de transmisión comercial", X Encuentro participación de la Mujer en la Ciencia, León Guanajuato (2013).

5. **K. Salas-Alcántara**, Rafael Espinosa-Luna, I Torres-Gómez**.** "Caracterización polarimétrica en fibra óptica de cristal fotónico", XXV Reunión Anual de Óptica. Michoacán Morelia (2012).

6. **K. Salas-Alcántara**, Rafael Espinosa-Luna, I Torres-Gómez. "Análisis polarimétrico de Mueller-Stokes en RPL inducida mecánicamente en Fibra de Cristal fotónico", IX encuentro participación de la Mujer en la Ciencia, León Guanajuato (2012).

7. **K. Salas-Alcántara**, I Torres-Gómez, D. Monzón Hernández, A. Martínez Ríos, "Sensor de micro-desplazamiento utilizando un interferómetro Mach-Zehnder con rejillas de periodo largo. XXIII Reunión Anual de óptica, Puebla, Puebla. (2010).

# Abstract

Although the formation of optical fiber gratings had been reported in 1978, intensive study on fiber gratings began after a controllable and effective UV method for their fabrication was devised in 1989. There are two types of fiber gratings: fiber Bragg gratings (FBGs) with a period of the order of the optical wavelength and long-period fiber gratings (LPFGs) with periodicities of several hundred wavelengths. Since Hill et al. and Vengsarkar et al. wrote the first FBG and LPFG in conventional fibers in 1978 and 1996 respectively, extensive studies have also been performed on new fabrication methods and novel applications of fiber grating.

Particularly, Long-period fiber gratings (LPFGs) are versatile components used in multiple applications. Although LPFGs were originally proposed as band-rejection filters, nowadays, they are capable of a much broader scope of operation in all-fiber devices. LPFGs have been studied for applications in optical fiber polarizers, optical sensors, and optical switching, among others. They have been used in the reshaping gain spectra of active fiber devices like erbium-doped fiber amplifiers (EDFAs) and fiber lasers. LPFGs have found practical application in the equalization spectral gain of EDFAs, and tunable and selective elements in fiber lasers. The optimal performance of the LPFGs in most of the applications is determined, in part, by the polarization properties, such as the polarization dependent loss (PDL), and the birefringence. Such parameters are critical for some specific applications of LPFGs and also for improving the LPFG fabrication process. In the sensing applications, it is necessary to reduce the transmission type polarization dependence to isolate the sensing parameter. In this sense, it is important to obtain a full description of the polarization properties of LPFGs.

In the thesis, an overview of long-period fiber gratings, including theoretical background, fabrication techniques and their applications are presented to explain fiber gratings properties, behavior and the importance of their characterization. The Mueller-Stokes matrix determination, as well as the concept of polarimetric metrics such as the depolarization index, the Q (M) depolarization scalar metric, the theorem of Gil-Bernabeu, and the degree of polarization, polarization dependent loss, are introduced to quantitatively describe the interaction of light with long-period gratings.

Abstract

For the first time, an explicit method for the complete determination of the Mueller matrix associated to both mechanically and UV induced long-period fiber gratings is presented. The Mueller matrix is determined through the Stokes vectors, which are measured using an incomplete, commercial, Stokes polarimeter. A review of two explicit methods for the entire determination of the Mueller matrix is presented. Some scalar polarimetric metrics are applied for the determination of the diattenuation, PDL, gain, attenuation, depolarization degree of anisotropy, among others have been investigated. The results show a clear dependence on the incident polarization states, which could be employed to design and control the output signal from these devices.

The outline of this dissertation is as follows. Chapter 1 is a review for the fabrication techniques of LPFGs and their application in optical communications and sensing fields. Additionally, the induced birefringence by the inscription of method and some compensation techniques are presented. Chapter 2 discusses the theoretical background required for the understanding the principle of operation and transmission basic properties of the LPFG based in the coupling mode theory. Also, a brief review of methods of Jones calculus matrix and polarization-scanning that have been used to calculate the polarization properties of the fiber devices, such PDL were presented. In Chapter 3 the elements to analyze the polarized light through the Stokes vectors and the Mueller matrix of an arbitrary optical system and some scalar polarimetric metrics are presented. For the first time, Experimental results of both mechanically and UV induced long-period fiber gratings by using two explicit methods for the entire determination of the Mueller matrix are presented, compared and discussed in chapter 4. Finally a summary of this research work is presented.

# Table of contents

# List of figures

.

# 1 The development of long-period fiber gratings

## 1.1 Long-period fiber grating and their applications

Long-period fiber gratings (LPFGs) were initially developed for use as band-rejection filters, and have been used for gain-flattening of erbium doped fiber amplifiers (EDFAs). The rejection bands of the LPFG can be being useful for polarization dependent loss compensation. The use of LPFGs as mode converters in two mode fibers and as wavelength selective polarizers has also been demonstrated. Long-period fiber gratings can be used to enhance coupling between different optical devices, such as, from a waveguide to a fiber, from a semiconductor laser to an optical fiber or between two fibers. On the other hand, by cascading two identical LPFGs is possible to obtain very narrow optical filters being therefore useful devices in wavelength division multiplexing or modal interferometers. Moreover, LPFGs also present unique opportunities as fiber optic sensors.

### 1.1.1 Gain equalizers

Erbium-doped fiber amplifiers can amplify multiple wavelengths within a gain bandwidth spectrum. However, the gain is not uniform over the entire bandwidth (from 1530 to 1560 nm). When an EDFA is used to amplify a multi-channel transmission, each channel experiences different gain. Eventually, the gain discrepancy between the channels can become sufficiently large to detrimental for WDM applications. There are two basic approaches to flattening the gain spectrum. The first approach involves tailoring the material properties of the erbium doped fiber. However, with this method, the gain spectrum of EDFA is still not flat enough for an advanced DWDM system and there still remain other problems. The second approach is to use gain flattening filters. In this case, filters are designed to approximate the inverse characteristics of the EDFA gain spectrum. Long-period fiber gratings are the most promising candidates for gain flattening over other techniques because they are passive, can be used in transmission and can be tailored to flatten the full required bandwidth [1-3]. In addition, they exhibit low insertion loss, and are relatively easy to manufacture in a cost effective and consistent manner.

The other major application of long-period fiber gratings to EDFAs is the suppression of the amplified spontaneous emission (ASE). In a cascaded chain of EDFAs, the buildup of ASE travels in both forward and backward directions with a power that is proportional to the amplifier gain during complete population inversion and high gain. For increasing gain, the stimulated emission by ASE grows to a value where it starts competing with the pumping rate which causes the excited erbium ions to return the ground state. Due to reduction in medium inversion, the amplifier gain saturates even in the absence of any input signal. Self-saturation can be prevented by periodically filtering the forward ASE noise power along the fiber [4]. In line, long-period fiber gratings with low insertion loss are ideal filter elements for this purpose.

## 1.1.2 Dispersion compensations

One of the factors restricting the bit rate in modern communication links is the chromatic dispersion of fibers, which causes broadening and even overlap of laser pulses carrying information. The group-velocity dispersion in standard fibers at a wavelength of 1.55 $\mu m$ is about 17 ps $nm^{-1}$ $km^{-1}$, so that, despite low losses in standard fibers (~0.2 dB $km^{-1}$), the data transfer distance for the 40- Gbit $s^{-1}$ transmission does not exceed 10 km. To increase this distance in operating fiber optic communication links, it is necessary to compensate their dispersion. This can be done by a compact fiber element, namely, a fiber Bragg grating with a variable period. Such a grating can introduce a certain time delay between the spectral components of a pulse, recovering in this way the initial pulse shape. But the use of fiber Bragg gratings requires the use of an expensive circulator besides the complexity of chirping the grating. Hence there has been a great interest to develop devices all-fiber dispersion compensators working in transmission mode. For this reason, the use of concatenated chirped long-period fiber gratings has been proposed for dispersion compensation [5-6]. Das and Thyagarajan [7] have proposed the use of a uniform LPFG, fabricated on fiber with relatively high index value, as an efficient dispersion compensator. He showed that by appropriately choosing the length of the grating and the refractive index modulation it is possible to achieve large dispersion compensation over a reasonable bandwidth with very low transmission loss, and negligible delay ripples.

### 1.1.3 Add/drop filter for CWDM systems.

Wavelength division multiplexing is one of the important enabling technologies for high speed communication network systems. This technique allows increasing the capacity of the networks by transmitting many channels simultaneously on a single optical fiber. While dense wavelength division multiplexing (DWDM) is mainly used for long haul applications, coarse wavelength division multiplexing (CWDM) is widely used in short and medium distance transmission systems. To date, multiplexing or demultiplexing components for WDM systems mainly fall into three categories, thin-film interface filters, fiber Bragg gratings, and array waveguide gratings [8]. Because a long-period grating provides both band-rejection and band-pass functions, it can be used as an all-fiber add/drop filter for CWDM systems with good channel isolation [9-10].

### 1.1.4 Long-period grating sensors.

Fiber grating sensors technologies are the most important application in optical fiber sensors. Long-period gratings have been demonstrated as highly sensitive temperature, axial strain and index of refraction sensors [11-16]. The response of these sensors is a strong function of the grating period, the fiber parameters and the order of the cladding mode. The wavelength shift in the broad resonance loss bands due to an external perturbation can be used to implement simple demodulation techniques. Additionally, the multiple bands of a single long-period grating can be employed for simultaneous strain and temperature sensing. Long-period gratings possess a high degree of versatility that can be used to configure various optical fiber-based sensing systems. Over the next few years these sensors are expected to find widespread use in commercial and military applications.

### 1.1.5 LPFG Temperature and Strain Sensing

Any modulation of the core and cladding guiding properties will modify the spectral response of LPFGs, which is essential for sensing purposes. The external perturbations are detected as wavelength-dependent loss modulation of an LPFG. In 1996, Bhatia and Vengsarkar first demonstrated LPFG optical sensors capable of measuring temperature or strain as well as the external refractive index [11, 17]. They found that the average temperature sensitivity of LPFGs is

much larger than that of the fiber Bragg gratings (FBG) and strongly fiber type and grating structure dependent. In their investigation, LPFGs were fabricated in four different types of fiber and their spectral behavior was examined for the cladding modes of different orders. It was noticed that the third-order cladding mode of an LPFG with a 210 μm period produced in the 980 nm single mode standard fiber exhibited the highest temperature sensitivity of 0.154 nm/°C, ten times higher than that of an FBG (0.014 nm/°C). It should be particularly pointed out that, in LPFG temperature and strain sensing, the wavelength shift of the cladding modes of LPFGs can be toward either short wavelengths (blue shift) or long wavelengths (red shift) [18-19], depending on the dispersion property of the waveguide.

### 1.1.6 Refractive index sensing

The response of the long-period fiber gratings to external refractive index (RI) was systematically analyzed by Patrick and co-workers [12]. They prove the high dependence of LPFG spectral response to the external refractive index on the grating period. The refractive index sensitivity of LPFGs arises from the dependence of the phase matching condition upon the effective refractive index of the cladding modes. The effective indices of the cladding modes are dependent of the difference between the RI of the cladding and that of the medium surrounding the cladding.

The central wavelengths of the attenuation bands thus show a dependence upon the RI of the medium surrounding the cladding, with the highest sensitivity being shown for surrounding refractive indices close to that of the cladding of the optical fiber, provided that the cladding has the higher RI. The highest sensitivity to the surrounding refractive indices is close to that of the cladding of the optical fiber. For surrounding refractive indices higher than that of the cladding, the central wavelengths of the resonance bands show a considerably reduced sensitivity.

The RI sensitivity of an LPG is dependent on the order of the cladding mode that is coupled, allowing the tuning of the sensitivity by appropriate choice of grating period, with 427.72, 203.18, 53.45 and 32.10 nm/refractive index unit (RIU) being reported for LPGs fabricated in SMF28 with periods 159, 238, 400 and 556 μm, respectively [12]. Another subject of further consideration is the geometry and composition of the fiber, with the sensitivity being shown to differ for the step index and W profile fibers and a progressive three-layered fiber [20]. In order to improve the sensitivity of

the long-period fiber gratings written in standard optical fiber configurations to surrounding RI, approaches such as tapering the fiber [21-24], or etching the cladding have been investigated [16, 25]. Different approaches that require the involvement of processing of the fiber, polishing, etching and tapering produce significant enhancements in sensitivity, but at the cost of requiring careful packaging to compensate the inevitable reduction in the mechanical integrity of the device.

The deposition of thin film overlays (thickness of the order of 200 nm) of materials with RI higher than that of the cladding has also been investigated for the enhancement of RI sensitivity [26-28]. In this studies has been shown previously experimentally and theoretically [29, 30] that the effective indices of the cladding modes, and thus the central wavelengths of the core-cladding mode coupling bands of LPFGs show a high sensitivity to the optical thickness of high RI coatings when the coating's optical thickness is such that one of the low order cladding modes is phase matched to a mode of the waveguide formed by the coating.

### 1.1.7 Bend sensors

Long-period fiber gratings have also been implemented as optical bend sensors [31-32]. Two techniques have been demonstrated to measure the bending curvature; one involves detecting the bend induced cladding mode resonance wavelength shift [33], and the other is based on measuring the asymmetry generated cladding-mode resonance splitting [31]. Also, the LPFGs are used for structural bend sensing by noting the changes in wavelength and attenuation strength of LPFGs under bending. A clear correlation between the applied bending curvatures and the resonance wavelength shift was identified for LPFGs produced by several specific fibers [34]. This detection sensing method has limitations associated with nonlinear response, fiber orientation and decaying of the attenuation band. Given that these limitations are hard to overcome, the implementation of real bend sensors devices could be highly problematic.

In comparison, the mode resonance splitting detection technique shows some advantages for bending curvature measurement. The mode splitting under bending can be attributed to the symmetry break of the fiber geometry. The imposed curvature in the fiber splits the degeneracy of the cladding mode of the circular fiber, leading to two closely separated cladding modes, one with

its field predominantly on the outer side of the cladding relative to the center of the bend, and the other with its field mainly on the inner side of the cladding. These separate cladding modes have correspondingly higher and lower effective index values compared to the value of the straight fiber.

## 1.2 Long-period fiber grating fabrication technique

The fabrication of LPFGs implies the introduction of a periodic index modulation of the core in the optical fiber. This can be obtained by permanent modification of the refractive index of the fiber core or by temporal physical deformation of the fiber, respectively. The magnitude of change of the refractive index (Δn) depends of certain factors, such as wavelength, intensity, material composition of the fiber core and fiber processing before an exposition to ultraviolet (UV) light. Techniques like UV irradiation, laser $CO_2$ exposure, electric arc discharge, mechanical microbends, etched corrugations, ion beam implantation, and femtosecond laser exposure, among others, have been used in the fabrication of this kind of devices in fiber optic [35]. The index profile and the fiber type give the response spectral of these rejection bands and these characteristics make of its sensitive to physical variables such as; bending, temperature, strain, torsion, and external refractive index. The strain and temperature response of a long-period grating can be either positive or negative, depending on the differential responses of the core and cladding. In the following section, a brief overview of the manufacture of LPFGs will be described.

### 1.2.1 LPFGs manufactured by UV radiation

The ultraviolet (UV) irradiation was the first method used to manufacture Bragg gratings in 1989 by Meltz et al., who used holographic interference between two coherent beams directed to the fiber axis [36]. The UV exposure method requires that the fiber first be made sensitive to UV irradiation, i.e. the fiber must be made photosensitive prior to writing the grating. It can be obtained by doping the fiber core with atoms (such as germanium, boron or a combination of these elements through the fabrication process) or by hydrogen loading exposing the fiber to high-pressure $H_2$ gas at elevated temperatures for a long period of time so that hydrogen diffusion into the core material takes place. The later method is preferable because hydrogen loading can be achieved in standard fibers, providing a cheaper and simpler way to obtain UV photosensitivity fibers [37].

The UV inscription method for LPFGs can be made in two ways. One of them consists on the irradiation of the photosensitive fiber to UV laser beam through an amplitude mask (AM) [18, 35]. The inscription occurs when the optical fiber placed directly behind the mask is sweep off by the UV radiation (see Figure 1.1 (a)). The exposure is repeated until the index modulation has reached a sufficient level to provide the desired attenuation depth in the LPFG transmission spectrum. This technique implies a permanent modification of the refractive index of the fiber core. The AM technique is wavelength specific since the periodicity is defined by the mask periodicity Λ. A second way to generate long-period gratings with UV irradiation is based on a periodic point by point modulation of the core refractive index until the desired grating length is obtained. In general, both techniques above described are considered expensive.

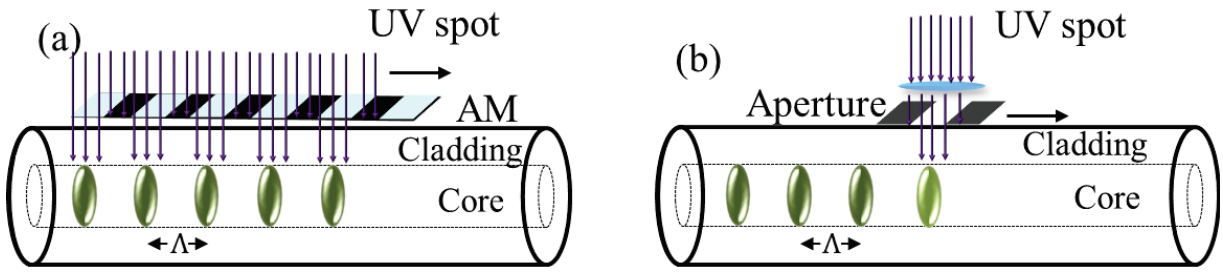


**Figure 1.1** LPFGs manufactured by UV radiation: a) phase amplitude mask and b) point by point technique

## 1.2.2 Mechanically induced long-period fiber gratings

The refractive index of glass can be changed under stress. Since the period of a LPFG can be as large as hundreds of micrometers, it is possible to induce it mechanically via the photoelastic effect. Different techniques of mechanically induced M-LPFGs have been reported in standard fibers and microstructured fibers, where corrugated plates, strings, grating period variations, twisting the fiber, etching of the fiber cladding, and springs have been used to apply periodic mechanical stress on the optical fiber in order to induce the effective index modulation to obtain the coupling of light from the fundamental mode to cladding modes [38-43]. One of the most relevant characteristics that share these techniques is their tunability by simple adjustment of the mechanical stress period, in addition of being erasable and reconfigurable in real time. Under this concept, M-LPFGs offer a tuning range at least one order of magnitude wider than other methods reported in tunable permanent recorded LPFGs with similar isolation loss and line-width. Figure 1.2(a) shows the

mechanical system designed and fabricated in our facilities which allow a fine tuning of the grating period by changing the angle between the fiber axis and grooves [44-45]. Each long-period fiber grating is obtained by applying a transverse force over a section of fiber using two grooved aluminum plates. The plates were mechanically polished in order to get rectangular grooves like are shown in Figure. 2(b)

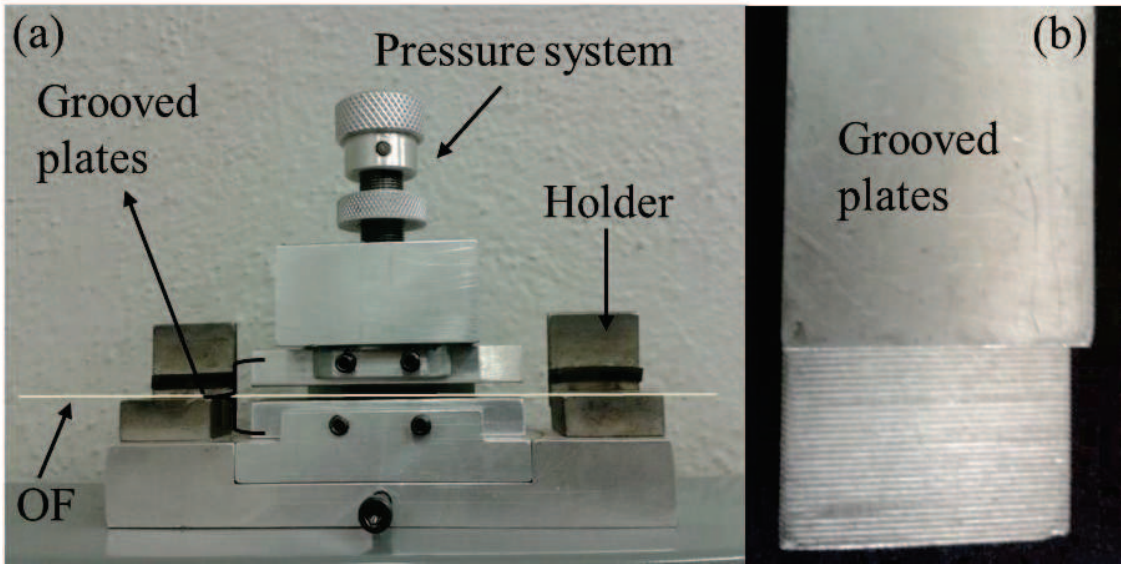


**Figure 1.2.** Experimental setup used to fabricate the M-LPFG, a) the mechanical system, b) Grooved plate [43]

## 1.2.3 Arc induced long-period gratings

The electric arc technique is one of the simplest methods to manufacture LPFGs, see Figure 1.3. It does not need expensive laser systems for its fabrication; the manufacture is done through a fusion splice machine. Besides enables the inscription of the LPFGs in almost any kind of fibers, because it is not necessary that the fibers be photosensitive. Moreover, this kind of LPFGs provides a high thermal stability.

The unjacketed fiber is held between the electrodes of the splice machine so that it can be pulled by a translation stage connected to a micro control motor. After applying an electric arc on the fiber, it is translated by a few micrometers in the longitudinal direction and the arc is applied again. The electric arc applied modifies the refractive index by diffusion of dopants, also changing the profile in the core as well as the cladding. During the fabrication process, the fiber is kept under tension. [46-48].

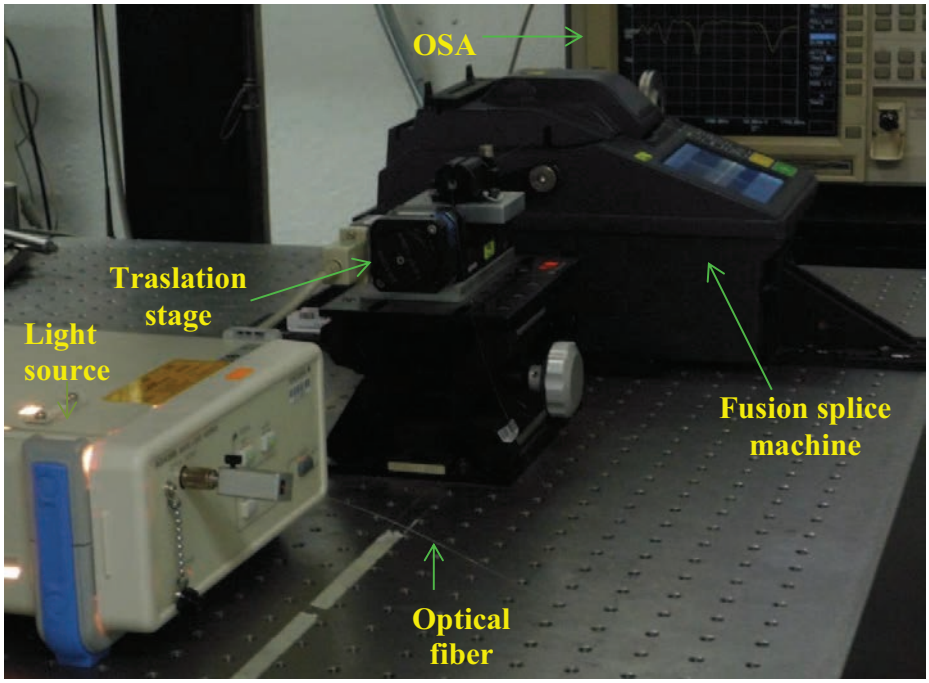


**Figure 1.3.** Manufacturing station of LPFGs by electric arc discharge [46]

## 1.2.4 $CO_2$ laser pulses exposure

Long-period fiber gratings fabricated by exposure to $CO_2$ laser pulses have been shown a high thermal stability. Attenuation bands characteristics are unchanged in resonant wavelength even when subjected to temperatures up to 1200 °C. Thus $CO_2$ laser induced long-period fiber gratings are candidates for both long lifetime and high temperature applications [49-50].

Typically, in most of LPFG fabrication setups employing a $CO_2$ laser, as shown in Figure 1.4, the fiber is periodically moved along its axis direction via a computer-controlled translation stage (this movement is indicated in the Figure 1.4 as 1st, 2nd), and the laser beam irradiates periodically the fiber through a shutter controlled by a same computer. A light source and an optical spectrum analyzer are employed to monitor the evolution of the grating spectrum during the laser irradiation. This is a typical point-to-point technique for writing a grating in an optical fiber. Such a LPFG fabrication system usually requires an exactly controlling of both the shutter and the translation stage to achieve a good simultaneousness of the laser irradiation and the fiber movement. Additionally, the vibration of the employed fiber, resulting from the periodic

movement of the fiber, could occur during the irradiation of the laser beam, which is of disadvantage to the stability and repeatability of the grating fabrication.

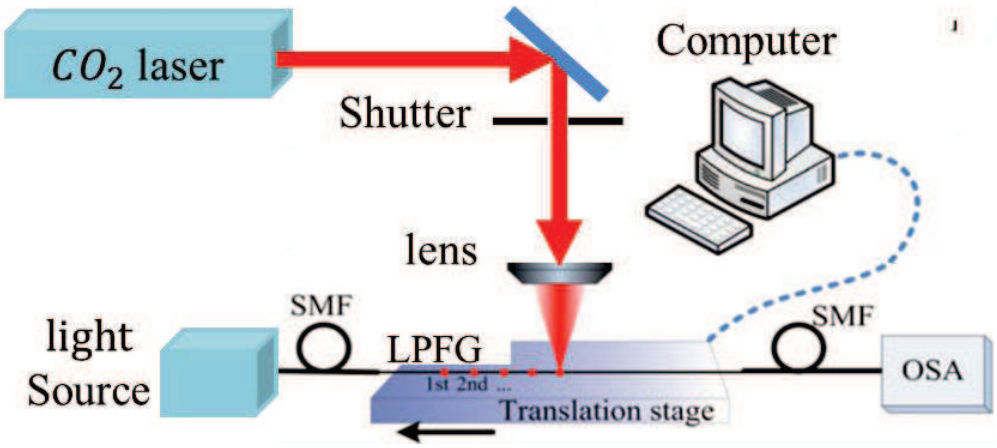


**Figure 1.4.** Schematic of the setup used for the fabrication of LPFG by $CO_2$ laser pulses exposure [50]

The table 1.1 shows the typical properties and some physical parameters of LPFG to manufacture with the technique described above.

**Table 1.1** Parameters reported in a LPFG with different fabrication methods [35].

| Parameters | UV | Residual thermal stress | Mechanical stress | Etching | $CO_2$ | Electric arc |
|---|---|---|---|---|---|---|
| Length (cm) | 2-4 | 2-5 | 3-5 | 2-3 | 3-5 | 2-3 |
| Isolation depth (dB) | 10-30 | 10-25 | 10-20 | 10-15 | 10-25 | 10-15 |
| $\Delta\lambda$ (nm) | >10 | >10 | >15 | >10 | >10 | >15 |
| Insertion loss (dB) | 0.1-0.2 | 0.1-1 | 0.1-0.5 | 0.1-0.3 | 0.1-2 | 0.1-0.2 |
| Modal birefringence | $2(10)^{-7}$ | $1.7(10)^{-6}$ | $1.7(10)^{-6}$ | -- | $1.7(10)^{-6}$ | -- |
| Grating period $\Lambda$ ($\mu$ m) | >100 | >300 | >250 | >500 | >400 | >500 |
| Temperature range of operation (°C) | < 250 | <1100 | <600 | <1200 | >1200 | >1200 |

## 1.3 Birefringence induced in LPFG

At a fundamental level, any standard optical fiber will exhibit low inherent randomly birefringence. In the telecommunication and sensor application fields, the presence of inherent and induced birefringence is crucial. Inherent or intrinsic birefringence is a fundamental property of an optical fiber and can be either low or high, depending on the fiber type. The presence of birefringence may cause an undesirable state of polarization change. In the case of high-speed data transmission on long distances, the polarization mode dispersion may occur. Due to this effect the light pulses are broadened. This may result in inter-symbol interference. In the case of sensor application, when the state of polarization is a carrier quantity, the possibility of output characteristic distortion and sensors sensitivity decreasing may occur. Birefringence is a non-vanishing difference of the propagation constants of the two fundamental mode polarizations; it may result in different spectral responses for two polarizations in fiber gratings [45]. On the other hand, the UV induced birefringence can be exploited to affect the polarization behavior of fibers and gratings, for a control of the output polarization of fiber lasers [51].

The polarization dependence of long-period fiber gratings results in undesirable polarization dependent loss (PDL) and polarization mode dispersion (PMD), thereby deteriorating the property of the LPFG as an optical communication device. Birefringence in long-period fiber gratings is manifest as a change in the grating resonant wavelength and attenuation band in the transmission spectrum, with changing polarization of incident light. If birefringence is present within a grating structure, then that grating will exhibit polarization dependent loss. The refractive index modulation is different for each state of polarization. Meanwhile for each state of polarization the amount of light coupled to the relevant cladding modes changes [49]. As a result of these changes that grating undergo, each incident of state of polarization will has a particular resonant wavelength and transmission spectrum. The sources of birefringence can be either inherent to the optical fiber or induced by a mechanism that creates the refractive index change. The birefringence induced in a long-period fiber grating depends on the fabrication technique employed.

### 1.3.1 Birefringence induced in long-period fiber gratings

There are three categories of long-period fiber gratings based on the locations of the birefringence over the fiber cross section: core birefringence, cladding birefringence, and both core and cladding birefringence. The third category represents the most general situation in LPFGs. The more popular technique to determinate the category an LPFG belongs can be established by measurement of the transverse refractive index profile over the grating region by use of computed tomography methods [52]. Figure 1.5 illustrates the location of birefringence for these categories over the optical fiber cross section: (a) core only birefringence, (b) cladding only birefringence, (c) core and cladding birefringence. Shade areas indicate the presence of birefringence in the cross section (right hand side). The raised portions of the line profiles (left hand side) indicate the same. $\Delta n$ is representative of birefringence. UV-induced LPFGs are the first example of long-period gratings that belong in the core birefringence. The main reason of this phenomenon is due to the presence of photosensitive dopants only in the fiber core; therefore, the index change is limited to this region. Birefringence in this type of LPFG has been studied extensively [50-54].

Long-period fiber gratings written in low-intrinsic birefringence optical fiber, in which an index change is induced over the optical fiber cross section, tend to belong in the cladding birefringence category. When the index change is over the entire fiber cross section, both the core and the cladding may be birefringent. For an azimuthally asymmetric refractive index that is not rapidly varying over the cross section, the index change in the core region can be azimuthally symmetric because the core covers a small portion of the overall fiber cross section. The birefringence in the core is much smaller than that in the cladding, therefore the core birefringence can be neglected and the cladding is the only portion of the fiber cross section that is birefringent. $CO_2$ induced, and electric arc LPFGs are a typical examples of this category [51].

Birefringence in both regions of a fiber can be due to the inherent properties of the fiber or to the induced index change. UV induced LPFGs fabricated in stress induced polarization maintaining fibers (PMF) possess birefringence in both, the core and the cladding, because of the inherent properties of PMF not because of UV exposure. LPFGs created by application of pressure with a grooved plate, also belong in this category [55]. Another type of LPFGs fabricated in etched

optical fibers by ion implantation belong in this category, for certain ion energy levels, the induced refractive index change covers the core and a portion of the cladding [56].

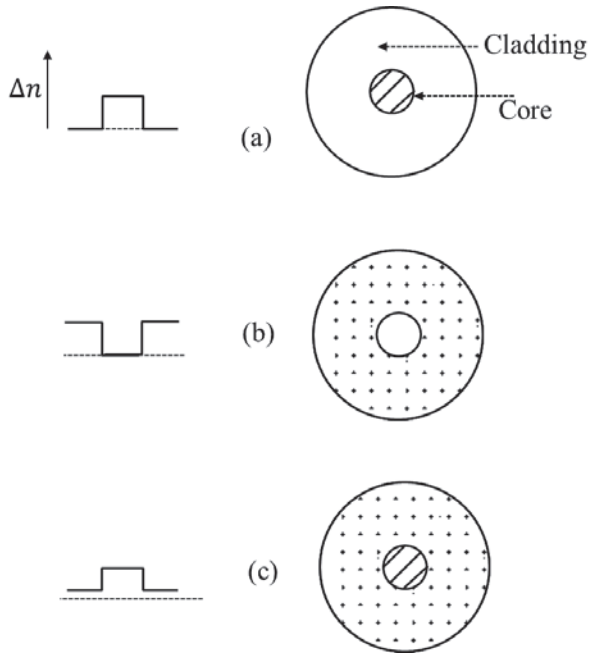


**Figure 1.5.** Illustration of the location of birefringence of long-period fiber gratings

## 1.3.2 Birefringence in mechanical-induced LPFG

Ceballos-Herrera and co-workers [40] characterized the spectral transmission of a long-period holey fiber grating mechanically induced in two different holey fibers. In the experiment (see Figure 1.6), they analyzed the twist sensitivity, tuning of the grating, and polarization response. The two long-period holey-fiber gratings (LPHFGs) were formed using two different holey fibers. The LPHFG was induced by pressing a section of holey fiber (HF) between two corrugated grooved plates (CGPs). In both cases, the results showed that the rejection bands of the grating split when each holey fiber was twisted prior pressure application and the splitting observed grows linearly with the increase in the twist rate. Additionally, results showed that the shift sensitivity in the splitting depends directly on the holey fiber structure. A white light source (WLS) and an optical spectral analyzer (OSA) were used for the spectral measurements. Additionally, a linear polarizing plate and the fluorescence of an ytterbium fiber laser (YFL) were included for the polarization spectra measurements.

Also, they measured the polarization response of the grating inscribed in both holey fibers. The results in Figures 1.7 and 1.8 shows that the rejection bands in the fiber 1 have higher polarization dependence than that in the fiber 2. In these figures it is observed that when the input polarization is changed from vertical (S), which coincides with the pressure direction of the grooved plates, to horizontal (P), each resonant peak is shifted 1.3 and 0.6 nm for fibers 1 and 2 [40]. This behavior varies slightly for different values of twist and it does not depend if the fiber is twisted clockwise or counterclockwise. This result agrees with the fact that the transverse structure of the fiber 1 shows an asymmetric microstructured cladding and consequently, a higher linear intrinsic birefringence. On the other hand, it is worth to mention that, in some applications, this polarization dependence is not attractive in LPFG based devices; nevertheless, it is possible to find alternative experimental setups that can reduce or eliminate this polarization response [40].

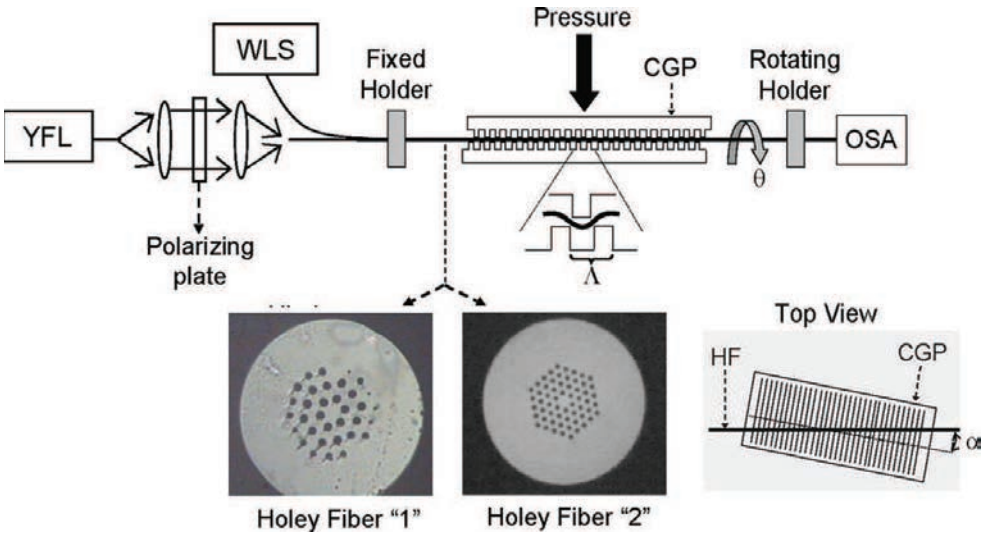


**Figure 1.6.** Schematic of experimental mechanically induced LPHFG set up under torsion [40].

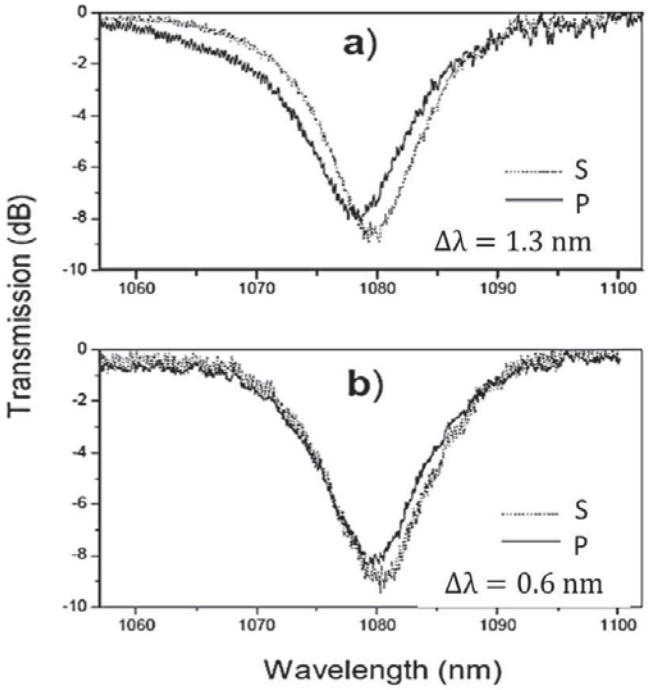


**Figure 1.7.** Polarization response of the rejection bands with: (a) fiber 1 and (b) fiber 2 with zero turns [40].

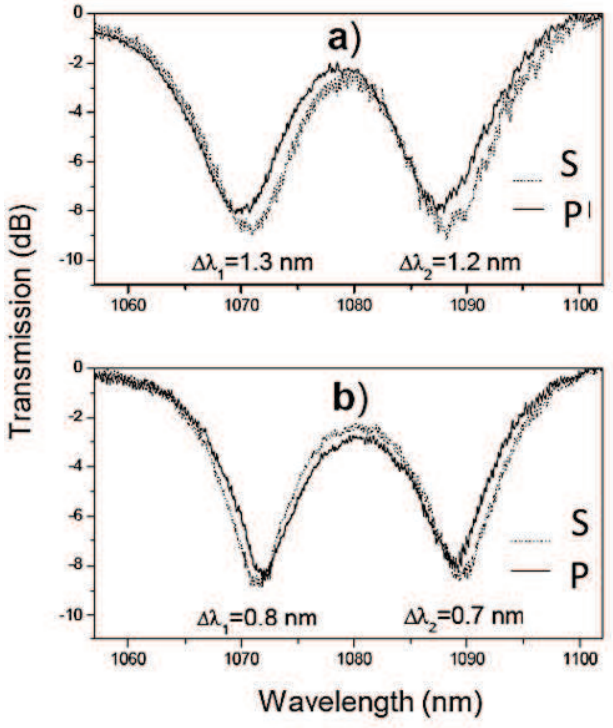


**Figure 1.8.** Polarization response of the rejection bands with: (a) fiber 1 with 4 turns and (b) fiber 2 with 15 turns, respectively [40].

### 1.3.3 Birefringence in arc-induced LPFGs

There are some important applications of LPFGs in optical communications in which, the performance of the optical filter is directly related to its polarization properties. Rego and coworkers [46] have investigated polarization dependent loss on arc induced long-period gratings by considering solely two orthogonal polarizations. They discuss the polarization dependent loss of arc induced gratings under different fabrication parameters.

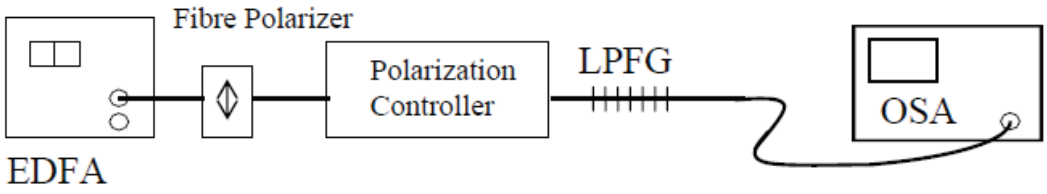


**Figure 1.9.** Experimental setup for polarization dependent loss measurement of electric arc long period fiber gratings

The polarization dependent loss of the arc induced long-period gratings were investigated using the setup shown in Figure 1.9. The PDL values were measured by searching at a particular wavelength in the vicinity of the resonant wavelength, for the maximum and minimum transmitted power. Afterwards, the spectrum of the grating corresponding to the fast and slow axis was registered and the PDL determined by the absolute difference of those spectra. The two extreme PDLmax values are shown in Figure 1.10(a). While, Figure 1.10(b) also shows that two gratings with similar wavelength separation (~1 nm) may exhibit completely different PDL values. Therefore, an important conclusion can be drawn of this experiment, that is, the PDL values depend not only on the wavelength separation, but also on the gratings strength and bandwidth [46].

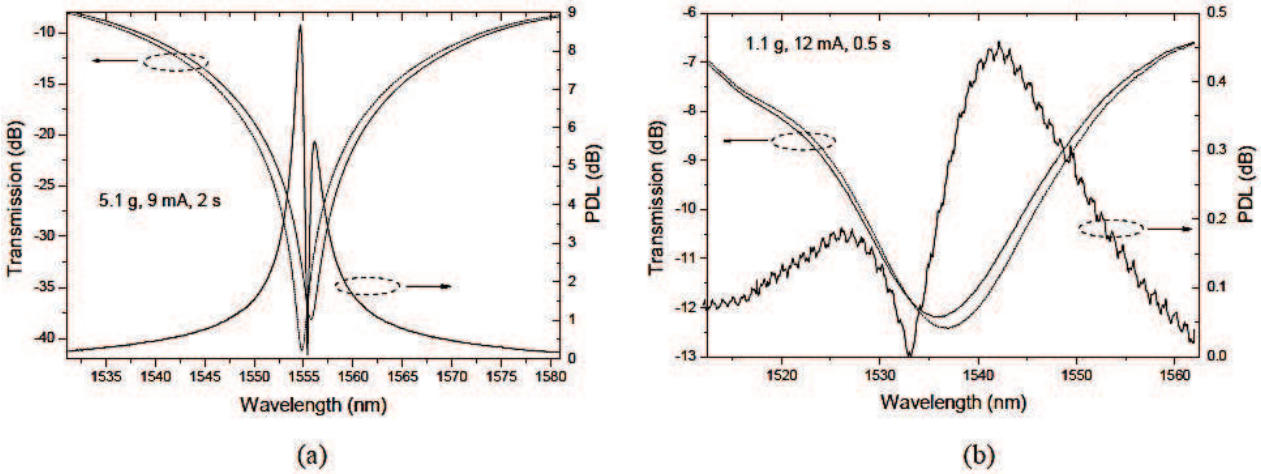


**Figure 1.10**. PDL values of two LPFGs manufactured by electric arc technique [46].

## 1.3.4 Birefringence in $CO_2$ laser exposure LPFG

Conventional LPFGs based on single-side $CO_2$ laser beam exposure could lead to asymmetric refractive index (RI) modulation, which could result in fiber grating birefringence and generate high PDL [52, 57]. Van Wiggeren et al calculated the energy distribution over fiber gratings fabricated by single-side $CO_2$ laser beam exposure and their results showed that the energy absorbed by the exposed side is much higher than that absorbed by the opposite side [58]. Consequently, fabricating LPFGs by single-side $CO_2$ laser beam exposure could lead to fiber birefringence and generate high PDL, which would compromise their application in optical communications and sensing systems.

Figure 1.11 shows the transmission characteristics of the LPFG with two orthogonally polarized lights, parallel (p) and vertical (s). The two loss peaks are separated by 1.0 nm in wavelength, whereas the maximum PDL is ~1.2 dB near 1524-nm wavelength. The small inset in Figure 1.11 shows the full transmission spectrum of the LPFG with a non-polarized light source. Since only one side of the fiber was exposed to the $CO_2$ laser, the distribution of stress relaxation across the fiber cross section was expected to be asymmetric.

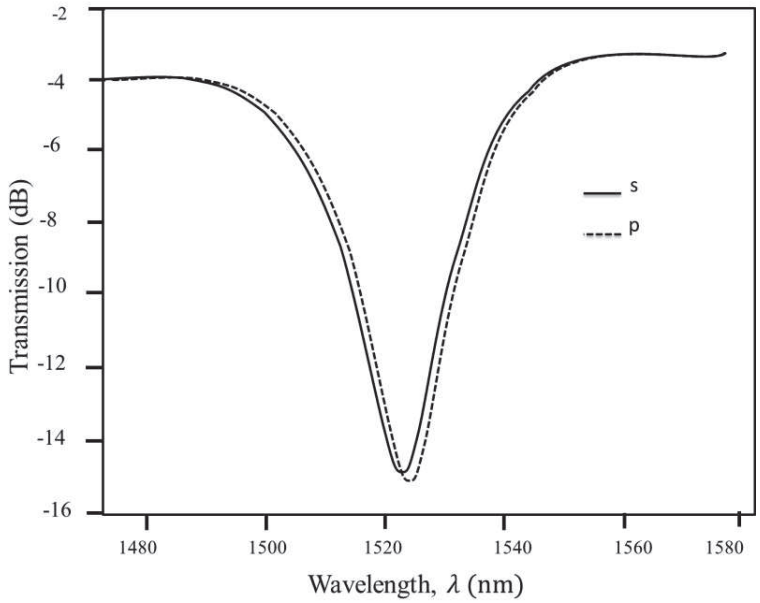


**Figure 1.11.** Polarization-dependent transmission spectrum modified [52]

## 1.4 Compensation techniques for unwanted induced birefringence in LPFGs

In the previous section, it has been explained how the birefringence in the LPFGs affects the input polarization state. Usually, the transformation of the input polarization state is often unwanted, if the fiber is used as carrier information. It is important to suppress the polarization mode dispersion in telecommunications applications, in order to avoid pulses broadening, which is caused mainly by linear birefringence. In the same way is also important to avoid the unwanted birefringence in polarimetric sensors applications. The fact showed above place demand for methods for unwanted birefringence suppression. The following lines present a brief overview of the selected methods. The methods differ in view of this principle, efficiency or usability in various applications.

### Reduction of induced birefringence in M-LPFGs

It is well known that mechanically induced long period fiber gratings (M-LPFGs) are sensitive to the polarization state of the input light [50-51]. This effect is caused by the linear birefringence induced when the fiber is pressed only in one direction by the flat plate over the grooved plate

[59]. To reduce this behavior, it is necessary to compensate the linear birefringence induced in the fiber. One method consists of using two identical LPFGs at 90 degrees from each other (see Fig. 1.12). Thus, two linear orthogonal polarizations that are transmitted along the gratings experience the same perturbations [59].

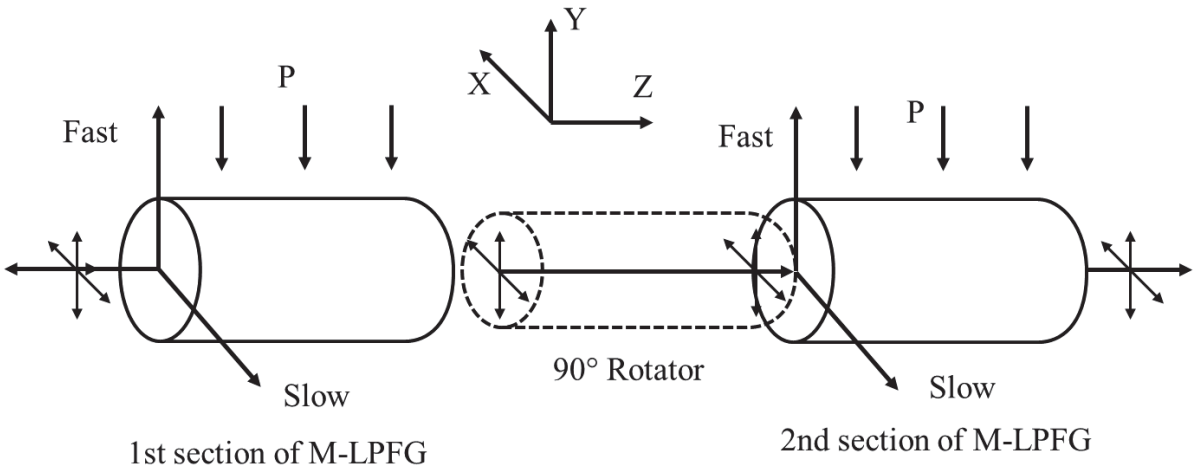


**Figure 1.12.** Concept of a birefringence compensation for M-LPFGs [59]

## Fiber twist method for reducing birefringence in UV LPFGs

One of the major causes of the birefringence in UV induced grating is the geometrical asymmetry of the writing process, UV induced refractive index changes are different between the incident side and the far side on the core and hence can give rise to birefringence. To avoid UV-induced birefringence along the fiber axis, the fiber is twisted during the UV exposure process and then is released after UV writing, this method was implemented by Kim and collaborators [60]. The transmission spectra of a LPFG is different according to the light polarized along the two birefringent orthogonal axes and that causes the PDL of a long-period fiber grating, as shown in Figure 13 there is a wavelength dependent PDL, agreed with the difference between spectra for two orthogonal axes.

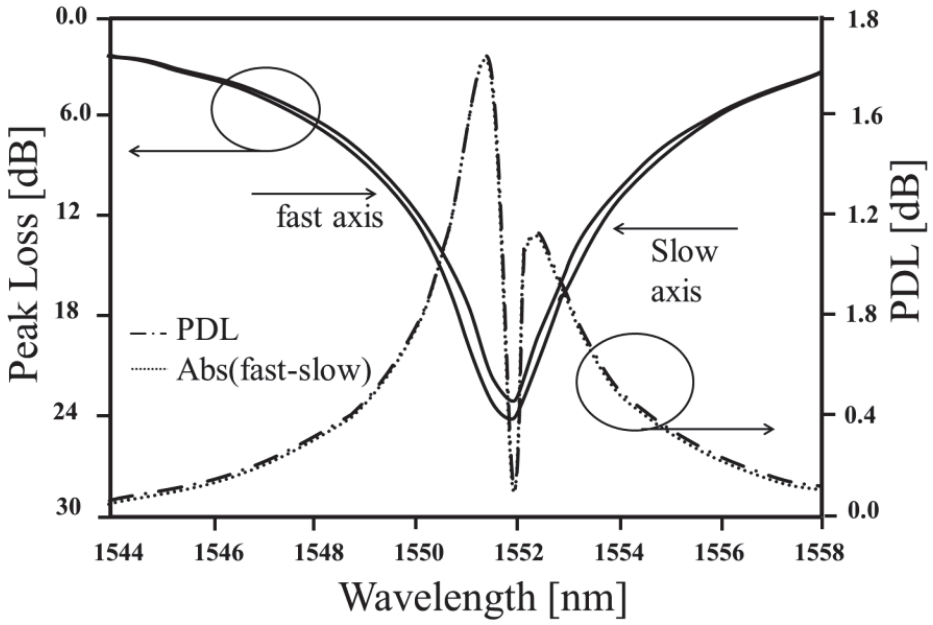


**Figure 1.13.** Transmission spectra and PDL for light linearly polarized in the fast and slow axis of a UV long-period fiber grating [60].

This fiber twist causes the refractive index changes of the core to be spiraled along the fiber axes and can hence reduce the birefringence along the fiber principal orthogonal axes. Figure 1.14 shows the transmission spectra for the light polarized along the two orthogonal birefringent axes of LPFG inscribed by a conventional side writing technique (a) and the fiber twist method (b). By using the twist method the PDL was reduced to about 60% compared with the side writing technique.

Research on transmission properties of LPFGs has revealed that PDL in LPFGs can vary over a widely range of less than 0.1 dB to more than about 1 dB, depending of the type of fiber and the type of filter. The PDL is proportional to $dL/d\lambda$, where $L$ is the grating length [61]. This implies that filters that have sharp features are more susceptible to PDL. Therefore, there is also a need for a method for reducing PDL after the grating has been written in the fiber

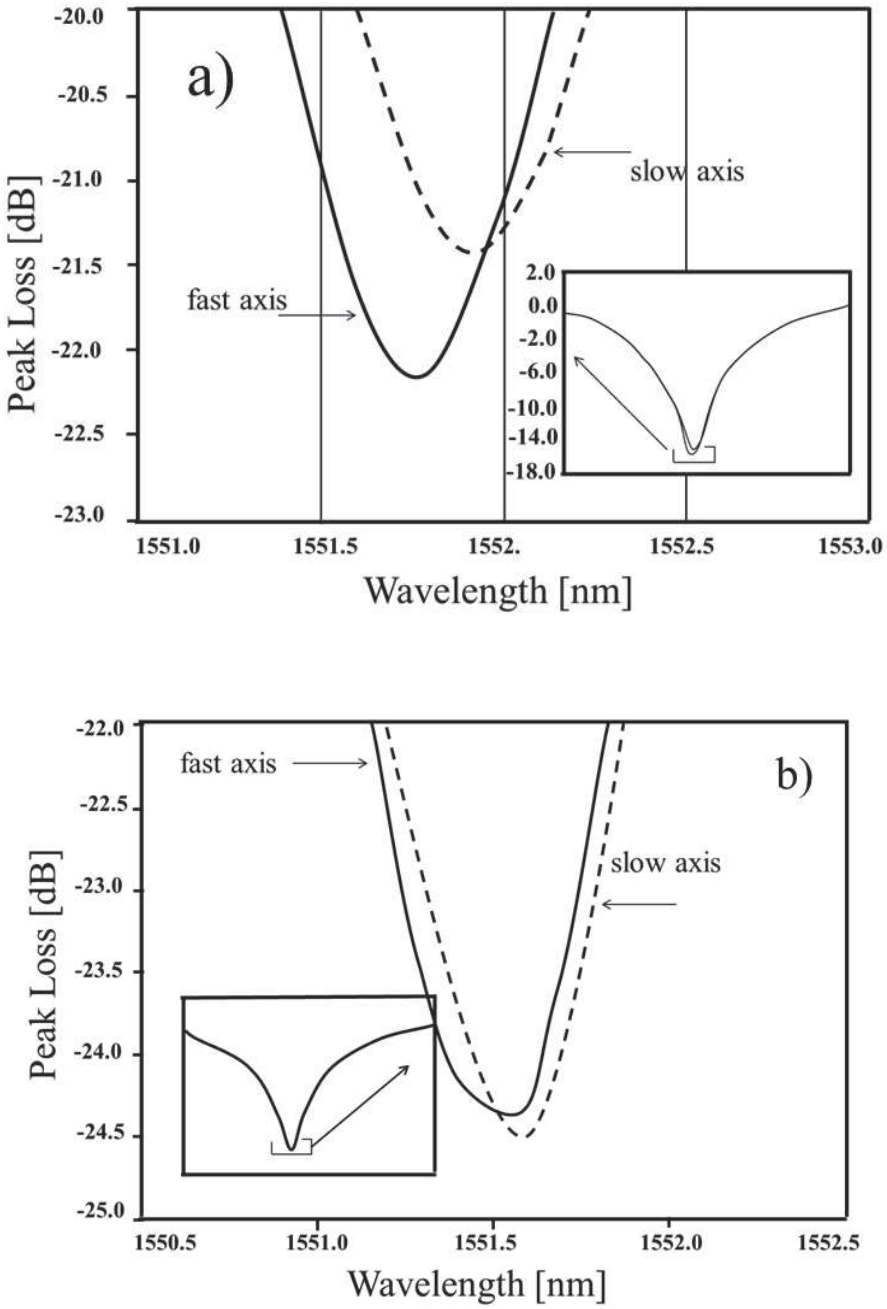


**Figure 1.14.** Transmission spectra and PDL for light polarized of a long-period fiber grating [60].

By twisting the LPFG, a circular birefringence is induced through the stress optic effect. The induced circular birefringence partially compensates the linear fiber birefringence that is intrinsic in most fiber. There is an optimum amount of twist for which the combination of linear and circular birefringence is minimized. Without twist, the linear birefringence dominates. With too

much twist, the fiber becomes highly circular birefringent. Both of these extremes produce PDL. The twist also changes the refractive index of the cladding more than that of the core of the fiber. This produces a peak wavelength shift, since the cladding mode is affected differently than the core mode. By twisting the LPFG, not only PDL may be reduced, but also the wavelegth may be tuned to control the peak wavelength of the LPFG within as little as 0.1 nm.

## 1.5 Polarimetric characterization of LPFGs

The equalization of the gain spectra of erbium doped fibre amplifiers (EDFAs) is one of the most important applications of long-period fibre gratings (LPFGs) in optical communications. In such application, the performance of the optical filter is directly related to its polarization properties. Several studies concerned with the polarization dependent loss (PDL) of gratings produced by UV, $CO_2$ laser radiation, mechanical stress and electric arc technique have been published [45, 60-61]. However, this property has been only described for considering solely two orthogonal polarizations and, therefore, they correspond somehow to an approximation.

It is well known that PDL measurements are largely based on the knowledge of the Mueller matrix elements of the optical component [62]. While PDL can readily be measured with well-established procedures [63], only a few Mueller matrix analyses of the polarization properties of LPGs have been proposed so far. The theoretical approach of LPFGs is based on coupled-mode equations, which describe co-directional coupling between the fundamental mode and high-order cladding modes. The mode coupling, however, is considered polarization-insensitive, and consequently, the results do not take into account polarization-dependent properties of the LPFG.

Using polarization-sensitive coupled-mode equations, Eftimov et al. derived explicit expressions for the Stokes parameters and the Mueller transfer matrix of a uniformly birefringent LPFG that allow calculating the state of polarization at the output of a birefringent LPFG. Explicit expressions for the PDL and the DoP of a LPG were also derived [64-65]. He established that LPFGs made of photonic crystal fiber exhibit cladding birefringence caused essentially by whole ellipticities. Eftimov performs a theoretical Mueller–Stokes analysis of a linearly birefringent LPFG and study the causes of its presence in LPFGs based on photonic crystal fibers (PCFs). He considers several specific cases and obtains explicit expressions for the PDL and the degree of

polarization (DoP) at the LPFG output. Figure 1.15 shows the PDLs for Y polarized input and DoP for two mutually orthogonal polarizations.

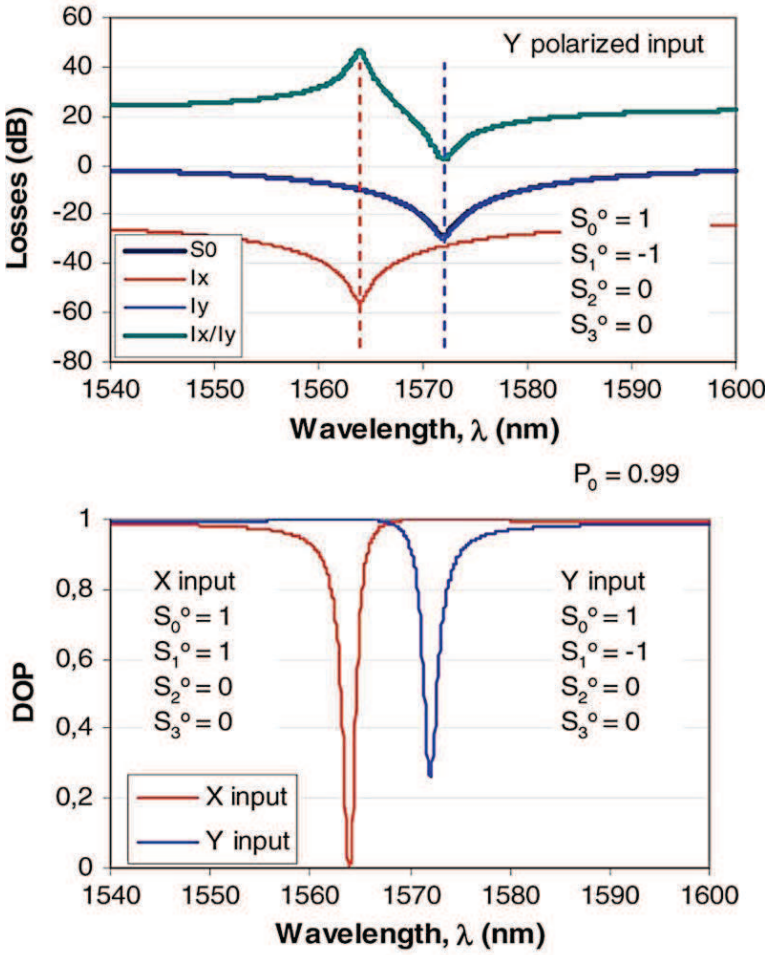


**Figure 1.15**. PDLs for Y polarized input and DoP for two mutually orthogonal polarizations [64].

Eftimov also obtained curves that show the evolution of the polarization on the Poincaré sphere in the LPFG for two almost orthogonal states of polarization (see Fig. 1.16).

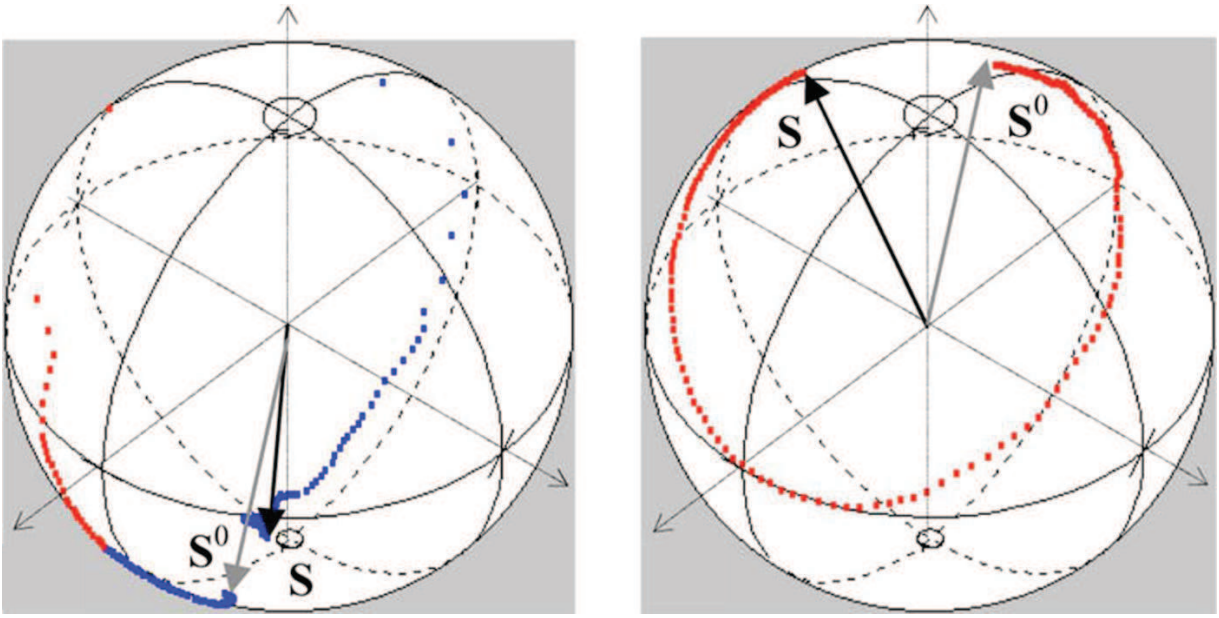


**Figure 1.16.** Evolution of the polarization on the Poincaré sphere in the LPFG [64]

Finally, polarization maintaining photonic crystal fiber (PM-PCFs) used for sensing applications attracts lots of research interests in recent years. The high birefringence can be introduced in PCF due to different air-hole diameters along the two orthogonal axes, which makes this kind of fiber an excellent candidate for fiber sensing based on the polarimetric technique, such as a torsion measurement [66].

## References

1. A. M. Vengsarkar, J. R. Pedrazzani, J. B. Judkins, P. J Lemaire," Long-period fiber-grating-based gain equalizers", Opt. Lett. **21**(5)1996.

2. M. Harumoto, M. Shigehara, H. Suganuma, "Gain-Flattening Filter Using Long-Period Fiber Gratings", J. Lightwave Tech., **20**(6)2000.

3. J. R. Qian, Chen H. F., "Gain flattening fiber filters using phase-shifted long period gratings," Electron. Lett. **34**(11)(1998).

4. M. K. Pandit, K. S. Chiang, Z. H. Chen, S. P. Chen Li, "Tunable long-period fiber gratings for EDFA Gain and ASE equalization," Microwave Opt. Technol. Let. **25**(3)2000.

5. M. Das, K. Thyagarajan, "Dispersion compensation in transmission using uniform long period fiber gratings", Optics Communications, **190**(1–6)2001.

6. D. B. Stegall and T. Erdogan, "Dispersion control with use of long-period fiber gratings," J. Opt. Soc. Am. **17**(2)(2000).

7. M. Das, K. Thyagarajan,"Wavelength-division multiplexing isolation filter using concatened chirped long-period gratings," Optics Communications, **197**, 2001.

8. C. R. Giles, V. Mizrahi, "Low-loss add/drop multiplexers for WDM lightwave networks," In Proc. IOOC´95 (1995).

9. M. J. Kim, T. J. Eom, U. C Paek, and B. H. Lee, "Tunable Add-Drop filter for CWDM using long period fiber gratings," in Proc. Optical Society of Korea, FD-V42(2006).

10. L. Fang, H. Jia,"Mode add/drop multiplexers of LP02 and LP03 modes with two parallel combinative long-period fiber gratings," Opt. Express **22**(10)2001.

11. V. Bhatia, A. M. Vengsarkar, "Optical fiber long-period grating sensors," Opt. Lett. **21**(9)1996.

12. H. J. Patrick, A. D. Kersey, F. Bucholtz, "Analysis of the response of long period fiber gratings to external index of refraction," J. Lightwave Technol. **16(**9)1998.

13. O. Duhem, J. F. Henninot, M. Warenghem, and M. Douay," Demonstration of long-period grating efficient couplings with an external medium of a refractive index higher than that of silica, Appl. Opt. **37**(31)1998.

14. B. H. Lee, Y. Liu, S. B. Lee, S. S. Choi,J. N. Jang," Displacements of the resonant peaks of a long-period fiber grating induced by a change of ambient refractive index," Opt. Lett. **22**(23)1997

15. I. D. Villar, I. R. Matias, F. J. Arregui,"Long-period fiber gratings with overlay of variable refractive index," IEEE Photon. Technol. Lett.**17**(9)2005.

16. A. Martinez-Rios, D. Monzon-Hernandez, I. Torres-Gomez, "Highly sensitive cladding-etched arc-induced long-period fiber gratings for refractive index sensing,"Opt. Commun. **283**(6)2010

17. V. Bhatia, D. Campbell, R. O. Claus, A. M. Vengsarkar, "Simultaneous strain and temperature measurement with long-period gratings," Opt. Lett. **22**(9)1997.

18. A. M. Vengsarkar, P. J. Lemaire, J. B. Judkins, V. Bhatia, T. Erdogan, and J. E, "Long-period fiber gratings as band-rejection filters," J. Lightwave Tech.14(1)1996.

19. X. Shu, T. Allsop, B. Gwandu, L. Zhang, and I. Bennion, a, T. Erdoerature sensitivity of long-period gratings in B/Ge co-doped fibe. Bennion, a, T. Techn. Lett. **13**(8) 2001.

20. T. Allsop, D. J. Webb, I. Bennion, "Bend and index insensitive long period grating in progressive three layered optical fibre," Electron. Lett. **39**(6)2003.

21. T. Allsop, F. Floreani, K. P. Jedrzejewski, P. V. S. Marques, R. Romero, D. J. Webb, I. Bennion. "Spectral characteristics of tapered LPG device as a sensing element for refractive index and temperature," J. Lightwave. Tech. **24**(2)2006.

22. J. F. Ding, A. P. Zhang, S. Li-Yang, Y. Jin-Hua, H. Sailing, "Fiber-taper seeded long-period grating pair as a highly sensitive refractive- index sensor," IEEE Photon. Technol. Lett. **17**(6)2005.

23. T. Allsop, R. Reeves, D. J. Webb, I. Bennion, R. Neal, "High sensitivity refractometer based upon a long period grating Mach–Zehnder interferometer," Rev. Sci. Instrum.**73**(4)2002.

24. K. C Patra, R.Singh, E. K. Sharma, Y. Yasumoto, "Analysis of transmission characteristics of long period gratings in tapered optical fibers". Appl. Opt. **48**(31)2009

25. S. Kim, Y. Jeong, J. Kwon, N. Park, B. Lee,"Control of the characteristics of a long-period grating by cladding etching," Appl. Opt. **39**(13)2000.

26. I. M. Ishaq, A. Quintela, W. J. Stephen, G. J. Ashwell, J. M. Lopez-Higuera, R. P. Tatam, "Modification of the refractive index response of long period gratings using thin film overlays," Sensors and Actuators B **107**(2)2005.

27. N.D. Rees, S.W. James, G.J. Ashwell, R.P. Tatam, "Optical fibre long-period gratings with Langmuir-Blodgett thin-film overlays," Opt. Lett. **27**(9)2002.

28. E. Davies, R. Viitala, M. Salomaki M, S. Areva S, L. Zhang, I. Bennion, "Sol–gel derived coating applied to long-period gratings for enhanced refractive index sensing properties," J. Opt. A: Pure Appl. Opt. **11**, 2009.

29. Z. Wang, J. R. Heflin, R. H. Stolen, S. Ramachandran, "Analysis of optical response of long period fiber gratings to nm-thick thin-film coatings, " Optics Express **13**(8)2005.

30. Z. Wang, J. R. Heflin, R. H. Stolen, and S. Ramachandran, "Highly sensitive optical response of optical fiber long period gratings to nm-thick ionic self-assembled multilayers," Appl. Phys. Lett. **86**, 2005.

31. Y. Liu, L. Zhang, J. A. R. Williams, and I. Bennion, "Optical bend sensor based on measurement of resonance mode splitting of long-period fiber grating," IEEE Photon. Tech. Lett., **12**(5)2000.

32. C. C. Ye, S. W. James, and R. P. Tatam, "Simultaneous temperature and bend sensing with long-period fiber gratings," Opt. Lett. **25**(14)2000.

33. H. J. Patrick, C. C. Chang, and S. T. Vohra, "Long period fiber gratings for structural bend sensing," Electron. Lett. **34**(18)1998.

34. Y. Liu, L. Zhang, J.A.R. Williams, I. Bennion, "Bend sensing by measuring the resonance splitting of long-period fiber gratings," Optics Communications, **193**(1–6)2001.

35. A. Martínez-Rios, D. Monzón-Hernández, I. Torres-Gómez, and G. Salceda-Delgado, "Long period fibre gratings," in Fiber Optic Sensors, M. Yasin, ed. Chap. 11 (InTech, 2012).

36. G. Meltz, W. Morey, and W. Glenn, "Formation of Bragg gratings in optical fibers by a transverse holographic method," Opt. Lett. **14**(15)1989.

37. K. O. Hill, Y. Fujii, D. C. Johnson, and B. S. Kawasaki, nd G. Salceda-Delgado, "Long period fibre gratings," in Fiber Optic Sensors, M. Yasin, ed. Chap. 11 (InTech, 2012**32**(10)1978.

38. I. K. Hwang, S. H, Yun, and B. Y. Kim, d B. S. Kawasaki, nd G. Salceda-Deln periodic microbends,re gratings,"**24**(18)1999.

39. D. E. Ceballos-Herrera, I. Torres-Gim, d B. S. Kínez-Rios, G. Anzueto-Sánchez, R. S. A, J. A. Álvarez-Chávez, J. J. Sánchez-Mondragon, "Ultra-widely tunable long-period holey-fiber grating by the use of mechanical pressure," Appl. Opt. **46**(3)2007

40. D. E. Ceballos-Herrera, I. Torres-Gómez "Torsion sensing characteristics of mechanically induced long period holey fiber gratings," IEEE Sens. J.**10**(7)2010.

41. C.Y. Lin, L. A. Wang, G. W. Chern, "Corrugated long-period fiber gratings as strain, torsion, and bending sensors," J. Lightwave Technol.**19**(8)2001.

42. B. U. Nair, V. P. S. Kumar, V. P. M. Pillai, and V. U. Nayar, "Wavelength shift of cladding mode resonances in a mechanically induced LPFG by twisting the fiber," Fiber and Integr. Optics. **26**(3)2007.

43. M. F. Valdez-Trejo, R. Serratos-Hernandez, "Diseño y fabricación de un dispositivo para el grabado temporal de rejillas de periodo largo en fibrá óptica, " Bachelor Thesis, Centro de Investigaciones en Óptica, México 2009.

44. I. Torres-Gnvestigaciones en Ópticanandez, "Diseño y fabricación de un dispositivo para el grabado temporal de rejillas de periodo larM. Yasin, ed. Chap. 11 (InT long period twisted holey fiber grating," Opt. Lett. **32**(23)2007.

45. G. Rego, "Polarization dependent loss of mechanically induced long-period fibre gratings, Optics Communications," Optics Communications. **281**(2)2008.

46. G. Rego, Arc-induced long-period fibre gratings: fabrication and their applications in optical communications and sensing, Doctor degree thesis, University of Porto, 2006.

47. K. M. Salas-Alcántara, Interferómetro Mach-Zehnder en fibra óptica utilizando rejillas de periodo largo, Masters in Science thesis, Centro de Investigaciones en Óptica, México, 2010.

48. L. A. García-de-la-Rosa, I. Torres-Gómez, A. Martínez-Ríos, D. Monzón-Hernández, J. Reyes-Gómez, "Background loss minimization in arc-induced long-period fiber gratings," Optical Engineering, **49**(6)2010.

49. Y. P. Wang, J. P. Chen, Y. J. Rao, "Torsion characteristics of long-period fibercgratings induced by high-frequency CO2 laser pulses," Journal of Optical Society of America B, **22**(6)2005.

50. Y. Wang, "Review of long-period fiber gratings written by CO2 laser, "Applied physics reviews. **108**(081101)2010.

51. L. B. Bachim, T. K. Gaylord, "Polarization-dependent loss and birefringence in long-period fiber gratings," ," Appl. Opt. **42**(34)2003.

52. H. S. Ryu, Y. Park, S. T. Oh, Y. Chung, and D. Y. Kim, "Effect of asymmetric stress relaxation on the polarization-dependent transmission characteristics of a $CO_2$ laser-written long-period fiber grating," Opt. Lett. **28**(3)2003.

53. Y. G. Han and B. L. Sang, "Discrimination of Strain and Temperature Sensitivities Based on Temperature Dependence of Birefringence in Long-Period Fiber Gratings," Japanese J. of Appl. Phys. **44**(1)2005.

54. T. Erdogan and V. Mizrahi, "Characterization of UV-induced birefringence in photosensitive Ge-doped silica optical fibers," J. Opt. Soc. Am. B. **11**(10)1994.

55. S. Savin, J. F. Digonnet, G. S. Kino, and H. J. Shaw, "Tunable mechanically induced long-period fiber gratings," Opt. Lett. **25**(10)2000.

56. M. Fujimaki, Y. Ohki, J. L. Brebner, and S. Roorda, "Fabrication of long-period optical fiber gratings by use of ion implantation," Opt. Lett. **25**(2)2000

57. H. S. Ryu, Y. Park, S. T. Oh, Y. Chung, and D. Y. Kim, "Effect of asymmetric stress relaxation on the polarization-dependent," transmission characteristics of a $CO_2$ laser-written long-period fiber grating," Opt. Lett. **28,** 2003.

58. G.D. VanWiggeren, "Axial rotation dependence of resonances in curved $CO_2$-laser-induced long-period fibre gratings", Electron Lett. **36**(16) 2000.

59. J. Y. Cho, K. S. Lee, "A birefringence compensation method for mechanically induced long-period fiber gratings," Opt. Commun. **213**(4-6)2002.

60. S.Y. Kim, S. Y. Yoon, M. S. Kim, K. H. Kwack,"Birefringence reduction long period gratings by the fiber-twist method ", Lasers and Electro-Optics, CLEO 2000.

61. J. A. Cline, G. E. Kohnke, "Twisted long-period fiber grating and method for reducing polarization dependent loss and shifting wavelength of a long-perion fiber grating" **US 6707966 B1,** 2004

62. X. S. Yao, "Measurements of polarization-dependent loss (PDL) and degree of polarization (DoP) using optical polarization controllers" **US 20090213453 A1**, 2009

63. T. Eftimov, "Müller matrix analysis of PDL components," Fiber and Integrated Optics,**23**, 2004.

64. T. A. Eftimov, W. J. Bock, J. Chen, and P. Mikulic, "Muller- Stokes analysis of long-period gratings part I: uniformly birefringent LPGs," J. Lightwave Technol. **27**(17)2009.

65. T. A. Eftimov, W. J. Bock, P. Mikulic, and J. Chen, "Analysis of long-period gratings part II: randomly birefringent LPGs," J. Lightwave Technol. **27**(17)2009.

# 2 Long-period fiber gratings

Fiber gratings have found many applications in lightwave communications. These applications include rare-earth doped fiber grating lasers, dispersion compensations, WDM demultiplexers, add/drop multiplexers, mode couplers, fiber amplifier gain control, grating-based sensors, nonlinear effect switches, etc. with the development of Dense Wavelength Division Multiplexing (DWDM) networks. This chapter gives an overview of long-period fiber gratings, including the theoretical background, transmission properties, and polarized light in LPFGs.

## 2.1 Theory of long-period fiber grating

Long-period gratings (LPFGs) are periodic structures that couple light from the fundamental guided mode to discrete cladding modes [1]. The periodicity of the refractive index modulation ranges in hundreds of micrometers and this causes light to couple from the fundamental guided mode to discrete forward propagating cladding modes. The response of this device is a strong function of the parameters of the host fiber, the grating period and the writing conditions. The principle of operation of LPFGs proposed by Vengsarkar et al [1] is depicted in Figure 2.1. Light in the fundamental $LP_{01}$ guided mode is perturbed by the presence of the grating in the fiber core. The difference between the propagation constant of the guided mode and the phase matching vector of the grating are equals the propagation constant of one or more cladding modes at appropriate wavelengths. Cladding modes result from the radiation modes that are trapped by cladding outer surface. These modes attenuate rapidly on propagation due to bends in the fiber and absorption due to the cladding, and hence light at the phase matched wavelengths is lost from de fiber.

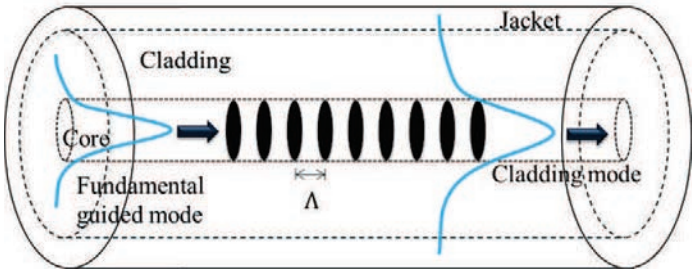


**Figure 2.1.** Coupling of the fundamental guided mode to cladding modes in a long-period fiber grating

## 2.2 Coupling mode equation

The transfer of power between two propagating modes has been analyzed since 1953[2]. In optical fibers, the power is transferred in the form of modes. In a lossless unperturbed system, each mode propagates without losing or gaining power along the fiber length. Nevertheless in reality, any small disturbance in the system can cause power to couple between two or more modes. Interesting and useful devices can be fabricated by utilizing the mode coupling in one or more fibers. These components include directional couplers [3], and gratings [4-5] that are finding increased applications in fiber optic systems. Hence to perform a comprehensive analysis of these devices it becomes necessary to understand the finesse of mode coupling in optical fibers.

### 2.2.1 Co directional coupling

By using the approach used by Taylor and Yariv [6] under the influence of a periodic perturbation is possible to present the solution to coupled mode equations for two modes propagating in the same direction. In the same way using coupled mode equations to depict the importance of phase matching condition between two modes for significant exchange of power.

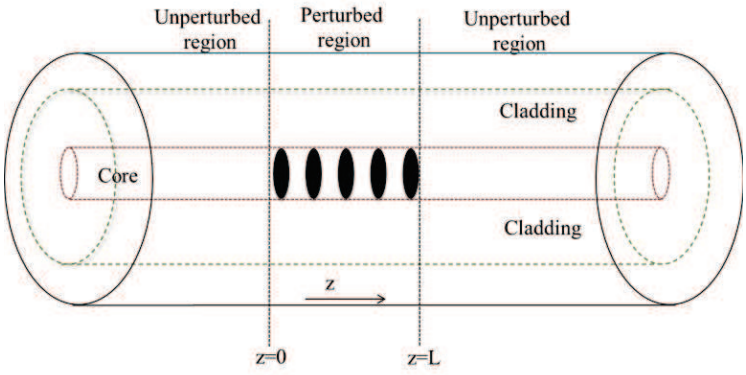


**Figure 2.2.** Optical fiber under perturbation

Consider an optical fiber of Figure that is disturbed by a periodic perturbation along of the fiber axis, originating at z=0 and ending at z=L. the perturbation can be caused by a periodic variation in the core index or simply by external bends in the fiber. Consider two modes denoted by $a_1$ and $a_2$ traveling in the positive $z$ direction with propagation constants $\beta_1$and $\beta_2$ respectively, such that,

$$a_1(z,t) = A_1(z)e^{j(\omega t-\beta_1 z)}$$
$$a_2(z,t) = A_2(z)e^{j(\omega t-\beta_2 z)} \quad (2.1)$$

Where $\omega$ is the angular frequency and $A_1(z)$ and $A_2(z)$ are complex normalized amplitudes and are independent of $z$ in an unperturbed fiber. The presence of a disturbance causes two modes to exchange energy such that $a_1$and $a_2$ become functions of the propagating distance. The electric field of the perturbed fiber is expressed as a linear combination of the two eigenmodes in equation (2.1) and substituting in the scalar wave equation for the perturbed system. Integrate over the fiber cross section to obtain two coupled, the equations describing this coupling can be written by:

$$\frac{dA_1(z)}{dz} = \kappa_{12}A_2(z)e^{-j\Delta z}$$
$$\frac{dA_2(z)}{dz} = \kappa_{21}A_1(z)e^{+j\Delta z} \quad (2.2)$$

Where $\kappa_{12}$ and $\kappa_{21}$ are the cross coupling coefficients and dictate the magnitude of coupling between the two modes, Δ is the phase mismatch between the propagating modes and is typically the difference in their propagation constants, such that

$$\Delta = \beta_1 - \beta_2 - \frac{2\pi}{\Lambda} \quad (2.3)$$

In the presence of a periodic perturbation Λ. Since $\beta_1$ and $\beta_2$ are functions of the optical wavelength the phase mismatching, Δ has a strong spectral dependence. For a synchronous transfer of power between the two modes, the value of Δ should ideally be zero. Using equation (2.3), the phase matching condition between two modes is,

$$\Delta\beta = \beta_1 - \beta_2 = \frac{2\pi}{\Lambda} \quad (2.4)$$

Where Δβ is their differential propagation constant.

The perturbation simply interacts with the mode $A_1$ to generate a propagating polarization wave that finally results in mode $A_2$. This mode further interacts with the perturbation to alter the energy in

mode $A_1$. This exchange of power between the two eigen modes is hence dependent of the differential propagation constants and the periodicity of the perturbation. For the phase matched case, the mode coupling is optimized and the power transference between the two modes is a function of the coupling coefficients. The magnitude of interaction between the two modes is expected to be negligible far away from the phase matching condition.

The total power carried by modes $a_1$ and $a_2$ is given by $|A_1(z)|^2$ and $|A_2(z)|^2$, respectively. Since in a lossless system, there is no variation of total power in the $z$ direction, and manipulating the equation 2 is possible to obtain [6],

$$\kappa_{12} = -{\kappa_{21}}^* \tag{2.5}$$

Where, * denotes the complex conjugate. If we assume that only mode $A_2$ carries power at $z = 0$, we get the following boundary conditions,

$$\begin{aligned} a_1(0) &= 0 \\ a_2(0) &= A \end{aligned} \tag{2.6}$$

Which can be used to solve the mode coupled equations. The complex modal amplitudes can be written as

$$A_1(z) = A\frac{2\kappa^2}{\sqrt{4\kappa^2+\Delta^2}}e^{-j\left(\frac{\Delta z}{2}\right)}\sin\left[\frac{1}{2}\left(\sqrt{4\kappa^2+\Delta^2}\right)z\right] \tag{2.7}$$

And

$$A_2(z) = Ae^{j\left(\frac{\Delta z}{2}\right)}\left\{\cos\left[\frac{1}{2}\sqrt{4\kappa^2+\Delta^2}z\right] - j\frac{\Delta}{\sqrt{4\kappa^2+\Delta^2}}\sin\left[\frac{1}{2}\left(\sqrt{4\kappa^2+\Delta^2}\right)z\right]\right\} \tag{2.8}$$

Where

$$\kappa^2 = |\kappa_{12}|^2 \tag{2.9}$$

The eigenmodes can now be obtained by substituting the values of the complex amplitudes $A_1$ and $A_2$ in equation (2.1). The power in the two modes is given by,

$$P_1(z) = |A_1(z)|^2 = P_0 \frac{sin^2\left[\kappa z\sqrt{1+\left(\frac{\delta}{\kappa}\right)^2}\right]}{1+\left(\frac{\delta}{\kappa}\right)^2} \tag{2.10}$$

And,

$$P_2(z) = |A_2(z)|^2 = P_0 \left\{\frac{cos^2\left[\kappa z\sqrt{1+\left(\frac{\delta}{\kappa}\right)^2}\right]+\left(\frac{\delta}{\kappa}\right)^2}{1+\left(\frac{\delta}{\kappa}\right)^2}\right\} \tag{2.11}$$

Where $\delta = \Delta/2$ is the detuning parameter and $P_0$ is the incident power in eigenmode $a_2 (P_0 = P_2(0) = |A|^2)$. the two modes have sinusoidal variations in the propagating power. The frequency and magnitude of power coupling is a function of the detuning ratio $\delta/\kappa$. The figure 2.2 shows the variation in the incident power normalized values of $P_1(z)$ and $P_2(z)$ as function of $\kappa z$ for two different values of detuning ratio. When $\delta \neq 0$, the mode coupling is small and becomes negligible for $\delta/\kappa \gg 1$. For the phase matching condition ($\delta = 0$), equations (2.10) and (2.11) can be modified to yield,

$$P_1(z) = P_0 sin^2(\kappa z) \tag{2.12}$$

and

$$P_2(z) = P_0 cos^2(\kappa z) \tag{2.13}$$

Which predict a large degree of interaction between the two modes depending on the value of the coupling coefficient, this can be observed in Figure 2.3(b) which shows that the modes continuously exchange power in the region of perturbation with a spatial period given by $\pi/\kappa$. The modal interaction ends at $z = L$. At that point the perturbation terminate, and the ratio $P_T$ ($P_T \leq 1$) of the power in mode $a_1$to the originally in $a_2$ can be determined from equations (2.10) and (2.11) as,

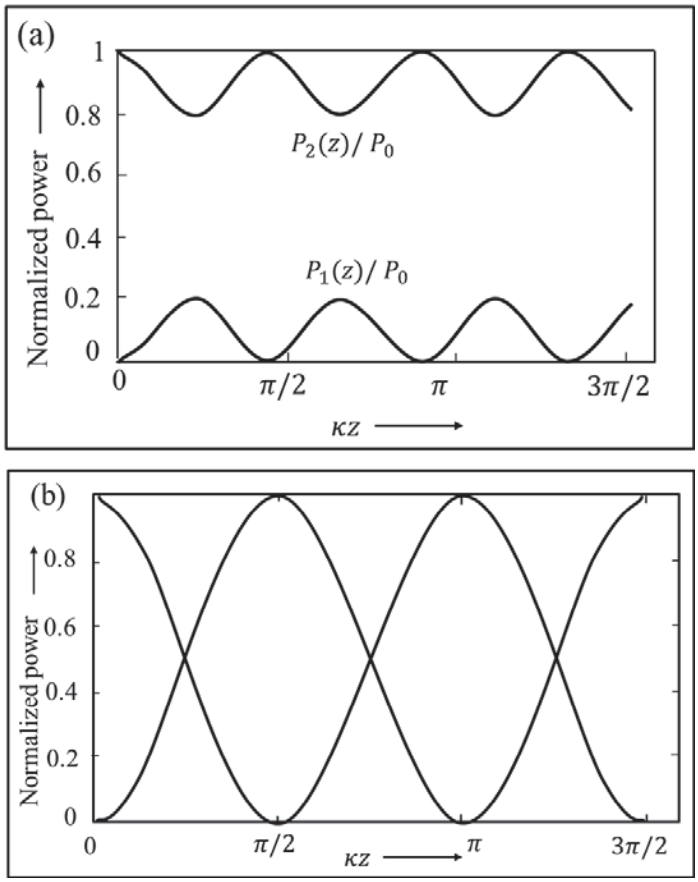


**Figure 2.3.** Variation of the power of the two co-propagating modes involved in coupling for (a) phase mismatched $\boldsymbol{\delta/\kappa = 2}$, and (b) phase matched $\boldsymbol{\delta/\kappa = 0}$ case. **[**6**]**

$$P_T = \frac{P_1(L)}{P_2(0)} = \frac{sin^2\left[\kappa L\sqrt{1+\left(\frac{\delta}{\kappa}\right)^2}\right]}{1+\left(\frac{\delta}{\kappa}\right)^2} \tag{2.14}$$

At $z = L$, the normalized power remaining $T$ in mode $a_2$ is simply given by $T = 1 - P_T$. For most applications the length L of the perturbation region is constant while the coupling coefficient $\kappa$ is varied to achieve complete power transfer from mode $a_2$ to $a_1$. Although the maximum power transfer occurs when $\kappa L = m\pi/2$, where $m$is an integer, the device operation is typically optimized for $m = 1$, which yields $\kappa = \pi/2L$.

In certain applications, it is essential to couple light from the $LP_{01}$ mode to other forward propagating guided modes. In next lines will be described briefly the operation and properties of

gratings that implement the transformation of one guided mode to another. The $\beta$ plot in Figure 2.4 depicts the mode coupling mechanism between two forward propagating guided modes. Since the differential propagation constant ($\Delta\beta$) is small in this case, large values of the grating periodicity are required to satisfy the phase matching condition (equation (2.4)). The periodicity of the resultant devices are typically hundreds of micrometers compared to less than one micrometer for fiber Bragg gratings. Long-period fiber gratings couple light between two guided modes. Hill was the first to propose the use of these gratings for guided mode coupling [8]. He used a point by point writing technique to couple the $LP_{01}$ mode to $LP_{11}$ mode employing a periodicity of $590\,\mu m$. Since coupling in this case occurs from a circularly symmetric to asymmetric mode, the grating needs to be blazed to arraign optimum mode coupling [7].


**Figure 2.4.** Mode coupling between two forward propagating guided modes

In 1991, Bilodeau and coworkers [8] proposed a grating that coupled the fundamental guided mode to the circularly symmetric $LP_{02}$ mode. The grating did not require blazing because both $LP_{01}$ and $LP_{02}$ modes possess circular symmetry. In the same year, Vengsarkar et al. demonstrated internally written gratings for coupling to the $LP_{11}$ mode in dual mode, elliptical core fibers [9]. In 1992, Johnson proposed long-period fiber gratings that couple light from one polarization component of the fundamental mode to the other in standard telecommunication fibers [10]. The differential propagation constant between the two orthogonal polarizations is very small, resulting in a large period. The rocking filter coupled light from one polarization to another with a 99% efficiency.

In Figure 2.4 [11] is shown a typical variation of the differential propagation constant ($\Delta\beta$) between two forward propagating guided modes. The value of ($\Delta\beta$) can be the same at two different operating wavelengths. Therefore, the same grating period might result in modal coupling at two values of wavelength ($\Delta\beta = 2\pi\Lambda$). The spectral dependence of the coupling coefficient might cause

a difference in the coupling magnitude at the two wavelengths. The wavelength at which the slope of $\Delta\beta$ versus $\lambda$ curve is zero, i.e., where the $LP_{01}$ and $LP_{11}$ modes have the same group velocity, is termed the equalization wavelength $\lambda_0$ [10].

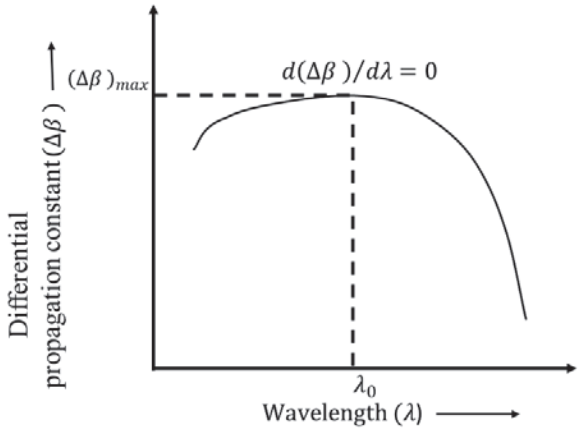


**Figure 2.5.** Typical variation of the differential propagation constant with wavelength for a two forward propagating modes [11]

The coupling between two modes propagating in the same direction is a strong function of the detuning ratio $\delta/\kappa$, where $\delta$ is the detuning parameter and $\kappa$ is the coupling coefficient of the grating. The detuning parameter is dependent on the proximity of the operating wavelength to the phase-matching wavelength for the grating. The coupling coefficient is a function of the index change and the modal overlap between the guided and cladding modes over the region of perturbation. It is typically desired that the value of the detuning ratio be as small as possible for maximum power transfer to occur which implies that the coupling coefficient should be optimized to improve the grating performance.

By use a function $\delta n(z)$ to describe the periodic refractive index modulation in the fiber core such that the modified profile $n(z)$ is possible to derive an expression for the coupling coefficient adopt the approach used by Snyder and Love [12], Such as

$$n(z) = n_1 + \delta n(z) \tag{2.15}$$

Where $n_1$ is the unperturbed core index of refraction. For a rectangular index modulation the function $\delta n(z)$ is given by $\delta n(z) = \Delta n \,\mathrm{rect}\,(\mathrm{z}/\Lambda)$. The periodic variation in the index can be expressed in terms of its Fourier series [13].

$$\delta n(z) = \Delta n \left[ A_0 + \sum_{N=1}^{\infty} A_N cos\left(\frac{2\pi N}{\Lambda} z\right)\right] \tag{2.16}$$

Where $\Lambda$ is the grating periodicity, $\Delta n$ is the peak index change and $A_N$ are the Fourier coefficients. For coupling to all cladding modes $N = 1$. The coupling coefficient $\kappa$ is given by the square root of the product of the two cross coupling coeficients $\kappa_{12}$ and $\kappa_{21}$ [12].

$$\kappa = \sqrt{\kappa_{12}\kappa_{21}} \tag{2.17}$$

The cross coupling coefficients $\kappa^{(m)}$ are functions of the order of the mode $m$ and yield [12].

$$\kappa^{(m)} = \frac{\mathrm{k}|A_N|}{2} \frac{\left|\int_0^a \Delta n E_{01}(r) E_{cl}^{(m)}(r) r dr\right|}{\sqrt{\int_0^\infty (E_{01}(r))^2 r dr \int_0^\infty \left(E_{cl}^{(m)}(r)\right)^2 r dr}} \tag{2.18}$$

Where $E_{01}(r)$ and $E_{cl}^{(m)}(r)$ are the electric field distributions of the fundamental guided mode and the circularly symmetric cladding mode of order $m$ respectively. The integration in the numerator is over the core only since the refractive index perturbation for the grating is confined to the fiber core. By assuming that the index modulation is small compared with unperturbed core index and hence from equation (15), $n^2(z) - n_1^2 = 2n_1\delta n(z)$. Defining the overlap integral $\eta^{(m)}$ as,

$$\eta^{(m)} = \frac{\left|\int_0^a \Delta n E_{01}(r) E_{cl}^{(m)}(r) r dr\right|}{\sqrt{\int_0^\infty (E_{01}(r))^2 r dr \int_0^\infty \left(E_{cl}^{(m)}(r)\right)^2 r dr}} \tag{2.19}$$

We can rewrite the coupling coefficient as,

$$\kappa^{(m)} = \frac{\pi|A_N|}{\lambda^{(m)}}\eta^{(m)} \tag{2.20}$$

Where we have assumed that the coupling coefficient is constant across the spectral width of a resonance band of order $m$ and centered at $\lambda^{(m)}$. The coupling coefficient for a LPFG hence has the same form as that for a FBG [14]. Since the coupling coefficient is directly proportional to the overlap integral, the modal distribution of the cladding mode will have a strong influence on its magnitude. Also since the index modulation has no azimuthal variation, the coupling of the guided mode can occur only to circularly symmetric cladding modes, and for all other cladding modes, the overlap integral is zero. Blazing the grating will give the index modulation an azimuthal dependence ($\Delta n = \Delta n(\phi)$) and result in coupling to cladding modes that have the same variation [15]. A typical rectangular amplitude mask used to write LPFG has a 50% duty cycle and yields the index modulation given by $\delta n(z) = \Delta n\,\mathrm{rect}(z/\Lambda)$. The Fourier series of the rectangular index modulation with a period Λ may be expressed as [10],

$$\delta n(z) = \Delta n\left[\frac{1}{2} + \frac{2}{\pi}\sum_{N=1}^{\infty}\frac{1}{N}\sin\left(\frac{N\pi}{2}\right)cos\left(\frac{2\pi N}{\Lambda}z\right)\right] \tag{2.21}$$

Comparing equations (16) and (2.21) we deduce that the Fourier coefficients (N>1) are

$$A_N = \frac{2}{\pi N}\sin\left(\frac{N\pi}{2}\right) \tag{2.22}$$

For $N = 1$, the Fourier coefficients is $A_1 = 2/\pi$ and $A_2 = 0$, and hence for a grating with a perfectly rectangular modulation the second order interaction between the guided and cladding modes does not exist. Thus the coupling coefficient for the first order of interaction in a LPFG with rectangular index modulation is given by

$$\kappa^{(m)} = \frac{2}{\lambda^{(m)}}\eta^{(m)} \tag{2.23}$$

Since the overlap integral is a dimensionless quantity, the coupling coefficient is expressed in the units of per unit length ($cm^{-1}$). Probst et al. [16] have shown that the coupling coefficient is a strong function of the order of the cladding mode, the operating wavelength, and the fiber parameters and power profile. For LPFGs, the index modulation during the writing process makes the coupling coefficient of the transmittance function of the amplitude mask and the peak index change.

# 2.3 Transmission properties

## Resonance band separation

To calculate the resonance band separation, it is necessary to calculate the wavelength difference between the band of order $m$ at $\lambda^{(m)}$ and $\lambda_{cut}$, the coupling wavelength corresponding to a mode with effective index equal to the index of refraction of the cladding $n_2$ [1]. By combining the expression for $u_{cl}^{(m)}$(See Appendix A) and the phase matching condition, we can obtain

$$\lambda^{(m)} - \lambda_{cut} = \frac{\lambda_{cut}^2 \Lambda}{8n_2} \frac{m^2}{b^2} \tag{2.24}$$

where the effective index of the guided mode is assumed to be equal at $\lambda^{(m)}$ and $\lambda_{cut}$ [1]. The maximum value of the cladding mode propagation constant yields a wavelength parameter termed $\lambda_{cut}$. Equation (2.24) reveals that the wavelength separation between $\lambda^{(m)}$ and $\lambda_{cut}$ is an increasing function of the order $m$ and the grating period $\Lambda$. Thus for a given period, the wavelength difference will increase as we move to higher order cladding modes.

If $m$ is small $\lambda^{(m)}$ and $\lambda_{cut}$ can be assumed to very close and the wavelength separation $\delta\lambda^{(m,m+1)}$ between the resonance bands of orders $m$ and $m+1$ can be obtained from equation (2.24)

$$\delta\lambda^{(m,m+1)} = \lambda^{(m+1)} - \lambda^{(m)} \approx \frac{\lambda_{cut}^2 \Lambda}{8n_2} \frac{2m+1}{b^2} \tag{2.25}$$

The wavelength separation between the resonance bands increases as the value of m is increased. Also the wavelength separation between any two attenuation bands increases as the cladding radius b is reduced. The ratio C of the power coupled to a cladding mode of order *m* to the initial power in the fundamental guided mode is approximated by [17].

$$C = \frac{P^{(m)}(L)}{P_{01}(0)} = \frac{sin^2\left[\kappa^{(m)}L\sqrt{1+\left(\frac{\delta^{(m)}}{\kappa}\right)^2}\right]}{1+\left(\frac{\delta^{(m)}}{\kappa^{(m)}}\right)^2} \tag{2.26}$$

Where L is the length of the grating and $\kappa^{(m)}$ and $\delta^{(m)}$ are the coupling coefficient and the detuning parameter for the corresponding cladding mode, respectively, the detuning parameter at a wavelength λ is defined by

$$\delta^{(m)} = \frac{1}{2}\left(\beta_{01} - \beta^{(m)} - \frac{2\pi}{\Lambda}\right) = \frac{\pi}{\Lambda}\frac{\left(\lambda^{(m)} - \lambda\right)}{\lambda^{(m)}} \tag{2.27}$$

And is zero at the phase matching wavelength $\lambda^{(m)}$. The normalized power T transmitted by the fundamental mode through the grating is given by

$$T = \frac{P_{01}(L)}{P_{01}(0)} = \frac{cos^2\left[\kappa^{(m)}L\sqrt{1+\left(\frac{\delta^{(m)}}{\kappa}\right)^2}\right] + \left(\frac{\delta^{(m)}}{\kappa^{(m)}}\right)^2}{1+\left(\frac{\delta^{(m)}}{\kappa^{(m)}}\right)^2} \tag{2.28}$$

Which at the phase matching wavelength reduces to expression for the attenuation band $T_0$ of the grating

$$T_0 = cos^2\left(\kappa^{(m)}L\right) \tag{2.29}$$

The grating normalized transmission is expressed in decibels (dB) and typically ranges from 5 dB (68.3%) to 35 dB (99.97% coupling). Equation (2.29) reveals that the minimum power in the guided mode is transmitted at the phase matched wavelength and depends on the coupling

coefficient and the length grating. Thus if the length of the grating is known, the coupling coefficient and hence the peak index change can be calculated by combining equations (2.18), (2.23) and (2.29). The condition of complete power transfer to the cladding mode corresponds to [1]

$$\kappa^{(m)} L = \frac{\pi}{2} \tag{2.30}$$

For gratings with the same period that are written for either complete power transfer or the same isolation, for a given order m, the coupling wavelengths will be functions of the grating length. The reason is because is necessary to maintain the product $\kappa^{(m)} L$ constant to satisfy equation (29). Which implies that if the wavelength dependence of the coupling coefficient is ignored, different values of L will require distinct peak index changes $\Delta n$ (equation (2.18)). The characteristics curves of a LPFG written in a SMF28 as function of $\Delta n$ are shown in Figure 6 [1].

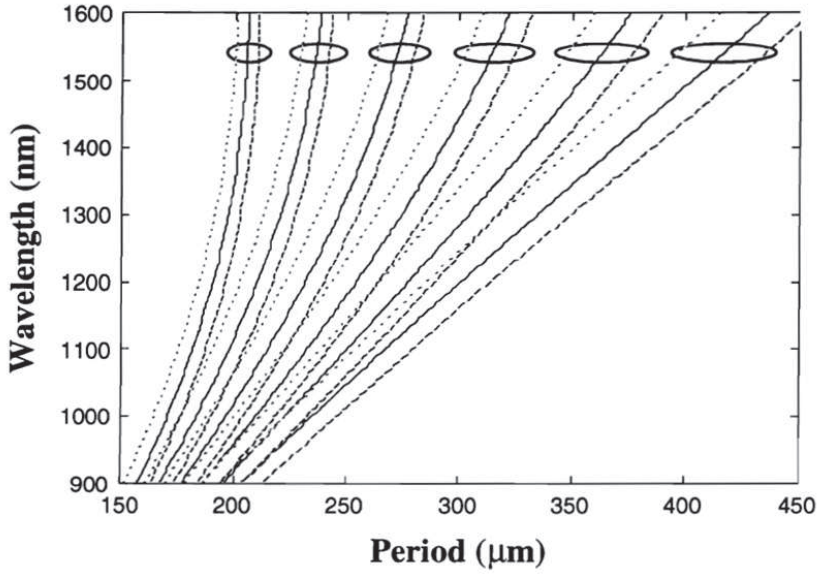


**Figure 2.6.** Typical curves of period versus wavelength obtained for LPFG written in SMF28 fiber when $\boldsymbol{\Delta n = 5 \times 10^{-4}}$ (solid lines), $\boldsymbol{\Delta n = 10^{-4}}$ (dashed curves), and $\boldsymbol{\Delta n = 10^{-3}}$ (dotted curves), respectively. Only modes with m=5 to 10 are presented [1].

Since the effective index of the mode changes during the inscription of the LPFG, a shift in the spectral position of the resonance band is also expected. Figure 2.7 shows the evolution of a

resonance band in a grating with a period of 360 $\mu m$ and a grating length of 2 $cm$ in a SMF28 fiber by UV exposure [1].

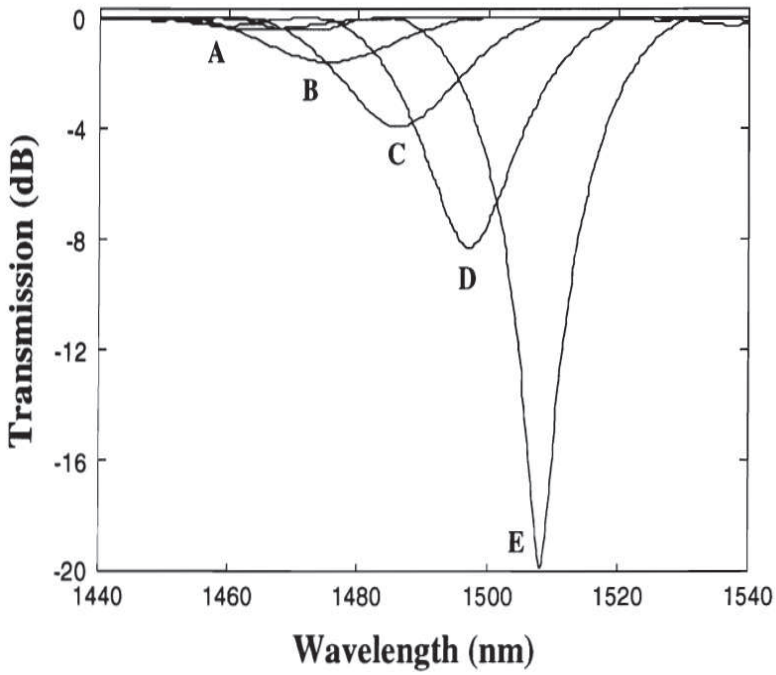


**Figure 2.7.** Evolution of simulated transmission spectrum of LPFG written in SMF28 fiber with $\boldsymbol{\Lambda = 360\ \mu m}$. The curves A through E represent the transmission spectrum at intervals of a one minute each from the time exposure was initiated [1].

For a resonance band of a LPFG and by assuming complete power transfer and putting $c = 1/2$ in equation (2.26) and using equation (2.29).

$$x^2 - 2sin^2\left(\frac{\pi x}{2}\right) = 0 \tag{2.31}$$

Where equation (26) gives

$$x = \sqrt{1 + 4L^2\left(\frac{\lambda^{(m)}}{\Lambda}\right)^2\left(\frac{1}{\lambda_s} - \frac{1}{\lambda^{(m)}}\right)^2} \tag{2.32}$$

By using the phase matching condition and assumed that the cladding mode effective indices at the 3 dB loss wavelength $\lambda_s$ and the coupling wavelength $\lambda^{(m)}$ can be approximated by the index

refraction of the cladding $n_2$ and substituting in equation (2.32) The solution for $x = 1.2798$ we obtain the FWHM $\Delta\lambda^{(m)}$ [1].

$$\Delta\lambda = 2\left|\lambda^{(m)} - \lambda_s\right| = \frac{0.8\lambda^{(m)}\Lambda}{L} \tag{2.33}$$

where we have assumed that $\lambda_s \approx \lambda^{(m)}$

Bandwidth of a resonance band is inversely proportional to the length of the grating L. thus the resonance band can be made narrower if the length of the grating is increased which is illustrated in Figure 2.8. The spectra will be offset due to different coupling coefficients and hence distinct $\Delta n$.

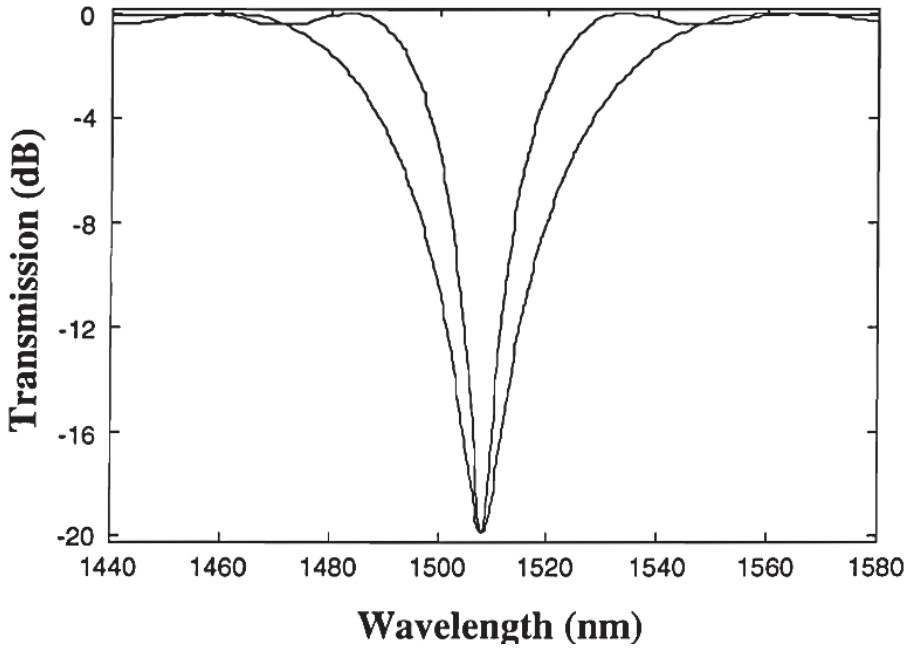


**Figure 2.8.** Simulated transmission spectra of two LPFG written in SMF28 fiber with $\boldsymbol{\Lambda = 360\ \mu m}$. The inner spectrum is for a grating length of 2 cm while than on the outside is for a grating with L=1 [1]

## Peak isolation

Figure 2.9 shows the transmission spectrum of a LPFG written in single mode fiber (SMF28) with period $\Lambda = 600\ \mu m$ and length $L = 4\ cm$ [18]. The peak isolation is 14 dB at a wavelength

of 1540 nm. The value of full width at half maximum (FWHM) gives LPFGs an advantage over other filters such as fiber Bragg gratings in broadband applications. For a grating written for complete power transfer, the resonance band typically has an isolation varying from 15 to 35 dB and FWHM between 20 and 30 nm. The out of band losses for wavelengths far off from the phase matching wavelength are 0.2 dB [1]. The small insertion loss enables concatenation of two or more such devices with similar resonant wavelengths for applications that require large isolation. The polarization mode dispersion and polarization dependent loss of a typical grating are 0.001 ps and 0.02 dB, respectively [1]. The polarization mode dispersion gives an estimate of time difference for grating transversal between two signals launched along the orthogonal axes of the fiber. The polarization dependent loss is a measure of the difference in the losses of the two orthogonal signals.

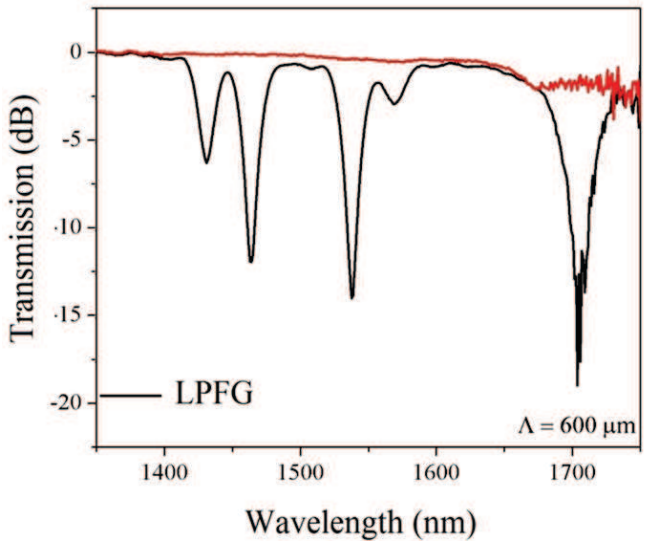


**Figure 2.9.** Transmission spectrum of a LPFG written in SMF28 with $\boldsymbol{\Lambda = 600\ \mu m}$ **and** $\boldsymbol{L = 4\ cm}$ using electric arc technique, the red line shows a transmission characteristics of white light source in the fiber [21]

The spectrum of the grating in figure 2.9 possesses a sideband on the lower wavelength side of the resonance peak. Typically, a LPFG can have two to three sidebands on the short wavelength side with peak loss ranging from 0.5 dB to 4 dB [1]. These gratings with sidebands on only one side of the phase matching wavelength are termed apodized gratings [19]. Apodization typically results from the variation of the peak refractive index modulation or the effective index of the

guided mode along the length of the grating. The effect of the grating length on the transmission serves to reduce the spectral width of the resonance bands of a grating.

The small back reflection of the LPFG is an attractive feature for a multimode sensing and communication systems where the optical feedback is a limiting factor. A typical optical feedback of less than -80 dB may be attributed to the small Fresnel reflections in the grating region and the resulting value of the peak index change ($\Delta n$) is calculated to be $5 \times 10^{-4}$[1]. Figure 2.10 shows the back reflection from a LPFG in AT&T dispersion shifted fiber [1].

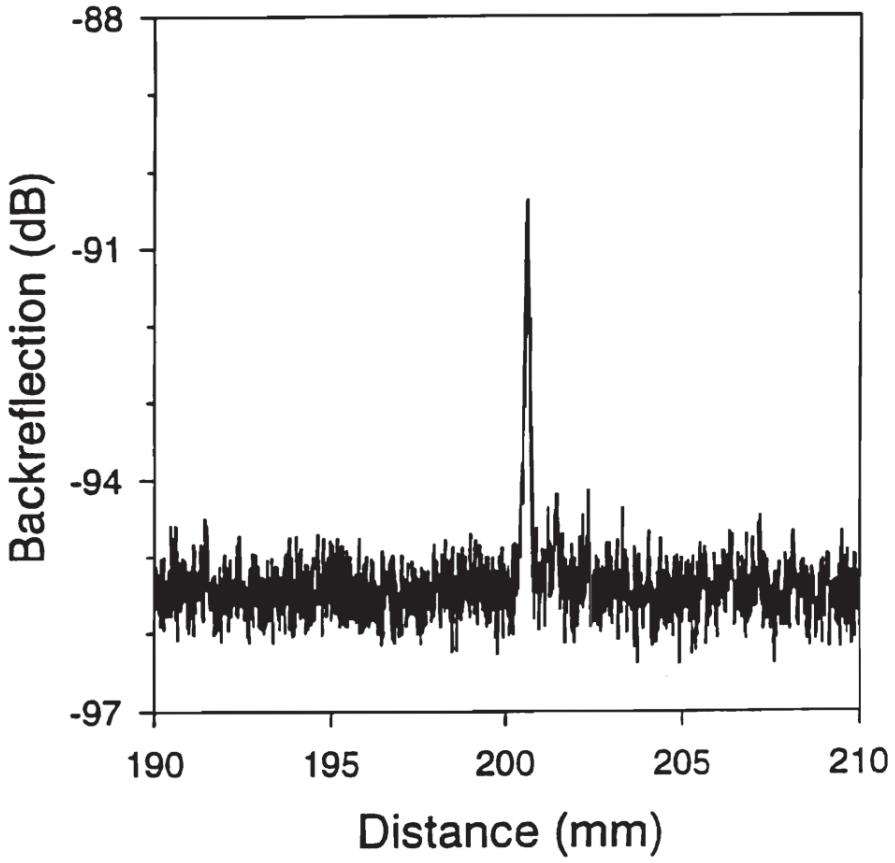


**Figure 2.10.** Optical coherence domain reflectometer back reflection measurement in a LPFG written in AT&T dispersion shifted fiber [1]

Polarization dependent loss refers to the maxim change in the power transmitted by an optical component or device as the input state of polarization is varied over all possible polarization

states. Polarization mode dispersion (PMD) is a fundamental characteristic of single mode optical fiber and fiber optic components that describes their propensity to split an optical signal into two orthogonal polarization modes with different propagation velocity, resulting in a different propagation time in each mode, called the differential group delay (DGD). The PDL and other polarimetric properties must therefore be characterized accurately in order to assess the potential impact on the performance of optical devices such as fiber gratings that becomes critically import for system design and evaluation.

# 2.4 Polarized light in LPFG [PDL]

There are two categories of PDL measurements techniques: deterministic and no deterministic [20-21]. The deterministic techniques compute the PDL value from the device´s Jones or Mueller matrices, which are obtained by measurements of Stokes parameter for a set of input polarization states [22]. The non-deterministic techniques determine the PDL value by measuring the maximum polarization sensitivity of a device over all possible input polarization states.

## 2.4.1The polarization-scanning method

The polarization-scanning method (called power min/max method) is a non-deterministic measurement technique [23-24]. A polarization controller and a power meter are needed to determine the maximun and minimum changes in power transmission trough the device (LPFG) over a large number of input polarization states. The polarization controller must be able to provide all possible ouput polarization states. The measurement set-up used for characterizing optical componets is shown in Figure 2.11. The 3 dB coupler must be removed for measurements in transmission.

A power calibration procedure is required to remove the PDL contributions of the polarization controller and other optical components in the set-up. Accounting for the system transmission variation, the PDL of the device under test (DUT) is then determined by

$$PDL\ (\lambda_i) = 10\log\left[max\left(\frac{P_j^{DUT}(\lambda_i)}{P_j^{cal}(\lambda_i)}\right)\right] - 10\ log\left[min\left(\frac{P_j^{DUT}(\lambda_i)}{P_j^{cal}(\lambda_i)}\right)\right] \tag{2.34}$$

Where $\{\lambda_i\}, i = 1,2, \dots, M$, refer to wavelegths within the wavelegth range of interest $\{P_i\}, j = 1,2, \dots, N\}$, refer to the transmission/reflection power at a set of polarization states 1 to $N$. $P^{cal}$ and $P^{DUT}$ denote the transmission/reflection power without the DUT (power calibration) and with the device under test (LPFG).

The polarization scanning is especially valuable for wavelength PDL measurements in broadband fiber optic components, since a large number of measurements must be obtained at each wavelength of interest to ensure measurements accuracy.

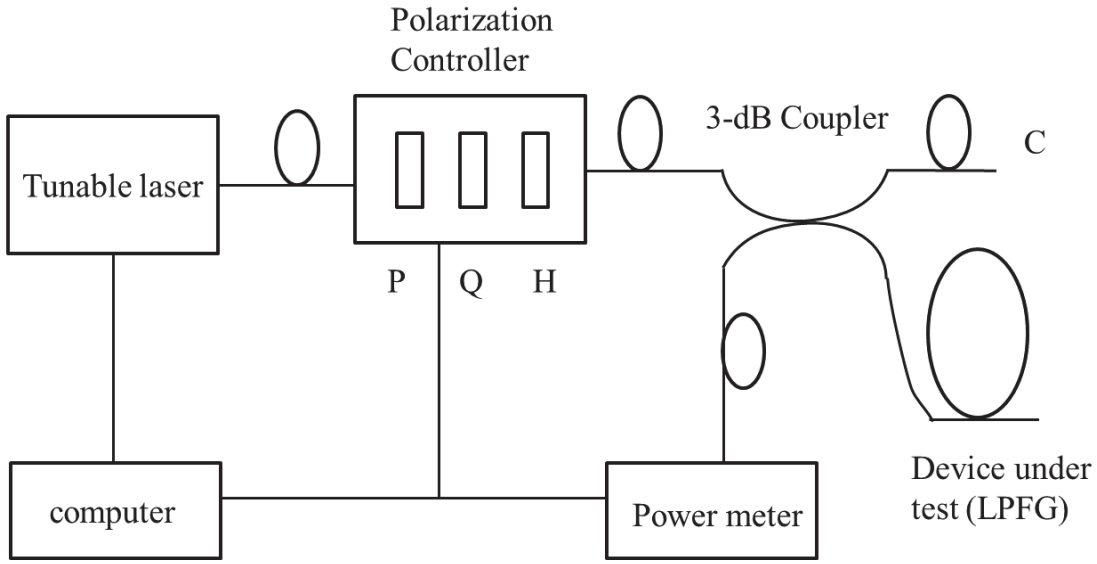


**Figure 2.11.** PDL measurement set-up used using the polarization scanning method . the polarization controller comprises a polarizer (P), followed by a quarter wave plate (Q) and a half wave plate (H). the oupt port C of the coupler us terminated to avoid back reflection. [23]

## 2.4.2 Jones Matrix method

The Jones matrix method measures the device´s polarization response to three input states of polarization at a wavelength of interest [24]. The PDL value of the DUT is the derived from these responses. The measurement set up used for characterizing optical components in reflection is shown in Figure 2.12. For measurements in transmission, de 3 dB coupler is removed. A polarization analyzer, having a polarization adjuster is used to set three linear

polarization states, measure the stokes parameter for the trhee states, calculate the Jones matrix and derive the PDL value.

In this measurements the Jones vector $x$ represents the input electric field. In transmission, the fiber pigtails interconnecting the DUT are represented by their Jones matrices $B$ and $F$. In reflection, $B$ and $F$ represent the backward and forward Jones matrices of the 3 dB optical coupler used shown un Figure 12, respectively. The DUT is represent by Jones matrix $A$. The output field through the optical coupler and the DUT are expressed as $BAFx$. The Jones matrix of the coupler and DUT combined is $J = BAF$, wich is obtained from the measured stokes parameter for three linear polarization states at 0, 60 and 120 degrees.

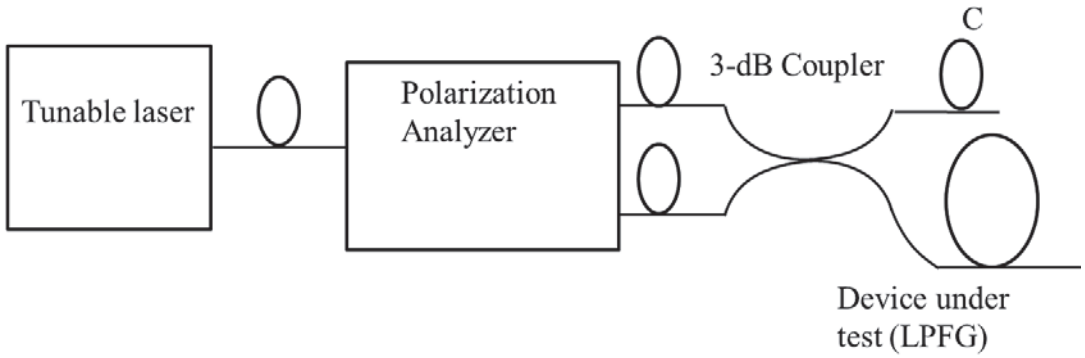


**Figure 12.** PDL measurement setup for characterizing a device using the Jones matrix method [25]

The intensity of an input field $x$ is proportional to the inner product $\langle x, x\rangle = x^{*t}\, x$, where $x^{*t}$ denotes the conjugate transpose of vector $x$, thus the intensity is constant and normalized. The intensity of the output field is proportional to the inner product $\langle Jx, Jx\rangle$. Measuring PDL involves finding the extrema of the inner product $\langle Jx, Jx\rangle$ over all input $x$. Since $\langle Jx, Jx\rangle = \langle J^{*t}Jx, x\rangle$ the latter represents the field of values of a Hermitian matrix $J^{*t}J$. Therefore the maximun and minimun reflected powers can be represented as $\lambda_i(J^{*t}J) = S_i^2(J)$ with $i = 1{,}2$ where $\lambda_1$ and $\lambda_2$ are the eigen values of $J^{*t}J$, and $S_i(J)$ are the singular values of matrix J. thus

$$PDL_{meas} = 10\log\left[\frac{T_{max}}{T_{min}}\right] = 10\,log\left[\frac{\lambda_2(J^{*t}J)}{\lambda_1(J^{*t}J)}\right] = 10\,log\left(\frac{S_2^2(J)}{S_1^2(J)}\right) = 10\,log\left(\frac{S_2^2(BAF)}{S_1^2(BAF)}\right) \tag{2.35}$$

Where $J^{*t}$ denotes the complex conjugate transpose of matrix J, and $PDL_{meas}$ denotes the measured PDL of device under test combined with the coupler.

In the case of polarization insensitive pigtails used for the intercinnection of the DUT in transmission, their Jones matrices $B$ and $F$ are unitary [25]. According to P. Lancaster [26], the singular values of a square matrix are invariant under a unitary transformation. Then the equation (2.35) becomes

$$PDL_{meas} = 10\ log\left(\frac{S_2^2(BAF)}{S_1^2(BAF)}\right) = 10\ log\left(\frac{S_2^2(A)}{S_1^2(A)}\right) = 10\log\left(\frac{\lambda_2(A^{*t}A)}{\lambda_1(A^{*t}A)}\right) = PDL_{DUT} \tag{2.36}$$

Where $PDL_{DUT}$ denotes the $PDL$ of DUT. It can be seen from equation (2.36) that the single mode fibers or components interconnecting the DUT will not impair the measurement accuracy as long as they are polarization independent.

Figure 2.13 shows the wavelength dependent PDL of a LPFG used in transmission for EDFA gain flattening by using the setups shown in Figures 2.11 and 2.12. In this case the coupler was removed and the LPFG connected directly either the polarization controller and a power meter, or the optical input and output ports of the polarization analyzer.

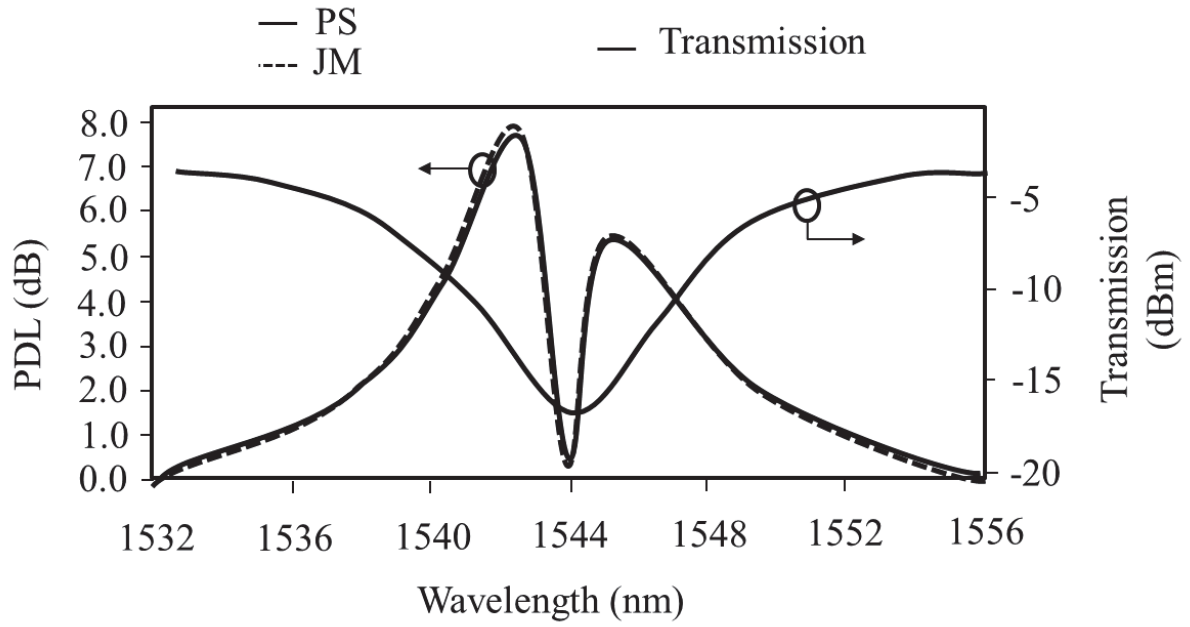


**Figure 2.13.** Measurements of PDL for a LPFG using the Jones matrix (JM) method, the polarization scanning method (PS) and the transmission response.

## References


1. A. M. Vengsarkar, P. J. Lemaire, J. B. Judkins, V. Bhatia, T. Erdogan, and J. E, "Long-period fiber gratings as band-rejection filters," J. Lightwave Tech. **14**(1)1996.
2. J. R. Pierce, "Coupling of modes of propagation, " J. Of Appl.Phys. **25**(2)1954.
3. D. Marcuse, Theory of Dielectric Optical Waveguides, Academic Press, New York, 1991.
4. K. O. Hill, B. Malo, K. Vineberg, F. Bilodeau, D. Johnson, I. Skinner, "Efficient mode-conversion in telecommunication fibre using externally written gratings, " Electr. Lett. **26**(16)1990.
5. T. Erdogan, J. E. Sipe, "Tilted fiber phase gratings," J. Opt. Soc. Amer. A. **13**(2)1996.
6. H. F. Taylor, A. Yariv, "Guided wave optics," Proceedings of the IEEE, 62(8)1974
7. D. Gloge, "Weakly guiding fibers" Appl. Opt. **10**(10)1971.
8. F. Bilodeau, K. O. Hill, B. Malo, , D. Johnson, I. Skinner, "Efficient narrowband $LP_{01} \leftrightarrow LP_{02}$ mode convertors fabricated in photosensitive fiber: Spectral response," Electr. Lett. **27**, 1991.
9. A. M. Vengsarkar, J. A. Greene, K. A. Murphy, "Photoinduced refractive-index changes in two-mode, elliptical-core fibers: sensing applications," Opt. Lett. **16**(19)1991.
10. D. C. Johnson, F. Bilodeau, B. Malo, K. O. Hill, P. G. J Wigley, G. I. Stegeman, "Long-length, long-period rocking filters fabricated from conventional monomede telecommunications optical fibers" Opt. Lett. **17**(22)1992.
11. V. Bhatia, K. A. Murphy, A. Wang, R. O. Claus, J. A. Greene,"Attometer resolution of wavelength shifts by use of fiber modal interferometers," Opt. Lett. **20**(1)1995.
12. A. W. Snyder, J. W Love, "Optical Waveguide Theory," Kluwer academic Publisher, New York, 2000.
13. H. Taub, D. L. Schilling, "Principles of Communications Systems, " McGraw-Hill,New York, 2008
14. R. Kashyap, "Photosensitive Optical Fibers: Devices and Applications, " Opt. Fiber Technol. **1**(17)1994.
15. D. Marcuse, "Microdeformation losses single-mode fibers, " Appl. Opt. **23**(7)1984.
16. C. B. Probst, A. Bjarklev, S. B. Andreasen, "Experimental verification of microbending theory using mode coupling to discrete cladding modes, " J. Lightwave Tech. 7(1)1989.

17. D. G. Hall, “Theory of Waveguides and Devices, ” in Integrated Optical Circuits and Components, L. D. Huctheson: Mercel-Dekker, New York, 1987
18. K. M. Salas-Alcántara, Interferómetro Mach-Zehnder en fibra óptica utilizando rejillas de periodo largo, Masters in Science thesis, Centro de Investigaciones en Óptica, México, 2010.
19. R. Kashyap, J. R. Armitage, R. Wyatt, S. T. Davey, D. L. Williams, “All-fibre narrowband reflection gratings at 1500 nm, “ Electr. Lett. **26**(11)1990.
20. C. D. Poole, R. E. Eagner, “Phenomenological approach to polarization dispersion in long single-mode fibers, ” Electr. Lett. **22**(19)1986.
21. TIA/EIA standard, FOTP-175, “Measurements of polarization dependent loss (PDL) of single-mode fiber optic components, ” May 1995
22. IEC international Standard 1300-3-2, Part 3-2: Examinaton and measurements polarization dependence of a single mode fiber optic device, 1995.
23. P. E. Green, “Optical Networking Update, ” IEEE J. Selected Areas in Communications, **14**(5)1996
24. P. Hemday, Chapter 12: “Dispersion measurements, ” Fiber Test and Measurements, Ed. Dennis D. Derickson, Prentice Hall, 1998.
25. B. L. Heffner, “Deterministic and analytically complete measurement of polarization dependent transmission through optical devices, ” IEEE Photonics Technolo. Lett. **4**,1992.
26. P. Lancaster, M. Tismendtshy, “The teory of matrices with applications, ” 2nd ed., Academic Press, 1985

# 3 Polarized light

Polarization effects play a key role in the operation of many important optical devices. The complete characterization of scattered light is described by Stokes vectors and Mueller matrices. The most general form of the scattering matrix coupled with polarizer and quarter wave plates demonstrates the physical relationships among the matrix elements and polarization measurements. The state of polarization in a lightwave signal can be used to carry information in an optical system. In this chapter, we show some elements to analyze the polarized light through the Stokes vectors and the Mueller matrix.

## 3.1 Description of lightwave polarization

In free space, light is a transverse wave, where the wave motion is perpendicular to the direction of propagation. Such a transverse electromagnetic wave can be divided into unpolarized and polarized. All field components of polarized light have a fixed phase difference to each other. Each state of polarization (SOP) can be split into any two orthogonal states.

When the superposition of both orthogonal states is oriented in only one direction of the transverse plane is called linearly polarized light. In an elliptical polarization state, both orthogonal states have a fixed phase between 0 and 90°. A special case is the circular polarization where the phase difference is 90° and both field components have the same magnitude. Then the electric field vector rotates by 360° within one wavelength (see Figure 3.1).

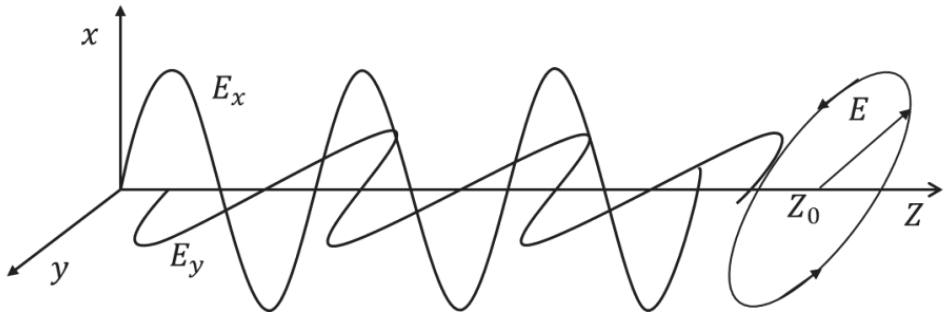


**Figure 3.1.** Electromagnetic wave in free space [1]

The complex electric field envelope can be expressed as [2-3]

$$\begin{aligned} E_x &= E_{x0}\cos(\omega t - kz) \\ E_y &= E_{y0}\cos(\omega t - kz - \delta) \end{aligned} \tag{3.1}$$

The vector of the electric field intensity *E (t)* is determined by the superposition of the *x* and the *y* component. At a fixed time, it points to a trace direction and has a defined magnitude. Figure 2 illustrates two-dimensional descriptions of various polarization states of polarized lights, such as linear polarization, circular polarization, and elliptical polarization.

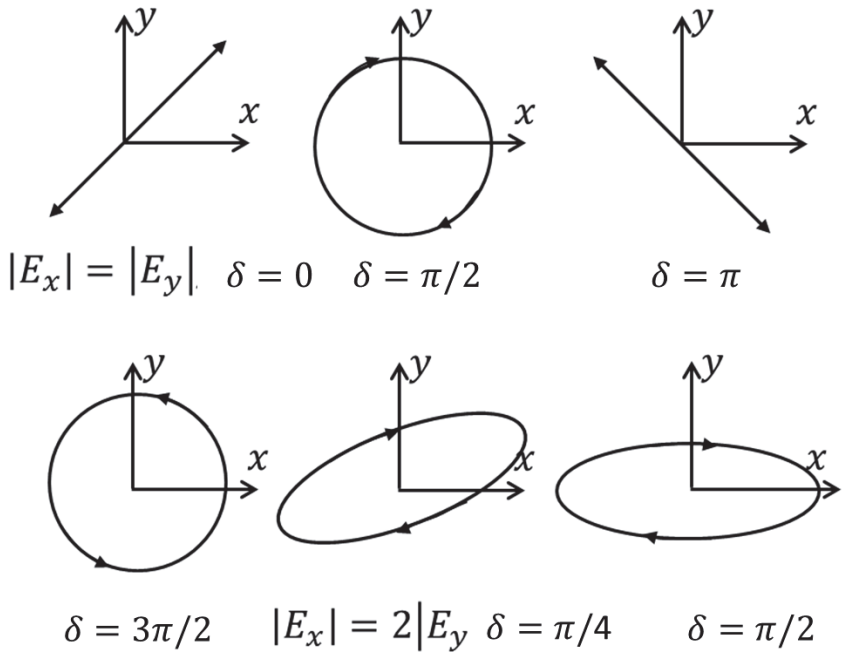


**Figure 3.2.** Two dimensional descriptions of various polarizations states of polarized light.

The pattern of the optical field traced on a fixed point in the *xy* plane can be described by the polarization ellipse,

$$\frac{E_x^2}{E_{x0}^2} + \frac{E_y^2}{E_{y0}^2} - 2\frac{E_x E_y}{E_{x0}E_{y0}}\cos\delta = \sin^2\delta \tag{3.2}$$

Generally, an optical signal may not be fully polarized. That means that the $x$ and $y$ components of the light are not completely correlated with each other; in other words, the phase difference $\delta$ between them may be random. Many light sources in nature are un-polarized, such as the sunlight, whereas the optical signal from lasers are mostly polarized.

An optical signal can usually be divided into a fully polarized portion and a completely un-polarized portion. The degree of polarization (DoP) is often used to describe the polarization characteristics of a partially polarized light; which is defined as [3]

$$DoP = \frac{P_{polarized}}{P_{polarized} + P_{unpolarized}} \tag{3.3}$$

Where $P_{polarized}$ and $P_{unpolarized}$ are the powers of the polarized portion and unpolarized portion, respectively. $DoP$ is therefore the ratio between the power of the polarized part and the total power. $DoP$ is equal to zero for an unpolarized light, and it is equal to unity for a fully polarized light.

## 3.2 Stokes parameters and the Poincaré sphere

The state of polarization of a lightwave signal is represented by the maximum amplitudes $of\ E_x, E_y$ , in the $x$ and $y$ directions, and a relative phase $\delta$ between them. In addition, if the signal is not completely polarized, the $DoP$ also has to be considered. The Stokes vector is one of the most popular tools to describe the state of any polarization associated to of an optical signal. A Stokes vector is determined by four independent Stokes parameters, which can be represented by optical powers in various specific reference polarization states. The Stokes vector is defined in terms of the orthogonal components of the electric field vector (Ep ,Es) as [4-5]

$$s^a\begin{pmatrix} s_o^a \\ s_1^a \\ s_2^a \\ s_3^a \end{pmatrix} = \begin{bmatrix} \langle E_p^a E_p^{a*}\rangle + \langle E_s^a E_s^{a*}\rangle \\ \langle E_p^a E_p^{a*}\rangle - \langle E_s^a E_s^{a*}\rangle \\ \langle E_p^a E_p^{a*}\rangle + \langle E_s^a E_p^{a*}\rangle = 2Re\langle E_p^a E_s^{a*}\rangle \\ \pm i\left(\langle E_p^a E_s^{a*}\rangle - \langle E_s^a E_p^{a*}\rangle\right) = \pm 2\mathrm{Im}\langle E_p^a E_s^{a*}\rangle \end{bmatrix}, \tag{3.4}$$

where $\mathrm{a} = \mathrm{incidence\ (i) or\ scattered\ (sc)}$. Angular brackets represent temporal averages and * indicates complex conjugation, $i^2 = -1$ is the complex number. The upper (lower) sign in the right hand side of $s_3^a$ corresponds to a description of polarization states as looking to the source (propagation direction). The normalized Stokes vectors can also be written in terms of the azimuthal $(0 \le \psi \le \pi)$ and the ellipticity $(-\pi/4 \le \chi \le \pi/4)$ angles of the polarization ellipse of the wave, respectively [6]

$$s = \langle s_0\rangle \begin{bmatrix} 1 \\ \cos(2\chi)\cos(2\psi) \\ \cos(2\chi)\sin(2\psi) \\ \sin(2\chi) \end{bmatrix}, \tag{3.5}$$

where $\langle s_o\rangle$ represents the intensity associated to the Stokes parameters; usually, it is fixed to the unitary value.

For a totally polarized beam of light, Eq. (3.4) is reduced to

$$\begin{aligned} s_o &= |E_p E_p^*| + |E_s E_s^*| = I_p + I_s, \\ s_1 &= |E_p E_p^*| - |E_s E_s^*| = I_p - I_s \\ s_2 &= 2E_p E_s \cos\delta = 2\sqrt{I_p I_s}\cos\delta, \\ s_3 &= \pm 2E_p E_s \sin\delta = \pm 2\sqrt{I_p I_s}\sin\delta, \\ \delta &= \delta_p - \delta_s \end{aligned} \tag{3.6}$$

The positive (negative) sign in $s_3$, Eq. (3.4) and Eq. (3.6), means the sense of circular light is measured as seen to the source (propagation direction) and $\delta$ is the phase difference between the orthogonal components of the electric field. Note that Eq. (3.4) implies, at least for the integrating time used for the detector employed, a spatial coherence among the orthogonal components is implicit.

The value of each normalized Stokes parameter ranges between -1 and +1. If the optical signal is fully polarized, the normalized vector endpoint is always on a sphere surface with unit radius, which is commonly referred to as Poincaré sphere. On the other hand, if the optical signal is partially polarized, the endpoint of the normalized Stokes vector should be inside the unit sphere and the length of the vector is equal to the DoP of the optical signal.

An appropriate way to display the state of polarization is the representation via the Poincaré sphere. The center of the Poincaré sphere is located in the origin of the Cartesian coordinate system. The Cartesian coordinates of any point on the Poincaré sphere represent the corresponding three normalized Stokes parameters $s_1$, $s_2$ and $s_3$ (Shown in figure 3.2).

Each point on the Poincaré sphere describes a defined state of polarization. The equator plane represents all possible linear states of polarization. The two poles represent the states of circular polarization (right or left-hand sense of rotation). All the other points on the upper (lower) half sphere correspond to elliptical polarizations with right (left) handed rotation. From a geometrical point of view, partially polarized states are represented as points inside the unitary sphere. [2]

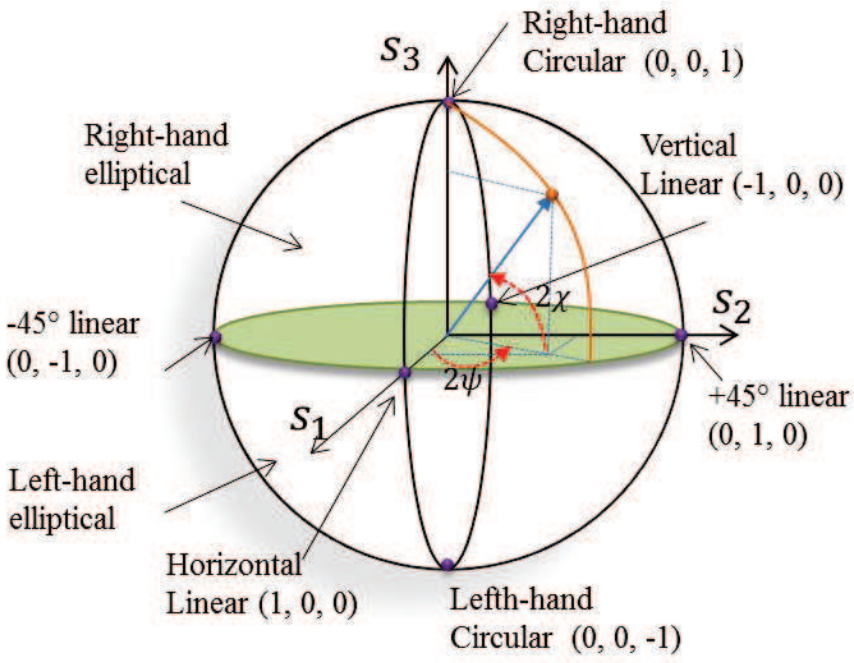


**Figure 3.3.** Polarization states represented on a Poincaré sphere

The value of each normalized Stokes parameter ranges between -1 and +1. If the optical signal is fully polarized, the normalized vector endpoint is always on the sphere (with unitary radius). On the other hand, if the optical signal is partially polarized, the endpoint of the normalized Stokes vector should be inside the unit sphere and the length of the vector is equal to the degree of polarization (DoP) of the optical signal. Observe that a totally un-polarized state must have a null DoP value, which is located at the center of the sphere. An unphysical sense is associated to points outside the Poincaré sphere.

## 3.3 Optical polarimeter

It is well known that an electromagnetic wave has four basic parameters: amplitude, frequency, phase, and the state of polarization. For an optical signal, its amplitude is represented by the brightness and its frequency is represented by the color. The brightness can be easily measured by an optical power meter and the wavelength can be measured by an optical spectrum analyzer. An optical polarimeter is an instrument used to measure the polarization state of light. The polarization states can be represented analytically, Eq. (3.1), by the Stokes parameters, Eq. (3.4), as points on the Poincaré sphere, among many other representations [2-3]. According to the definition of Stokes parameters given by Equations (3.4) and (3.6), they can be obtained by measuring the optical powers after the optical signal passes through polarization-sensitive optical devices such as linear polarizer and retarders.

## 3.4 The Mueller matrix method

The Mueller matrix method is most generally suited for describing irradiance-measuring instruments, including most polarimeter, radiometers and spectrometers. In the Mueller matrix method, the Stokes vector S is used to describe the polarization state of a light beam, and the Mueller matrix (MM) to describe the polarization-altering characteristics of a sample. This sample may be a surface, a polarization element, an optical system, biological tissues, and any other light-matter interaction which produces a reflected, refracted, diffracted, absorption, and scattering of the light beam.

Popular theories of polarized light interaction with optical elements or scattering media may be divided into two groups: Jones matrix, which assumes a coherent addition of waves; and the Stokes-Mueller matrix, which assumes an incoherent addition of waves. In both approaches, one usually starts a theoretical analysis with severely restrictive assumption. In the Jones matrix, one starts out with Maxwell´s equations, whereas in the Mueller matrix, it starts by postulating a linear relation between the input Stokes vector and the output Stokes vector emerging from the optical medium. The development of the Mueller analysis is heuristic and has an advantage in that it deals with intensities rather than field vectors.

A Mueller Matrix represents the polarization rotation characteristics of an optical device such as an optical fiber, which is determined by the relationship between a set of input polarization vectors and their corresponding output polarization vectors. The linear response of a physical system can be expressed in terms of the intensities, through the relation, [2, 4]

$$S^0 = MS^i \Rightarrow \begin{pmatrix} s_o^o \\ s_1^o \\ s_2^o \\ s_3^o \end{pmatrix} = \begin{bmatrix} m_{00} & m_{01} & m_{02} & m_{03} \\ m_{10} & m_{11} & m_{12} & m_{13} \\ m_{20} & m_{21} & m_{22} & m_{23} \\ m_{30} & m_{31} & m_{32} & m_{33} \end{bmatrix} \begin{pmatrix} s_o^i \\ s_1^i \\ s_2^i \\ s_3^i \end{pmatrix} = \begin{bmatrix} m_{00}s_o^i + m_{01}s_1^i + m_{02}s_2^i + m_{03}s_3^i \\ m_{10}s_o^i + m_{11}s_1^i + m_{12}s_2^i + m_{13}s_3^i \\ m_{20}s_o^i + m_{21}s_1^i + m_{22}s_2^i + m_{23}s_3^i \\ m_{30}s_o^i + m_{31}s_1^i + m_{32}s_2^i + m_{33}s_3^i \end{bmatrix} \tag{3.7}$$

where M is called the Mueller matrix of the system, represented as a $4 \times 4$ matrix of real elements, and S is the Stokes vector. S represents the polarization state of light, defined in terms of the orthogonal components of the electric field vector (Ep ,Es).

A typical polarimeter arrangement consists of a Source + PSG + Sample + PSA + Detector. See Figure 3.4. The incident Stokes vectors are generated by a Polarizer State Generator, PSG, and a source; while the out Stokes vector from the sample under study is analyzed or "filtered" by a Polarizer State Analyzer, PSA. The sample under study is an optical fiber. The exiting intensity from the PSA is measured by a sensor or detector device. Usually a PSA is named as a Polarization State Detector, PSD, when the analyzer is a system composed of a PSA plus a sensor (detector) of intensity. It is common to find a mirror-symmetry order between the optical components that constitutes a PSG (linear polarizer + half-wave retardation plate + quarter-wave retardation plate) and a PSA (quarter-wave

retardation plate + half-wave retardation plate + linear polarizer). For a passive Ideal Polarimeter Arrangement, IPA, the output Stokes vector reaching the detector is given as

$$S^{\det} = AMS^{i} = AS^{o} = \sum_{j=0}^{3} a_{ij} \sum_{k=0}^{3} m_{jk} s_{k}^{i} \tag{3.8}$$

Where A is the Mueller matrix that describes the action of the PSA on the Stokes vector scattered ($S^o$) from the sample (M). An IPA arrangement is formed by classical, passive, optical polarization elements, like linear polarizers based in calcite crystal (of the Glan-Thompson, Glan-Laser, Glan-Taylor, Rochon, of Wollaston-type), wave-plate retarders made of mica, quartz, polarizing thin-films, among many other possibilities, and where the theoretical linear response is supposed to be ideal. Indeed, there is not any formal restriction if the passive retarders of an IPA are changed by Liquid Crystal Variable Retarders, LCVR, set to a fixed voltage and with an oscillatory high frequency value. This is true if the integration time for the detector used is larger than the period associated to the oscillating frequency applied to the voltage of the LCVR and the sample under study is passive.

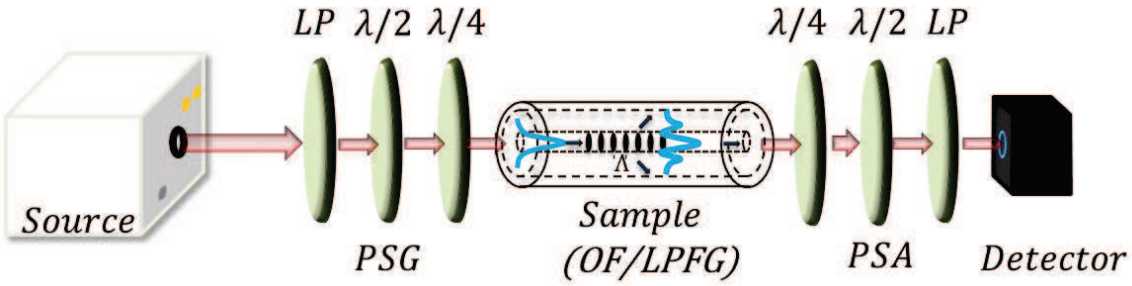


**Figure 3.4.** A typical passive ideal polarimeter arrangement (IPA)

## 3.4.1 Four- Mueller matrix method

For an arbitrary optical system and by considering an IPA setup, it has been shown that the 16 Mueller elements can be obtained from a set of 4 incident Stokes vectors (PSG) and 4 states filtered or analyzed (PSA): p, s, +45, and r [4]. The incident Stokes vectors correspond to linear polarization states parallel (p), perpendicular (s), and to +45 degrees

(+) respect to the incidence plane, respectively, and to a right-hand (r) polarization state. The polarized states mentioned above, form a tetrahedron inscribed into the Poincaré sphere, whose vertex are contained on the surface. The 16 arbitrary Mueller elements can be determined from the following 16 intensity-measurements taken from the so detected Stokes element [5]:

$$
\begin{aligned}
I_{pp} &= \frac{1}{2}\left(m_{00}+m_{01}+m_{10}+m_{11}\right); I_{ps} = \frac{1}{2}\left(m_{00}+m_{01}-m_{10}-m_{11}\right) \\
I_{p+} &= \frac{1}{2}\left(m_{00}+m_{01}+m_{20}+m_{21}\right); I_{pr} = \frac{1}{2}\left(m_{00}+m_{01}+m_{30}+m_{31}\right) \\
I_{sp} &= \frac{1}{2}\left(m_{00}+m_{10}-m_{01}-m_{11}\right); I_{ss} = \frac{1}{2}\left(m_{00}+m_{11}-m_{01}-m_{10}\right) \\
I_{s+} &= \frac{1}{2}\left(m_{00}+m_{20}-m_{01}-m_{21}\right); I_{sr} = \frac{1}{2}\left(m_{00}+m_{30}-m_{01}-m_{31}\right) \\
I_{+p} &= \frac{1}{2}\left(m_{00}+m_{02}+m_{10}+m_{12}\right); I_{+s} = \frac{1}{2}\left(m_{00}+m_{02}-m_{10}-m_{12}\right) \\
I_{++} &= \frac{1}{2}\left(m_{00}+m_{02}+m_{20}+m_{22}\right); I_{+r} = \frac{1}{2}\left(m_{00}+m_{02}+m_{30}+m_{32}\right) \\
I_{rp} &= \frac{1}{2}\left(m_{00}+m_{03}+m_{10}+m_{13}\right); I_{rs} = \frac{1}{2}\left(m_{00}+m_{03}-m_{10}-m_{13}\right) \\
I_{r+} &= \frac{1}{2}\left(m_{00}+m_{03}+m_{20}+m_{23}\right); I_{rr} = \frac{1}{2}\left(m_{00}+m_{03}+m_{30}+m_{33}\right)
\end{aligned}
\tag{3.9}
$$

where $I_{mn} = (s^0)_{mn}$ denotes the intensity measured when an m-polarized state illuminates the sample and an n-polarized state is analyzed. The Mueller matrix is obtained by solving the equation (3.7) for each of the 16 $m_{ij}$ elements [4, 5].

Indeed, it has been shown explicitly the existence of four-equivalent sets for the PSG and PSA configurations for the complete determination of the MM of a given optical system [6]. As a matter of fact, there are an infinite number of four-sets for the PSG and for the PSA configurations that fulfills the condition they describe a regular tetrahedron inscribed into the Poincaré sphere, able to be used for the determination of the complete MM elements. It has been shown this number of measurements provides an optimized, stable result [4, 6-8].

In the following paragraphs we will present an explicit method for the experimental determination of the complete Mueller matrix of a given general system, employing a partial Stokes polarimeter analyzer.

The normalized Stokes vector is:

$$S^{PAX} = \begin{pmatrix} 1 \\ s'_1 \\ s'_2 \\ s'_3 \end{pmatrix} \tag{3.10}$$

It is considered as an "incomplete" polarimeter because the first element is not displayed explicitly by the automated system. In order to obtain the complete, un-normalized detected Stokes vector, it is necessary to multiply the four Stokes parameters for the total intensity present into each incident polarization state. From Eq. (3.7), the scattered Stokes vector incident onto the PSD is closely related to the incident Stokes vector on the sample. For the set of incident polarization states (i = p, s, +45, and r), the scattered Stokes vectors from the sample $s^{io}$ are expressed, respectively, as

$$S^{po} = \begin{pmatrix} m_{00}+m_{01} \\ m_{10}+m_{11} \\ m_{20}+m_{21} \\ m_{30}+m_{31} \end{pmatrix}, \quad S^{so} = \begin{pmatrix} m_{00}-m_{01} \\ m_{10}-m_{11} \\ m_{20}-m_{21} \\ m_{30}-m_{31} \end{pmatrix}, \quad S^{+o} = \begin{pmatrix} m_{00}+m_{02} \\ m_{10}+m_{12} \\ m_{20}+m_{22} \\ m_{30}+m_{32} \end{pmatrix}, \quad S^{ro} = \begin{pmatrix} m_{00}+m_{03} \\ m_{10}+m_{13} \\ m_{20}+m_{23} \\ m_{30}+m_{33} \end{pmatrix} \tag{3.11}$$

The "power" detected is given by the total intensity associated to each scattered Stokes vector, according to

$$s_0^{pd} = m_{00}+m_{01}, \quad s_0^{sd} = m_{00}-m_{01}, \quad s_0^{+d} = m_{00}+m_{02}, \quad s_0^{rd} = m_{00}+m_{03} \tag{3.12}$$

On the other hand, the detected normalized Stokes vectors ($S^{id}$) are displayed as

$$S^{pd}=\begin{pmatrix}1\\ s_1^{pd}\\ s_2^{pd}\\ s_3^{pd}\end{pmatrix}=\frac{1}{s_0^{pd}}\begin{pmatrix}m_{00}+m_{01}\\ m_{10}+m_{11}\\ m_{20}+m_{21}\\ m_{30}+m_{31}\end{pmatrix},\quad S^{sd}=\begin{pmatrix}1\\ s_1^{sd}\\ s_2^{sd}\\ s_3^{sd}\end{pmatrix}=\frac{1}{s_0^{sd}}\begin{pmatrix}m_{00}-m_{01}\\ m_{10}-m_{11}\\ m_{20}-m_{21}\\ m_{30}-m_{31}\end{pmatrix} \tag{3.13}$$

And

$$S^{+d}=\begin{pmatrix}1\\ s_1^{+d}\\ s_2^{+d}\\ s_3^{+d}\end{pmatrix}=\frac{1}{s_0^{+d}}\begin{pmatrix}m_{00}+m_{02}\\ m_{10}+m_{12}\\ m_{20}+m_{22}\\ m_{30}+m_{32}\end{pmatrix},\quad S^{rd}=\begin{pmatrix}1\\ s_1^{rd}\\ s_2^{rd}\\ s_3^{rd}\end{pmatrix}=\frac{1}{s_0^{rd}}\begin{pmatrix}m_{00}+m_{03}\\ m_{10}+m_{13}\\ m_{20}+m_{23}\\ m_{30}+m_{33}\end{pmatrix} \tag{3.14}$$

The 16 elements of the Mueller matrix are obtained from equation (3.12)

$$\begin{aligned}
&m_{00}=\frac{1}{2}\left(s_0^{pd}+s_0^{sd}\right),\ m_{01}=\frac{1}{2}\left(s_0^{pd}-s_0^{sd}\right),\ m_{02}=s_0^{+d}-m_{00},\ m_{03}=s_0^{rd}-m_{00}\\
&m_{10}=\frac{1}{2}\left(s_1^{pd}s_0^{pd}+s_1^{sd}s_0^{sd}\right),\ m_{11}=\frac{1}{2}\left(s_1^{pd}s_0^{pd}-s_1^{sd}s_0^{sd}\right),\ m_{12}=s_1^{+d}s_0^{+d}-m_{10},\ m_{13}=s_1^{rd}s_0^{rd}-m_{10}\\
&m_{20}=\frac{1}{2}\left(s_{21}^{pd}s_0^{pd}+s_2^{sd}s_0^{sd}\right),\ m_{21}=\frac{1}{2}\left(s_2^{pd}s_0^{pd}-s_2^{sd}s_0^{sd}\right),\ m_{22}=s_2^{+d}s_0^{+d}-m_{20},\ m_{23}=s_2^{rd}s_0^{rd}-m_{20}\\
&m_{30}=\frac{1}{2}\left(s_3^{pd}s_0^{pd}+s_3^{sd}s_0^{sd}\right),\ m_{31}=\frac{1}{2}\left(s_3^{pd}s_0^{pd}-s_3^{sd}s_0^{sd}\right),\ m_{32}=s_3^{+d}s_0^{+d}-m_{30},\ m_{33}=s_3^{rd}s_0^{rd}-m_{30}
\end{aligned} \tag{3.15}$$

## 3.4.2 Six-Mueller matrix method

The Mueller matrix elements were obtained now from a set of six incident Stokes vectors, where we have added the -45 degrees linear polarization and also the left-hand circular polarization state to the 4-incident polarization method. In practice, the method of 6-incident polarization states provides more stable, less noise, results than the 4-incident polarization states method [5, 7-8].

The incident and the output Stokes vectors correspond to linear polarization states parallel (p), perpendicular (s), to +45 degrees (+), and to -45 degrees (-) respect to the horizontal plane of the working optical table, respectively, and to a right-hand (r) and a left-hand

polarization state (l). The total intensity associated with each incident polarization state ($s^i$ is denoted as the "power" and is measured in dBm units.

For the set of incident polarization states (i = p, s, ±45, r, and l), the scattered Stokes vectors from the sample ($S^{io}$) are expressed, respectively, as

$$S^{po}=\begin{pmatrix} m_{00}+m_{01} \\ m_{10}+m_{11} \\ m_{20}+m_{21} \\ m_{30}+m_{31} \end{pmatrix},\quad S^{so}=\begin{pmatrix} m_{00}-m_{01} \\ m_{10}-m_{11} \\ m_{20}-m_{21} \\ m_{30}-m_{31} \end{pmatrix},\quad S^{+o}=\begin{pmatrix} m_{00}+m_{02} \\ m_{10}+m_{12} \\ m_{20}+m_{22} \\ m_{30}+m_{32} \end{pmatrix},\quad S^{-o}=\begin{pmatrix} m_{00}-m_{02} \\ m_{10}-m_{12} \\ m_{20}-m_{22} \\ m_{30}-m_{32} \end{pmatrix} \tag{3.16}$$

$$S^{ro}=\begin{pmatrix} m_{00}+m_{03} \\ m_{10}+m_{13} \\ m_{20}+m_{23} \\ m_{30}+m_{33} \end{pmatrix},\quad S^{lo}=\begin{pmatrix} m_{00}-m_{03} \\ m_{10}-m_{13} \\ m_{20}-m_{23} \\ m_{30}-m_{33} \end{pmatrix}$$

The "power" is given by the total intensity associated to each scattered Stokes vector, according to

$$s_0^{pd}=m_{00}+m_{01}, s_0^{sd}=m_{00}-m_{01}, s_0^{+d}=m_{00}+m_{02}, s_0^{-d}=m_{00}-m_{02}, s_0^{rd}=m_{00}+m_{03}, s_0^{rd}=m_{00}-m_{03} \tag{3.17}$$

On the other hand, the detected normalized Stokes vectors ($S^{id}$) are displayed as

$$S^{pd}=\begin{pmatrix} 1 \\ s_1^{pd} \\ s_2^{pd} \\ s_3^{pd} \end{pmatrix}=\frac{1}{s_0^{pd}}\begin{pmatrix} m_{00}+m_{01} \\ m_{10}+m_{11} \\ m_{20}+m_{21} \\ m_{30}+m_{31} \end{pmatrix},\quad S^{sd}=\begin{pmatrix} 1 \\ s_1^{sd} \\ s_2^{sd} \\ s_3^{sd} \end{pmatrix}=\frac{1}{s_0^{sd}}\begin{pmatrix} m_{00}-m_{01} \\ m_{10}-m_{11} \\ m_{20}-m_{21} \\ m_{30}-m_{31} \end{pmatrix}, \tag{3.18}$$

$$S^{+d}=\begin{pmatrix} 1 \\ s_1^{+d} \\ s_2^{+d} \\ s_3^{+d} \end{pmatrix}=\frac{1}{s_0^{+d}}\begin{pmatrix} m_{00}+m_{02} \\ m_{10}+m_{12} \\ m_{20}+m_{22} \\ m_{30}+m_{32} \end{pmatrix},\quad S^{-d}=\begin{pmatrix} 1 \\ s_1^{-d} \\ s_2^{-d} \\ s_3^{-d} \end{pmatrix}=\frac{1}{s_0^{-d}}\begin{pmatrix} m_{00}-m_{02} \\ m_{10}-m_{12} \\ m_{20}-m_{22} \\ m_{30}-m_{32} \end{pmatrix}, \tag{3.19}$$

and

$$S^{rd}=\begin{pmatrix} 1 \\ s_1^{rd} \\ s_2^{rd} \\ s_3^{rd} \end{pmatrix}=\frac{1}{s_0^{rd}}\begin{pmatrix} m_{00}+m_{03} \\ m_{10}+m_{13} \\ m_{20}+m_{23} \\ m_{30}+m_{33} \end{pmatrix},\quad S^{ld}=\begin{pmatrix} 1 \\ s_1^{ld} \\ s_2^{ld} \\ s_3^{ld} \end{pmatrix}=\frac{1}{s_0^{ld}}\begin{pmatrix} m_{00}-m_{03} \\ m_{10}-m_{13} \\ m_{20}-m_{23} \\ m_{30}-m_{33} \end{pmatrix} \tag{3.20}$$

The 16 elements of the Mueller matrix are obtained from equations (3.17)

$$
\begin{aligned}
&m_{00}=\frac{1}{2}\left(s_0^{pd}+s_0^{sd}\right),\ m_{01}=\frac{1}{2}\left(s_0^{pd}-s_0^{sd}\right),\ m_{02}=\frac{1}{2}\left(s_0^{+d}-s_0^{-d}\right),\ m_{03}=\frac{1}{2}\left(s_0^{rd}-s_0^{ld}\right)\\
&m_{10}=\frac{1}{2}\left(s_1^{pd}s_0^{pd}+s_1^{sd}s_0^{sd}\right),\ m_{11}=\frac{1}{2}\left(s_1^{pd}s_0^{pd}-s_1^{sd}s_0^{sd}\right),\ m_{12}=\frac{1}{2}\left(s_1^{+d}s_0^{+d}-s_1^{-d}s_0^{-d}\right),\ m_{13}=\frac{1}{2}\left(s_1^{rd}s_0^{rd}-s_1^{ld}s_0^{ld}\right)\\
&m_{20}=\frac{1}{2}\left(s_2^{pd}s_0^{pd}+s_2^{sd}s_0^{sd}\right),\ m_{21}=\frac{1}{2}\left(s_2^{pd}s_0^{pd}-s_2^{sd}s_0^{sd}\right),\ m_{22}=\frac{1}{2}\left(s_2^{+d}s_0^{+d}-s_2^{-d}s_0^{-d}\right),\ m_{23}=\frac{1}{2}\left(s_2^{rd}s_0^{rd}-s_2^{ld}s_0^{ld}\right)\\
&m_{30}=\frac{1}{2}\left(s_3^{pd}s_0^{pd}+s_3^{sd}s_0^{sd}\right),\ m_{31}=\frac{1}{2}\left(s_3^{pd}s_0^{pd}-s_3^{sd}s_0^{sd}\right),\ m_{32}=\frac{1}{2}\left(s_3^{+d}s_0^{+d}-s_3^{-d}s_0^{-d}\right),\ m_{33}=\frac{1}{2}\left(s_3^{rd}s_0^{rd}-s_3^{ld}s_0^{ld}\right)
\end{aligned}
\tag{3.21}
$$

The above development has been realized under the consideration that the experimental setup has been calibrated with respect to the incident intensity associated to each polarization state. This is an essential step, in order to assign a physical sense to the measured Mueller matrix. It means that in the absence of any polarization-sensitive effects in the optical medium placed between the PSG and the PSA, any polarization state detected corresponds to the same polarization state generated.

## 3.5 Depolarization scalar metrics

When the Mueller matrix has been obtained, it is convenient to analyze the polarimetric properties associated to the system under study. In this sense, a very important property associated to an optical system is its capability to depolarize light, which is measured by using some of the following depolarization scalar metrics. The depolarization index, DI(M), and its physical realizable limits are defined by [4-5, 8-17 ]:

$$
0 \le DI(M)=\left\{\sum_{j,k=0}^{3} m_{jk}^2 - m_{00}^2\right\}^{1/2} / \sqrt{3}m_{00} \le 1 \tag{3.22}
$$

DI(M) is directly related to the Mueller matrix elements only. This means this metric can be applied only to the Mueller matrix elements associated to the optical system under study and not to the outgoing beam of light emerging from the system under consideration.

The degree of polarization, DoP(M,S), and its physical realizable limits have been defined by [5, 8-9]:

$$0 \le DoP(M,S) = \frac{\sqrt{(s_1^o)^2 + (s_2^o)^2 + (s_3^o)^2}}{s_0^o} = \frac{\left[\sum_{j=1}^{3} (m_{j0}s_0^i + m_{j1}s_1^i + m_{j2}s_2^i + m_{j3}s_3^i)^2\right]^{\frac{1}{2}}}{m_{00}s_0^i + m_{01}s_1^i + m_{02}s_2^i + m_{03}s_3^i} \le 1 \tag{3.23}$$

DoP(M,S) is directly related to both, the Mueller matrix elements of the system under study and the incident Stokes vector. The DoP(M,S) usually is measured directly from the Stokes vector emerging of the system under study and the measured value is associated to the outgoing light; however, it is inherently related to the optical response of the system, as can be noted from Eq. (3.7).

The upper limit associated to both, DI(M) and DoP(M,S), means the optical system does not depolarize, the lower limit is associated to total depolarization, and the medium limits correspond to partial depolarization.

The anisotropic degree of depolarization, Add, is a relationship that gives insight into the isotropy or anisotropy depolarization capability of the medium. It has been defined by [6, 8]

$$0 \le Add = \frac{(DoP)_{Max}^o - (DoP)_{\min}^o}{(DoP)_{Max}^o + (DoP)_{\min}^o} \le 1 \tag{3.24}$$

where the lower limit, 0, is interpreted as the depolarization generated by the system under study is isotropic. The upper limit, 1, is associated to a medium totally anisotropic. The intermediate values are associated to a partially anisotropic medium.

The Diattenuation, D(M), and the Polarizance parameters, P(M), are respectively defined by [9]

$$0 \le D(M) = \sqrt{m_{01}^2 + m_{02}^2 + m_{03}^2} / m_{00} \le 1 \tag{3.25}$$

and

$$0 \le P(M) = \sqrt{m_{10}^2 + m_{20}^2 + m_{30}^2} / m_{00} \le 1 \tag{3.26}$$

By consider the decomposition of a Mueller matrix as a valuable complementary tool for characterizing the properties of systems, as well as the non-depolarizing properties of the media we can write the Diattenuation and the polarizance linear and circular parameters as [2]:

$$DL = \sqrt{m_{01}^2 + m_{02}^2} \Big/ m_{00} \qquad DC = \sqrt{m_{03}^2} \Big/ m_{00}$$
$$PC = \sqrt{m_{30}^2} \Big/ m_{00} \qquad PL = \sqrt{m_{10}^2 + m_{20}^2} \Big/ m_{00} \tag{3.27}$$

The diattenuation parameter is a measure of the absorption of light by the sample and the polarizance parameter is a measure of the capacity to polarize light by the sample.

The Q(M) metric and its physical realizable bounds are defined as [15,16]

$$0 \le Q(M) = \frac{\sum_{j=1,k=0}^{3} m_{jk}^2}{\sum_{k=0}^{3} m_{0k}^2} = \frac{3[DI(M)]^2 - [D(M)]^2}{1 + [D(M)]^2} = \frac{\left\{\sum_{j,k=1}^{3} m_{jk}^2\right\} / m_{00}^2 + [P(M)]^2}{1 + [D(M)]^2} \le 3 \tag{3.28}$$

Where $Q(M) = 0$ for a totally depolarizing optical system; $0 < Q(M) < 1$ for a partially depolarizing optical system; if $1 \le Q(M) < 3$ and $0 < DI(M) < 1$ the system partially depolarizes also, but if $DI(M) = 1$, it is a non-depolarizing diattenuating optical system; and $Q(M) = 3$ for a non-depolarizing non-diattenuating optical system, respectively [4, 8, 15-16].

There exists a common criterion to test when a Mueller matrix is derivable from a Jones matrix, named the theorem of Gil-Bernabeu [11]

$$Tr(M^t M) = 4m_{00}^2 \tag{3.29}$$

The physical meaning can be understood in this way: If a Mueller matrix fulfills the theorem, then it is associated to a non-depolarizing system; otherwise, it is associated to a depolarizing optical system. This criterion is valid for any passive optical system.

The polarization dependent loss, PDL, is the maximum change in transmission/reflection with respect to polarization states *x, y*. Many fiber-optic components, such as isolators, couplers, circulators, fiber gratings, exhibit PDL. The polarization dependent loss is defined in terms of the Mueller parameters, as [8].

$$PDL = 10\log(T\max/T\min) = 10\log\left[\frac{m_{00} + \left(m_{01}^2 + m_{02}^2 + m_{03}^2\right)^{1/2}}{m_{00} - \left(m_{01}^2 + m_{02}^2 + m_{03}^2\right)^{1/2}}\right] \tag{3.30}$$

where $T_{max}$ and $T_{min}$ are the maximum and the minimum values of the transmittance, respectively.

Another way to calculate the PDL is by using the Diattenuation as follow:

$$PDL = 10\log(T\max/T\min) = 10\log\left[\frac{1+D(M)}{1-D(M)}\right] \tag{3.31}$$

PDL is a random phenomenon and their value has a statistical distribution depend upon wavelength and the environment (temperature, vibration, etc.). Therefore, the characterization and the measurement of PDL in optical fiber and fiber optic devices are very important for optical fiber systems design and evaluation.

## References

1. S. Yin, P. B. Ruffin, F. T. S. Yu, "Fiber Optic Sensors," 2nd ed., Taylor and Francis Group, Rochester New York.

2. M. Born, E. Wolf, "Principles of Optics, " 7th ed., Cambridge University Press.

3. Edward Collett, " Polarized Light: Fundamentals and Applications, " Dekker, 1992.

4. R. Espinosa-Luna, G. Atondo-Rubio, and A. Mendoza-Suarez, "Complete determination of the conical Mueller matrix for one-dimensional rough metallic surfaces," Opt. Commun. **257**(1)2006.

5. K. M. Salas-Alcántara, R. Espinosa-Luna, and I. Torres-Gómez, "Polarimetric Mueller-Stokes analysis of photonic crystal fibers with mechanically induced long-period gratings," Opt. Eng. **51(**085005)2012.

6. G. Atondo-Rubio, R. Espinosa-Luna, and A. Mendoza-Suárez, "Mueller matrix determination for one-dimensional rough surface with a reduced number of measurements," Opt. Commun. **244**(1-6)2005.

7. J. S. Tyo, "Design of optimal polarimeters: maximization of signal-to-noise ratio and minimization of systematic error," Appl. Opt. **41**(4)2002.

8. K. M. Salas-Alcántara, R. Espinosa-Luna, and I. Torres-Gómez, Yuri O. Barmenkov, "Determination of the Mueller matrix of UV-inscribed long-period fiber grating, " Appl. Opt. **53**(2)2014.

9. R. Espinosa-Luna, G. Atondo-Rubio, E. Bernabeu, and S. Hinojosa-Ruíz, "Dealing depolarization of light in Mueller matrices with scalar metrics," Optik **121**(12)2010.

10. J.J. Gil, E. Bernabeu, "A depolarization criterion in Mueller matrices," Opt. Acta, **32**(3)1985.

11. J.J. Gil, E. Bernabeu, "Obtainment of the polarizing and retardation parameters of a nondepolarizing optical system from the polar decomposition of its Mueller matrices," Optik, **76**(2)1987

12. S.Y. Lu, R. A. Chipman, "Mueller matrices and the degree of polarization, " Opt. Commun. **146**(1-6)1998

13. B. DeBoo, J. Sasian, R. Chipman, "Degree of polarization surfaces and maps for analysis of depolarization, " Opt. Express, **12**(20)2004

14. R. Chipman, “Depolarization index and the average degree of polarization,” Appl. Opt. **44**(13)2005.

15. R. Espinosa-Luna, E. Bernabeu, “On the Q(M) depolarization metric,” Opt. Commun., **277**(2)2007

16. R. Espinosa-Luna, E. Bernabeu, G. Atondo-Rubio, “Q(M) and the depolarization index scalar metrics, ” Appl. Opt., **47**(10)2008.

17. J.J. Gil, “Polarimetric characterization of light and media,” Eur. Phys. J. Appl. Phys. **40**(1)2007.

# 4 Polarimetric characterization of long-period fiber gratings.

One of our main interests in this thesis work is just to know the behavior of fiber optics devices to polarized light. In this chapter, we focus our attention to a Mueller-Stokes analysis of the polarization characteristics of both mechanical and ultra-violet long-period fiber gratings. Some scalar depolarization metrics are applied for the determination of the diattenuation (absorption), PDL, gain, attenuation, depolarization degree of anisotropy, among others important parameters. The Mueller matrix (MM) is determined through the Stokes vectors, which are measured using an incomplete, commercial, Stokes polarimeter.

## 4.1 Mueller Matrix of the mechanically induced long-period fiber grating

The Four-incident polarization states method has been used for the determination of the MM associated to a mechanically induced long-period fiber grating (M-LPFG) in a photonic crystal fiber, in an open space measurement [1-2]. Results show an increasing in the birefringence when the LPFG is present in the fiber. The PDL values of the UV-LPFG are intrinsically high in comparison to the grating produced by ultraviolet induced technique.

### 4.1.1 Experiments and results

To show the quality of the polarization states generated and detected by the polarimetric system, the equipment was self-calibrated with respect to the air where we have obtained the following numerical results for the Four-incident polarization states method, explained in Chapter two.

$$\begin{aligned} s_0^{pdf} &= -19.7\ dBm = 10.71\ \mu W; \quad s_0^{sdf} = -19.8\ dBm = 10.47\ \mu W; \\ s_0^{+45df} &= -19.6\ dBm = 10.96\ \mu W; \quad s_0^{rdf} = -19.8\ dBm = 10.47\ \mu W. \end{aligned} \tag{4.1}$$

Observe the power measurements are very similar (ideally they should have the same value for any incident polarization state), where a He-Ne un-polarized laser has been used as the source (emitting at 632.8 nm) and the PSG consists of a linear polarizer of the Glan-Thompson type and a liquid crystal variable retarder (LCVR) [3], see Figure 4.1.

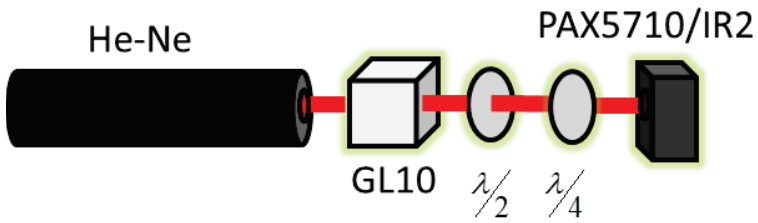


**Figure 4.1.** Setup employed for the complete determination of the Mueller-Matrix for the air.

The normalized experimental Mueller matrix for the air, at room temperature, is given by

$$M_{air} = \begin{bmatrix} 1.00 & 0.00 & 0.00 & 0.00 \\ 0.00 & 1.00 & 0.00 & 0.00 \\ 0.00 & 0.00 & 1.00 & 0.00 \\ 0.00 & 0.00 & 0.00 & 0.99 \end{bmatrix} \tag{4.2}$$

The wavelength employed here is to show the capacity of the experimental arrangement to generate and to detect polarization states of high quality, which are easier to handle in the visible than in the infrared spectral region. We have obtained an eccentricity of 0.99 for the right-hand circular polarization state, which is greater than the usually obtained in practice [2]. The deviation from the ideal eccentricity (1.00) is due to the lack of control to generate and to detect circular polarization (here we are considering the eccentricity as the ratio of the minor to the major axis of the polarization ellipse). This experimental condition can be easily identified within the $m_{00}$ value, when the system under study is the air.

Figure 4.2 shows the results obtained for the gain (employing un-normalized Mueller matrix elements), the degree of polarization, the Poincaré output sphere, and the attenuation, when the system under study is the air.

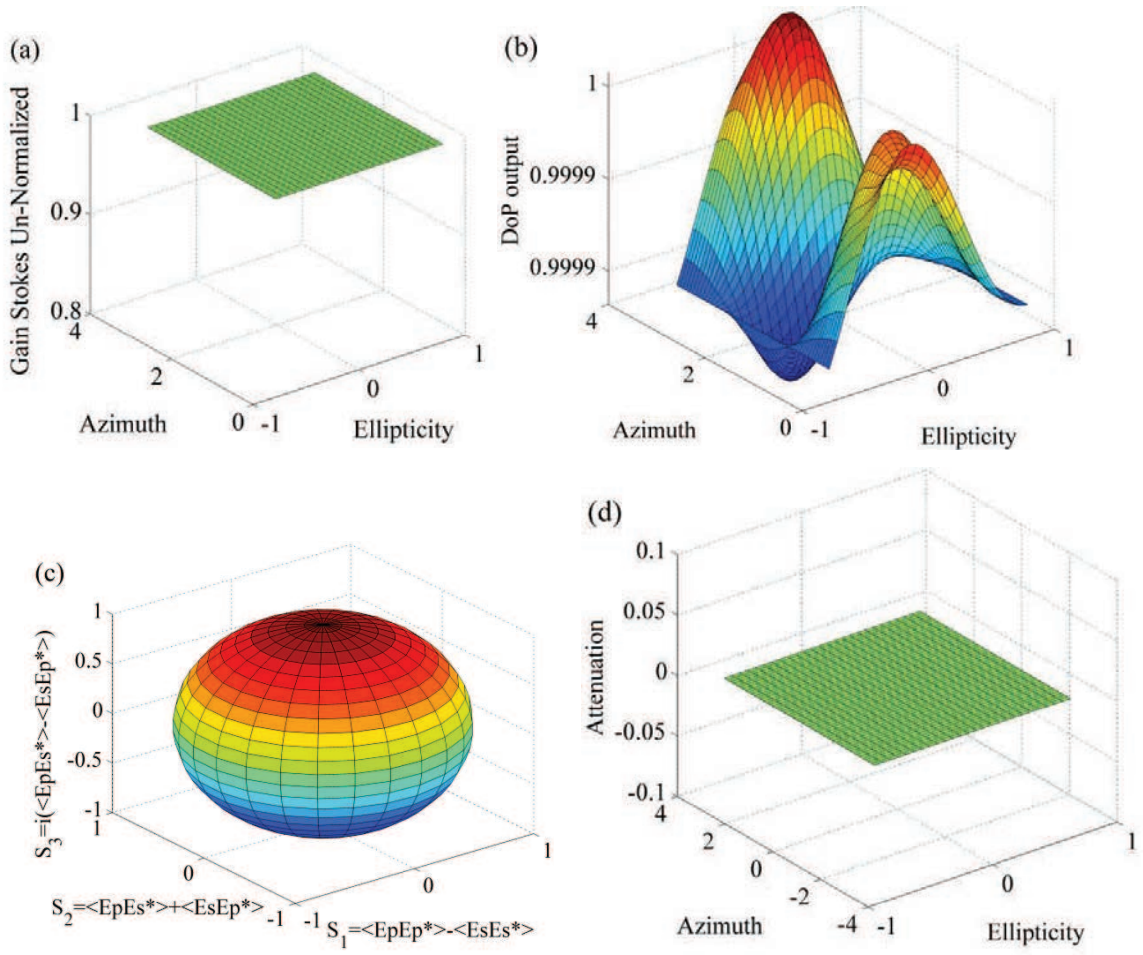


**Figure 4.2.** Results obtained for a) the gain (employing un-normalized Mueller matrix elements), b) the degree of polarization (DoP), c) the Poincaré output sphere, and d) the attenuation, when the system under study is the air.

The gain has the unitary value for all the incident polarization states, according to Figure 4.2(a). The output degree of polarization is close to one, for any incident polarization state (Figure. 4.2(b)). The anisotropic degree of depolarization has a value of 0.0039, instead of 0.0000 (the air is an isotropic non-depolarizing medium at short distances). This deviation is a consequence of the instrumentation restrictions present in the generation and detection employed here (we could not get a better condition). As a consequence, the lack of perfect control on the generation and the detection of polarization states also affect the both DoP output and the Poincaré output

response Figure 4.2(b) and Figure 4.2(c) respectively. The Poincaré output sphere maps almost identically the polarization states taken from the unitary Poincaré input sphere, Figure 4.2(c). Observe that our measurements are within the accuracy and resolution parameters provided by the manufacturer of the equipment (see the PAX manual).

To characterize the polarization response of the long-period fiber grating, it was necessary to analyze the photonic crystal fiber (PCF) first. We have used the experimental setup depicted schematically in Figure 4.3. It consists of a partial Stokes polarimeter analyzer (Thorlabs, model PAX5710/IR2) and an infrared source (Ytterbium Doped Fiber Laser with CW at 1064 nm, from IPG Photonics, PYL-10LP). This laser illuminates the polarizer state generator, PSG, which consists of a linear polarizer of the Glan-Laser type whit high polarization purity and an extinction ratio of 100000:1 (Thorlabs, model GL10), a half-wave plate (Thorlabs, WPMH05M-1064), and a quarter-wave plate (Thorlabs, WPMQ05M-1064). The polarizer is used to obtain a linear polarization with a great extinction rate at the output source (the source provides a 30:1 extinction ratio, a truly poor quality for our requirements). The half-wave plate acts as a rotator for the linear polarization (when the fast axis of the plate is set to an angle $\theta$ with respect to the linear polarization plane, generates a $2\theta$ rotated linear polarization). The quarter-wave plate transforms the linear polarization into right-hand circular polarization when the fast axis of the plate is set to +45° with respect to the linear polarization plane. A couple of microscope objectives of numerical aperture 0.65 and focal length 4.48 mm are employed to concentrate the light from the PSG into the PCF (a distance of 10 cm separates one microscope objective from the other).

The PCF is a commercial photonic crystal fiber F-SM10 that has a core/cladding diameter of 10/125 μm, with a 3.4 μm hole diameter and lattice pitch of 6.8 μm, and shows an almost perfect hexagonal arrangement of holes without asymmetry in its cladding structure (Figure 4.4). The PCF is connected directly to the polarizer state analyzer, PSA (Thorlabs Polarimeter, PAX5710/IR2) and the measurements are taken for the 4-incident polarization states p, s, +45 , r. For each polarization state generated, the polarimeter analyzes the outgoing Stokes vector from the PCF.

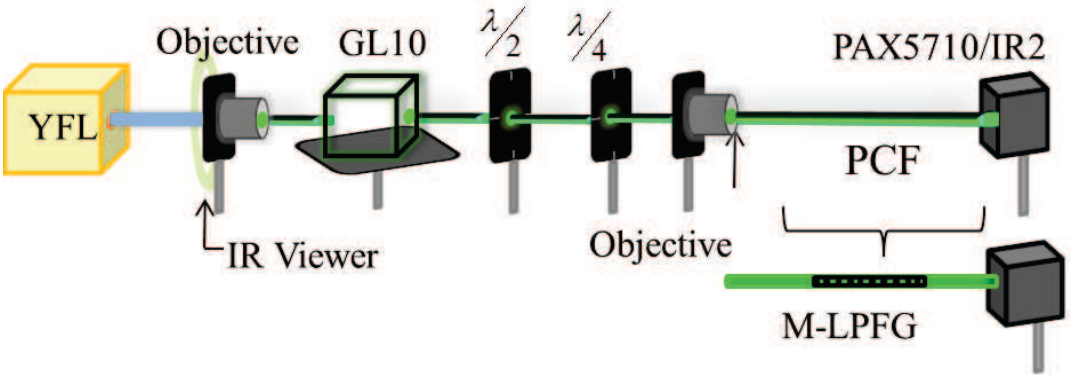


**Figure 4.3.** Experimental setup employed for the determination of the Mueller matrix associated to a Photonic Crystal Fiber and to a Photonic Crystal Fiber with a Mechanically-Induced Long-Period Fiber Grating, respectively.

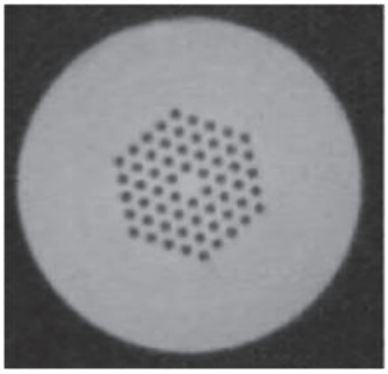

**Figure 4.4.** Cross sectional view of the F-SM10.

The experimental configuration shown in Figure (4.3) also was used to characterize de long-period fiber grating. The Mechanically-Induced LPFG was generated by pressing a section of the Photonic Crystal Fiber, between two corrugated grooved plates (CGPs). The dimensions of both grooved plates were 70 mm long and 24 mm wide, and each one had a square groove pattern with 480 μm of period. The PCF was placed between the CGP by a fixed and rotational holder. Figure 5 shows the transmission wavelength response of the M-LPFG.

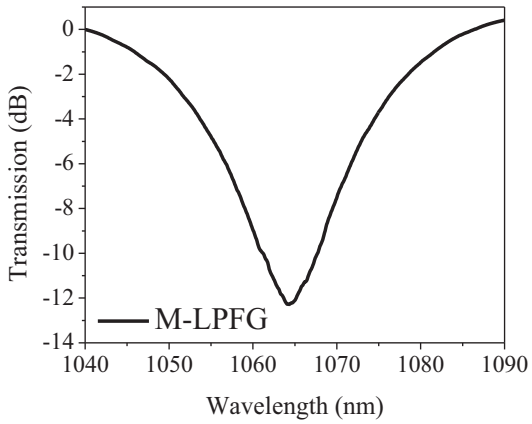


**Figure 4.5.** Transmission wavelength response of M-LPFG.

The experimental setup of Fig. 4.3 has also been self-calibrated, where an azimuth angle of -18 degrees for the setup of the polarimeter has been used. Figure 6 shows the results obtained for the gain (output energy/input energy), the degree of polarization, and the Poincaré output sphere, when the system under study is the PCF.

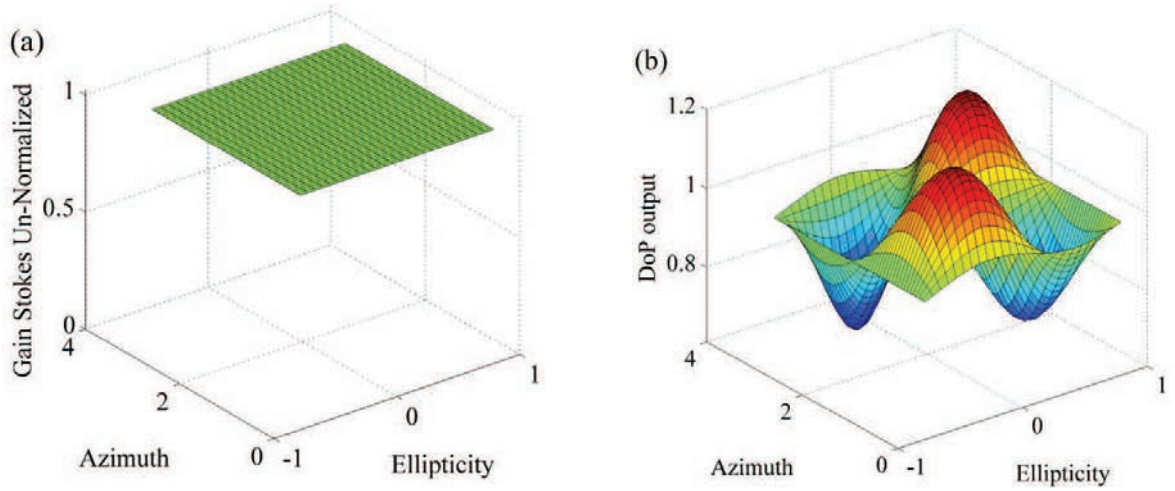

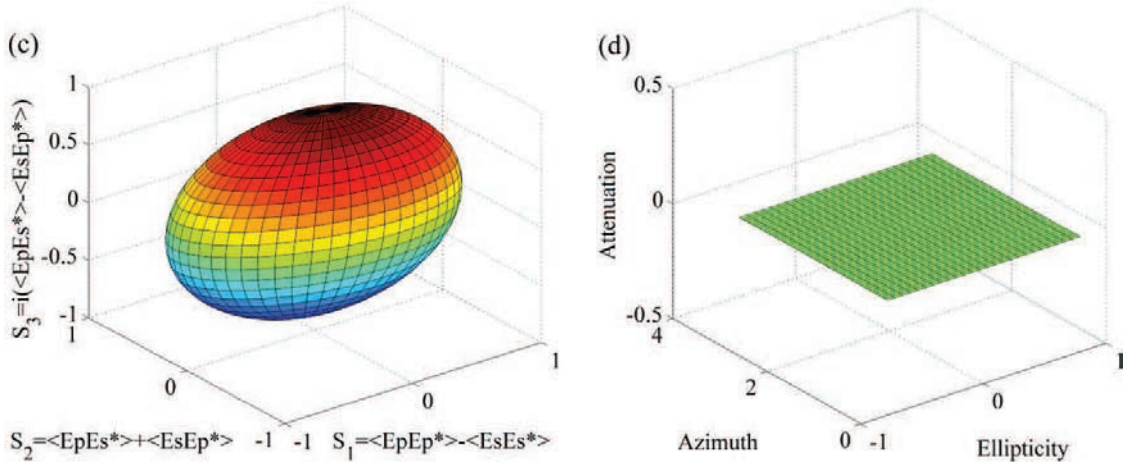


**Figure 4.6.** Analysis of the Mueller matrix associated to the PCF. Figures a) show the gain, b) the output degree of polarization, and c) the Poincaré output sphere.

## 4.1.2 Discussion

The gain has the unitary value for all the incident polarization states, according to Figure 4.6(a). The output degree of polarization varies around the unitary value and the PCF has a strongly dependence on the input polarization states (Fig. 4.6(b)). The anisotropic degree of depolarization provides a value of 0.1718. This value is two-orders of magnitude greater than the condition for the illumination under a free space setup (and for another incident wavelength). We believe this value reflects an intrinsic anisotropic depolarization behavior associated to the PCF, which cannot be identified if only the orthogonal polarizations p and s are used. Finally, the Poincaré output sphere suffers a slightly deformation with respect to the spherically symmetric Poincaré sphere associated to the input polarization states.

The normalized Mueller matrix obtained for the PCF, is given by

$$M_{PCF} = \begin{bmatrix} 1.0000 & 0.0000 & 0.0000 & 0.0000 \\ 0.0014 & 0.9970 & 0.2206 & -0.1641 \\ 0.0128 & -0.0669 & 0.9183 & -0.1641 \\ 0.0220 & -0.0250 & -0.3109 & 0.9651 \end{bmatrix} \tag{4.3}$$

Where, one can observe the main diagonal Mueller parameters are close to the unitary value, which indicates a tendency to maintain the incident polarization states. The first row indicates there is not diattenuation. However, the presence of non-zero values on the upper and the lower side of the main diagonal indicates the presence of phase retardation and depolarization effects also. The depolarization of light by an optical system is generally due to selective absorption or correlation of pure states related to the sample. This information could not be obtained if only the p- and the s-polarization states were employed.

We have measured the polarimetric response of a PCF when a long-period fiber, has been formed by the Mechanical-Induced Pressure Method. The results obtained are shown in Figure 4.7 where, we can observe that the gain, Figure 4.7(a), and the DoP, Figure 4.7(b), have some kind of anisotropy-behavior dependent on the ellipticity angular values of the incident polarization states. This behavior can be understood if the anisotropic degree of depolarization, can be associated to a partially anisotropic depolarizing medium (i.e., some incident pure states, are more affected than others). In this case, the Mueller matrix provides a value of 0.1751 for this parameter. The Add value increases with the presence of the LPFG on the PCF, which means the system becomes more anisotropic as depolarizer. On the other hand, the Poincaré output sphere has not a spherical symmetry, which can be interpreted as a depolarization effect due to the presence of the LPFG on the PCF (Figure 4.7(c)). Observe that the poles rotate; this behavior is interpreted as an increasing in the birefringence associated to the M-LPFG.

The normalized Mueller matrix obtained for the PCF with LPFG, is given by

$$M_{PCF+LPG} = \begin{bmatrix} 1.0000 & 0.0187 & -0.2004 & -0.3463 \\ -0.0812 & -0.3471 & 0.5622 & -0.4761 \\ -0.0070 & 0.4730 & 0.5138 & 0.0762 \\ -0.0077 & 0.8056 & -0.3759 & -0.3266 \end{bmatrix} \tag{4.4}$$

The form of this matrix suggests effects clearly associated to the presence of the induced LPFG. One evident effect is the presence of diattenuation (first row) and a marked depolarization effect (main diagonal values). In this case there is an increase of phase retardation and depolarization

effects also, according to the values shown in the upper and the lower diagonal parts of the Mueller matrix given by Eq. (4.4).

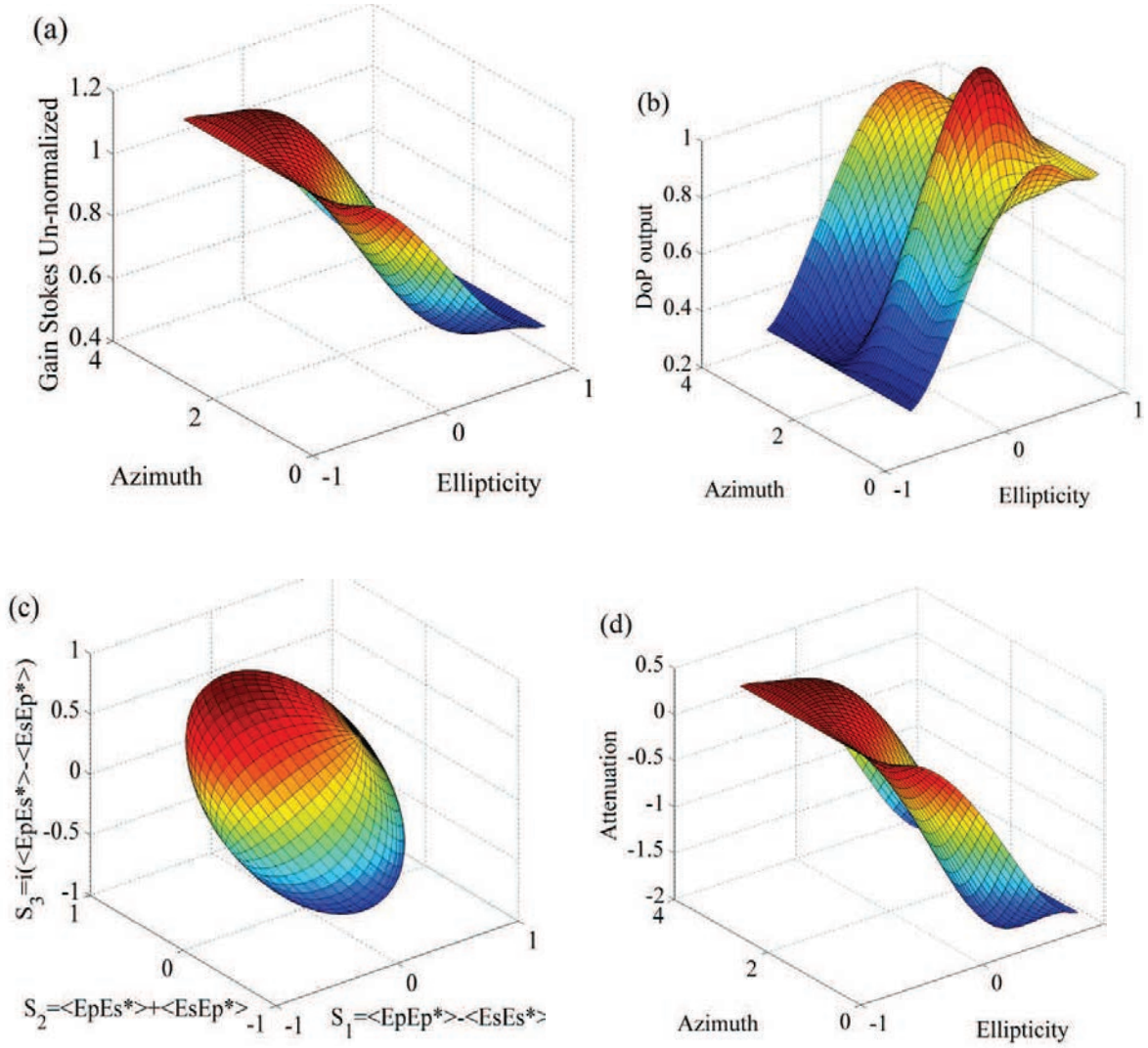


**Figure 4.7**. Analysis of the Mueller matrix associated to the PCF with the M-LPFG. Figures a) show the Gain, b) the output degree of polarization, c) the Poincaré output sphere and, (d) the attenuation.

Comparing the Figures 4.6 and 4.7, some considerable differences are found between them. These differences are mainly due to the presence of the LPFG in the PCF. With the LPFG, the gain (Figures 4.6(a) and 4.7(a)) depends strongly on the polarization state incident in the optical fiber. On the other hand, the output degree of polarization (Figures 4.6(b) and 4.7(b)) shows a tendency to polarize light linearly and to depolarize with the presence of the LFPG; however, the

un-perturbed PCF exhibits an intrinsic tendency to slightly depolarize the transmitted light. Finally, the Poincaré output sphere (Figures 4.6(c) and 4.7(c)) confirms the previous arguments: a reduction of the unitary radius is associated to isotropic depolarization effects, and a deviation of the spherical shape is associated to an anisotropic degree of depolarization, and the rotation of the axis is associated to the presence of birefringence. These effects increase with the presence of the LPFG in the photonic crystal fiber.

Additional information about the behavior of the PCF with and without a LPFG can be obtained from the polarimetric data. The PCF is a self-calibration, see Table 4.1.

**Tabla 4.1**. Polarimetric data obtained from the Mueller matrix associated to the PCF and to the PCF+M-LPFG.[1]

| | **D(M)** | **P(M)** | **DI(M)** | **Q(M)** | **$Tr(M^TM)/4(m_{00})^2$** | **PDL(dB)** | **Add** |
|---|---|---|---|---|---|---|---|
| **PCF** | 0.0000 | 0.0255 | 0.9914 | 2.9489 | 0.9872 | 0.0000 | 0.1718 |
| **PCF+LPFG** | 0.4006 | 0.0818 | 0.8604 | 1.7755 | 0.8052 | 8.4864 | 0.1751 |

From Table 4.1, the following information can be deduced. The diattenuation parameter, D(M), that indicates the LPFG generates a diattenuation effect, not present without the induced grating (which is used here as the reference). In this sense the polarizance, P(M), increases 320% with the presence of the LPFG. This behavior can be understood as follows: The period of the LPFG induced in the PCF has been designed to show resonance at the wavelength employed (1064 nm). In this way, the transmission is reduced because the resonance occurs; that is, the diattenuation (absorption) is increased. The LPFG affects the response to the transmitting polarization also. We can observe that transmitting an un-polarized state reaches a great output degree of polarization when the LPFG is present in the PCF. This means the polarizance parameter value increases. The physical mechanism responsible of this behavior must be associated to a dichroic, highly birefringent behavior due to the LPFG induced. The depolarization index, DI(M), the Q(M) depolarization scalar metric, and the theorem of Gil-

Bernabeu, all of them provide consistent results that indicate the presence of the LPFG increases in a 15% the effect of depolarization. These numerical results are coherent with the qualitative behavior presented with the deformation spherical shape of the Poincaré output sphere, Figure 7(c). We can also observe that the PDL parameter value just indicates that the PCF is affected by the presence of the LPFG. Even more when the response to each of the four polarization incident states generates a high degree of polarization output states (see Table 4.1), the arithmetic average behavior shows a tendency to a loss of the DoP for any PSG when the LPFG is on the PCF.

## 4.1.3 Conclusions

The Four-incident polarization states method has been used for the determination of the Mueller matrix associated to a photonic crystal fiber (PCF) with and without a long-period grating (LPFG). Results show the diattenuation, D(M), and the polarizance parameters, P(M), increases greatly with the Mechanically-Induced Long-Period Fiber Grating present in the PCF. The depolarization index, DI(M), the Q(M) depolarization scalar metric, the theorem of Gil-Bernabeu, the degree of polarization, DoP, and the anisotropic depolarization degree, Add, provide consistent results that indicate the existence and the increasing of depolarization effects due to the presence of the LPFG in the PCF. Finally, the polarization dependent loss, PDL, also increases for the PCF with the MLPFG. It should be noted that the method employed here to determine the scalar depolarization metrics provides more accurate information than the usually reported similar experimental works where only two orthogonal linear polarizations are used [5-6]. The basic difference is provided just by the phase difference between the two orthogonal linear polarizations, which contains additional information. One important result we have found here is just that the PCF we have employed has an intrinsic anisotropic degree of depolarization.
It is very hard to obtain experimentally a perfect generation and analysis of the polarization states, mainly for circular polarization. This is the fundamental reason why the output degree of polarization is slightly up to its physical limit. However, the results we reported here are as close as possible within the precision values considered by the manufacturer of our equipment.

## 4.2 Mueller Matrix of the UV long-period fiber grating for the Four-incident polarization states method

In Section 3.1.1, the Mueller matrix for a mechanically induced long-period grating was showed. Now, the Four-incident polarization states method has been used for the determination of the Mueller matrix and the polarimetric characterization associated to the long-period fiber grating (UV-LPFG) in a $H_2$ pre-loading fiber.

### 4.2.1 Experiment and results

In order to determine the Mueller matrix of the ultraviolet long-period fiber grating (UV-LPFG), the setup shown in Figure 4.8 was used [6]. The light source is a semiconductor laser tunable within 1450-1590 nm range (Anritsu, Tunics Plus SC). This laser is connected to a Deterministic Polarization Controller (Thorlabs, model DPC5500) input. The output signal from the DPC is used as a PSG for the fiber under study, which is connected directly to the polarizer state analyzer PSA (Thorlabs, model PAX5710/IR3) and the measurements are taken for the four incident polarization states p, s, +45, and r, respectively. A computer controls the PSG and the PSA, and a computer program provides the results obtained. For each polarization state generated, the polarimeter analyzes the Stokes vector of the light beam leaving the system under study.

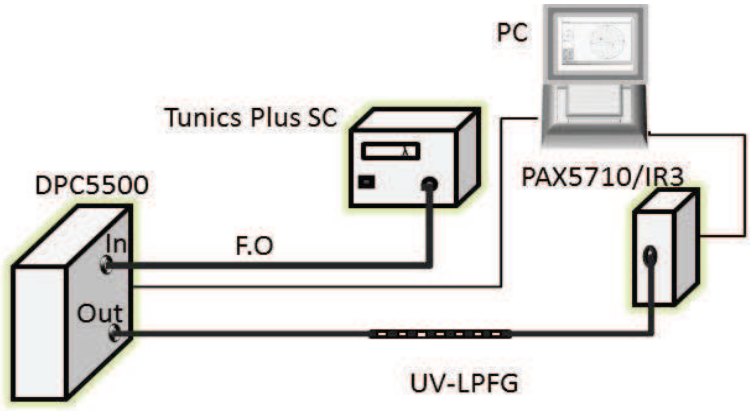


**Figure 4.8.** Experimental setup applied for the determination of the Mueller matrix associated to a UV-LPFG.

Figure 4.9 shows the transmission spectra of the UV-LPFG, and it has a transmission wavelength response centered at 1543 nm. The grating was manufactured by O/E Land Inc., model OEFBG-100. The UV-LPFG transmission spectra have been measured using an un-polarized source (white-light source AQ4305) and an optical spectrum analyzer (AQ6315A) with a wavelength resolution of 2 nm.

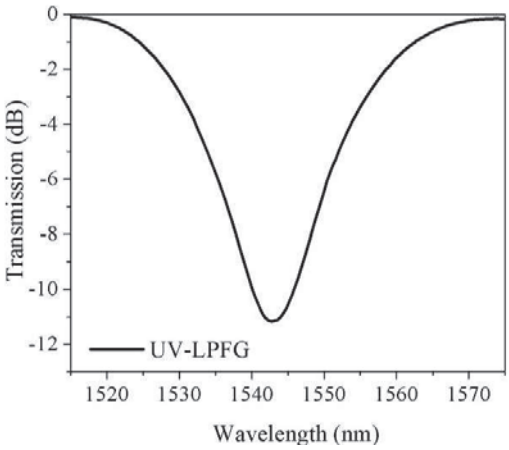


**Figure 4.9.** Transmission wavelength response of the UV-LPFG fiber under study, the resonance is centered at 1543 nm.

For the analysis of the polarimetric properties, the Mueller matrix of the fiber with and without the UV-LPFG at the main resonance (1543 nm) was determinate. The normalized Mueller matrix obtained for the fiber without grating, at 1543 nm, is given by

$$M_{Fiber} = \begin{bmatrix} 1.0000 & 0.0000 & 0.0000 & 0.0000 \\ 0.0166 & 0.4351 & -0.7746 & 0.4540 \\ -0.0483 & 0.1339 & -0.4294 & -0.8235 \\ -0.0007 & 0.8884 & 0.4444 & -0.1343 \end{bmatrix} \tag{4.5}$$

One can obtain some insight about the polarimetric characteristics of a given system, by analyzing the form of its associated Mueller matrix. The form of this matrix, Eq. (4.5), suggests a depolarization effect (the presence of non-zero values on the upper and the lower side of the main diagonal) and phase retardation also. It should be noted that this information could not be obtained if only the p- and the s-polarization states were employed as the incident Stokes states.

To show the general potential from the MM obtained, Eq. (4.5), the polarimetric response for some characteristic parameters (Table 4.2 and Figure 4.10) has been calculated. The gain has the unitary value for all the incident polarization states, according to Figure 4.10(a). The degree of polarization DoP, Figure 4.10(b), has some kind of anisotropy behavior dependent of the incident polarization states. The deterioration mechanism in the polarization degree is based on the assumption that an arbitrary incident polarized light is split into two separate eigen-polarization modes, which propagate at different group velocity values. Calculating the anisotropic degree of depolarization, a value of 0.022 is obtained. The Poincaré output response, Figure 4.10(c), has not a spherical symmetry, which can be interpreted as the presence of depolarization effects due to the reduction of the degree of polarization of light at the propagation through the optical fiber. As a consequence of the birefringence, due to possible deviations of the core from the circular cross section, as well as transverse stress, the poles of the sphere rotate.

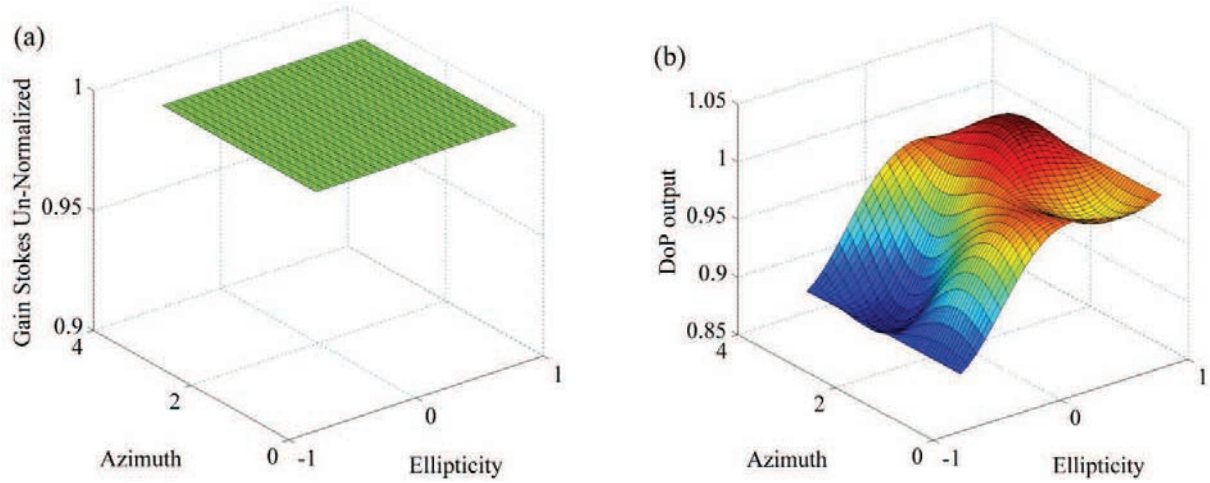

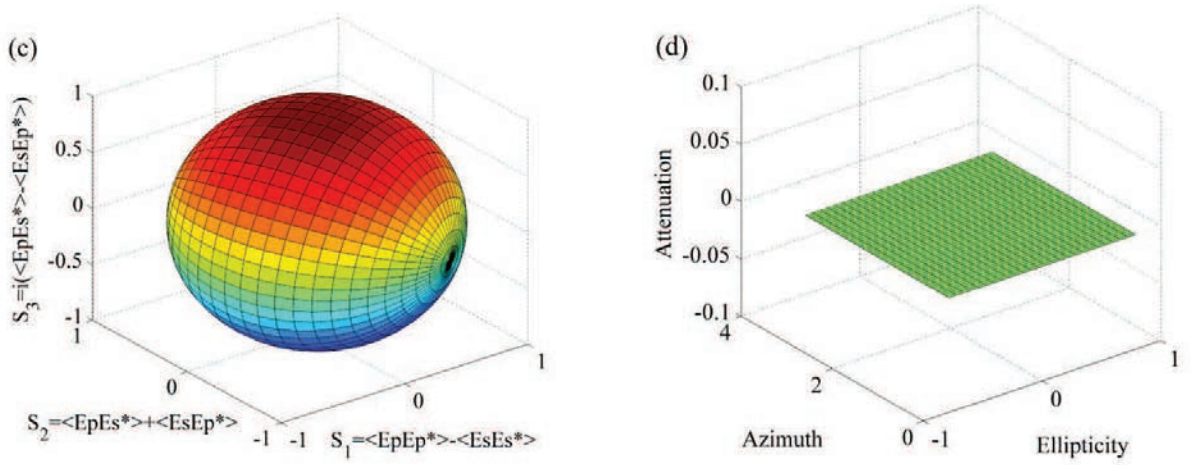


**Figure 4.10.** Mueller matrix associated to the fiber studied here at 1543 nm with (a) un-normalized gain, (b) output degree of polarization, (c) the Poincaré output sphere, and (d) attenuation.

In order to investigate the influence of UV-LPFG on the fiber, at 1543 nm, the corresponding (normalized) Mueller matrix obtained is given by

$$M_{LPFG_{1543}} = \begin{bmatrix} 1.0000 & 0.0023 & -0.0069 & -0.0067 \\ 0.0331 & 0.1139 & 0.3532 & -0.8735 \\ 0.0421 & -0.2451 & 0.8472 & 0.3487 \\ 0.0092 & 0.9611 & 0.2047 & 0.0971 \end{bmatrix} \tag{4.6}$$

The form of this matrix, suggests the presence of diattenuation effects, polarizance and a marked depolarization effect that can be attributed to the presence of UV-LPFG in the fiber (the exposure of the fiber to the UV beam creates an index change in the core). The grating coupling strength occurs at 1543 nm for un-polarized broadband white light source. In this way, the transmission is reduced; that is, the diattenuation increases also. The results obtained are shown in Figure 4.11 and Table 4.2.

According to Figure 4.11(a), the gain depends strongly of the polarization state incident in the optical fiber (basal plane indicates all the possible incident polarization states from the Poincaré sphere); the variation is due to the intrinsic birefringence of the fiber. On the other hand, the output degree of polarization, Figure 4.11(b), shows a tendency to polarize light linearly and to

depolarize slightly for some incident polarization states. The Poincaré sphere representation of the output polarization states, Figure 4.11(c), confirms the presence of depolarization effects and an increase of birefringence induced in the fiber core due to the UV radiation exposure. The attenuation, Figure 4.11(d), shows a strong dependence of the polarization state incident in the optical fiber, which is caused because the transmission is reduced due to the presence of the UV-LPFG.

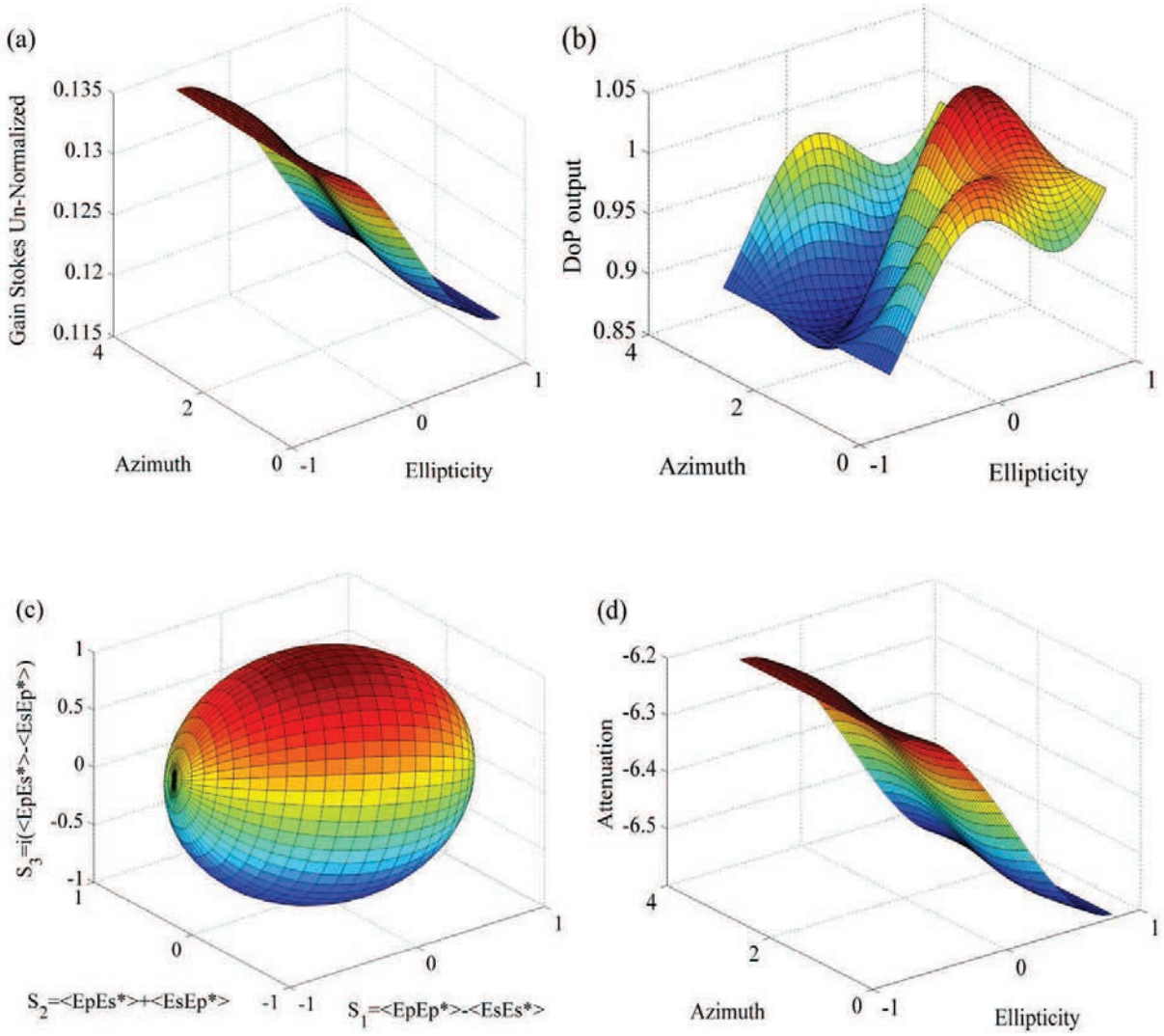


**Figure 4.11.** Mueller matrix associated with the UV-LPFG with (a) un-normalized gain, (b) the output degree of polarization, (c) the Poincaré output sphere, (d) the attenuation.

Additional information about the behavior of the fiber, with and without an ultraviolet long-period fiber grating, can be obtained from the polarimetric data (Table 4.2).

**Table 4.2.** Polarimetric data obtained from the Mueller matrix associated to the fiber without and with UV-LPFG.

| | D(M) | P(M) | DI(M) | Q(M) | Tr | PDL | Add |
|---|---|---|---|---|---|---|---|
| **Fiber** | 0.0000 | 0.0511 | 0.9804 | 2.8834 | 0.9709 | 0.0000 | 0.0222 |
| **UV-LPFG** | 0.0671 | 0.0543 | 0.9631 | 2.7658 | 0.9547 | 1.3449 | 0.0574 |

## 4.2.2 Discussion

From previous results (Table 4.2), one can build the following information: The diattenuation parameter, D(M), indicates the UV-LPFG generates a diattenuation effect, not present without the induced grating. In this sense the diattenuation, D(M), increases greatly with the presence of the UV-LPFG. This behavior can be understood as follows: The period of the LPFG shows a resonance wavelength at 1543 nm. In this way, the transmission is reduced because the resonance occurs; that is, the diattenuation is increased. The LPFG affects the response to the transmitting polarization also. The physical mechanism responsible of this behavior must be associated to a dichroic, highly birefringent change in the core due to the UV-LPFG. The depolarization index, DI(M), the Q(M) depolarization scalar metric, and the theorem of Gil-Bernabeu, all of them provide consistent results that indicate effect of depolarization. We can also observe that the PDL parameter value just indicates that the fiber is affected by the presence of the UV-LPFG as a consequence of the birefringence present in the grating structure. The PDL values are intrinsically low in comparison to gratings produced by other techniques used to fabricate them like through mechanical stress [5, 7-8], electric arc discharges, gratings produced by $CO_2$ laser radiation, among others. Even more when the response to each of the four polarization incident states generates a high degree of polarization output states (see Table 4.2), the arithmetic average behavior shows a tendency to a loss of the DoP for any PSG when the UV-LPFG is on the fiber.

### 4.2.3 Conclusions

The Four-incident polarization states method has been used for the determination of the Mueller matrix associated to UV induced long-period fiber gratings. Because the performance of the optical fiber is directly related to its polarization properties, the depolarization index, DI(M), the Q(M) depolarization scalar metric, the theorem of Gil-Bernabeu, the degree of polarization, DoP, and the anisotropic depolarization degree, Add was calculated. These depolarization scalar metrics provide consistent results that indicate an increasing in the birefringence when the LPFG is presented in the fiber. The PDL values of the UV-LPFG are intrinsically low in comparison to gratings produced by the mechanically induced technique.

## 4.3 Mueller Matrix of the UV long-period fiber grating for the Six-incident polarization states method.

In the following section a description of the full determination of the Mueller matrix associated to a commercial ultraviolet long-period fiber grating (UV-LPFG) is presented. The Mueller matrix elements were obtained now from a set of six incident Stokes vectors, where we have added the -45 degrees linear polarization and also the left-hand circular polarization state to the 4-incident polarization method [2-3]. In practice, we have found the method of Six-incident polarization states provides more stable, less noise, results than the Four-incident polarization states method.

### 4.3.1 Experiments and results

For the measurements of polarization properties of the ultraviolet long-period fiber grating, the same experimental setup sketched in Figure 4.8 was used. In order to obtain the UV-LPFG response and make an analysis of its polarimetric properties, the Mueller matrix of the fiber with and without the grating at two symmetrically-spaced wavelengths around 1543 nm was determined. The normalized Mueller matrix obtained for the fiber without grating, at 1543 nm, is given by

$$M_{Fiber} = \begin{bmatrix} 1.0000 & 0.0000 & 0.0000 & 0.0000 \\ 0.0166 & 0.4351 & -0.7641 & 0.4664 \\ -0.0483 & 0.1339 & -0.4744 & -0.8704 \\ -0.0007 & 0.8884 & 0.4365 & -0.1548 \end{bmatrix} \quad (4.7)$$

The form of this matrix, Eq. (4.7), suggests a depolarization effect (the presence of non-zero values out of the main diagonal), and also the phase retardation. From the Mueller matrix obtained, the polarimetric response for the most important characteristic parameters was calculated. The results obtained are shown in Figure 4.12. The gain has the unitary value for all the incident polarization states, according to Figure 4.12(a). The degree of polarization DoP (see Figure 4.12(b)), has some kind of anisotropic behavior dependent of the incident polarization states. Calculating the anisotropic degree of depolarization, a value of 0.0179 is obtained. The Poincaré sphere (see Figure 4.12(c)) does not have a spherical symmetry, which can be interpreted as small depolarization effects due to the reduction of the degree of polarization of light propagated through the core of the optical fiber without long-period grating inscribed. As a consequence of the birefringence arising from possible geometrical deviations of the core from the circular cross section, from uncontrollable transverse stress, as well as from some other achievable reasons, the poles of the sphere are rotated. One should note that the fiber attenuation is practically zero due to the length fiber is short (a few centimeters long) [3], see Figure 4.12(d).

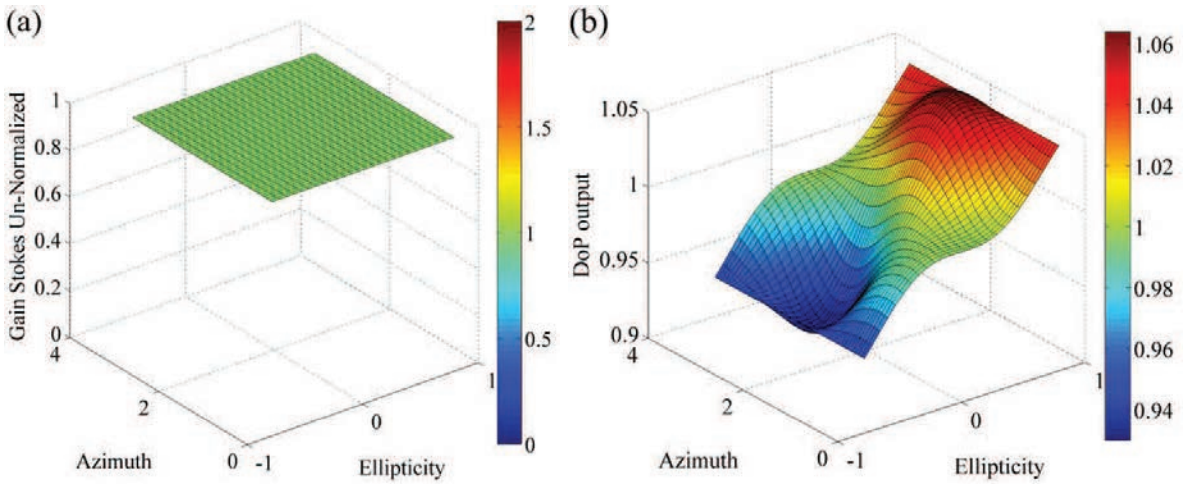

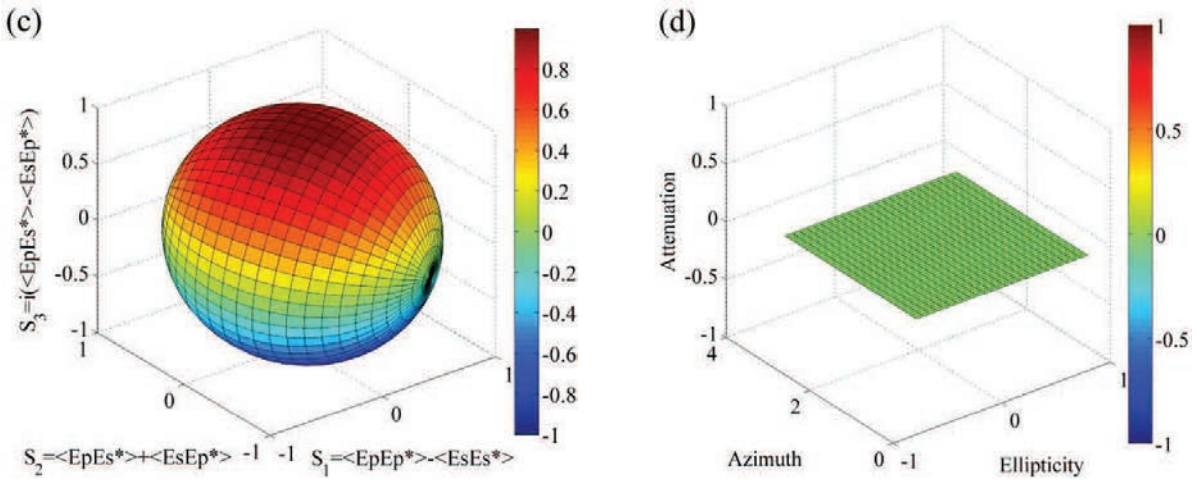


**Fig. 4.12.** Mueller matrix associated to the fiber studied here at 1543 nm with (a) unnormalized gain, (b) output degree of polarization, (c) the Poincaré output sphere, and (d) attenuation.

The normalized Mueller matrix obtained for the UV-LPFG at 1543 nm, is given by

$$M_{UV-LPFG_{1543}} = \begin{bmatrix} 1.0000 & 0.0023 & 0.0213 & -0.0288 \\ 0.0331 & 0.1139 & 0.3761 & -0.8831 \\ 0.0421 & -0.2451 & 0.8766 & 0.3569 \\ 0.0092 & 0.9611 & 0.1828 & 0.1241 \end{bmatrix} \tag{4.8}$$

## 4.3.2 Discussion

The matrix form suggests the presence of diattenuation effects (non-zero values in the first row) and polarizance (non-zero values in the first column). Moreover, one can observe a marked depolarization effect that can be attributed to the presence the UV-LPFG on the fiber core. According to this, we can infer that the exposure of the fiber to the UV light beam used for the grating writing creates a slight birefringence in the fiber core [4-5]. The wavelength of resonance of the UV-LPFG occurs at 1543 nm for un-polarized broadband white light source. In this way, the grating transmission decreases, that corresponds to the diattenuation increasing. The results obtained are shown in Figure 4.13.

The following information can be deduced of the graphical elements of the Mueller matrix. According to Figure 4.13(a), the gain depends strongly of the polarization state incident in the UV-LPFG; meanwhile, the gain variation is due to the intrinsic birefringence of the fiber. On the other hand, the output degree of polarization (see Figure 4.13(b)) shows a tendency to polarize the light linearly and to depolarize slightly for some others incident polarization states. The Poincaré sphere representation of the output polarization states, Figure 4.13(c), confirms the presence of depolarization effects and an increase of birefringence induced in the fiber core due to the UV radiation exposure. The attenuation, Figure 4.13(d), shows a strong dependence of the polarization state incident in the optical fiber, which is caused primarily by existence of UV-LPFG inscribed in the fiber core.

Figure 4.13(e) shows the total-, the linear-, and the circular- diattenuation and the polarizance contributions for the incident light at various wavelengths of the tunable laser (1533, 1538, 1543, 1548, and 1553 nm). The main contribution in the total diattenuation D depends of the linear diattenuation DL, which is greater for the main resonance (1543 nm) and decreases at detuning from this. The observed circular diattenuation DC, has smaller, but non-negligible values. Another parameter calculated in this work is the polarizance; the total polarizance, P, increases with the presence of the UV-LPFG, and the linear- and the circular polarizance, PL and PC, are also wavelength-dependent (see Figure 4.13(e)). The linear polarizance is bigger than the circular polarizance; however, its contribution also decreases with wavelength detuning from the grating main resonance. Figure 4.13(f) shows the total diattenuation, D, and the total polarizance, P, of the fiber with and without the grating. When the UV-LPFG is presented on the fiber, the polarizance increases to 106%; from this Figure, one can see that the contribution of the circular polarizance is greater in the fiber with the grating but anyway, the contribution of the linear polarizance is dominant.

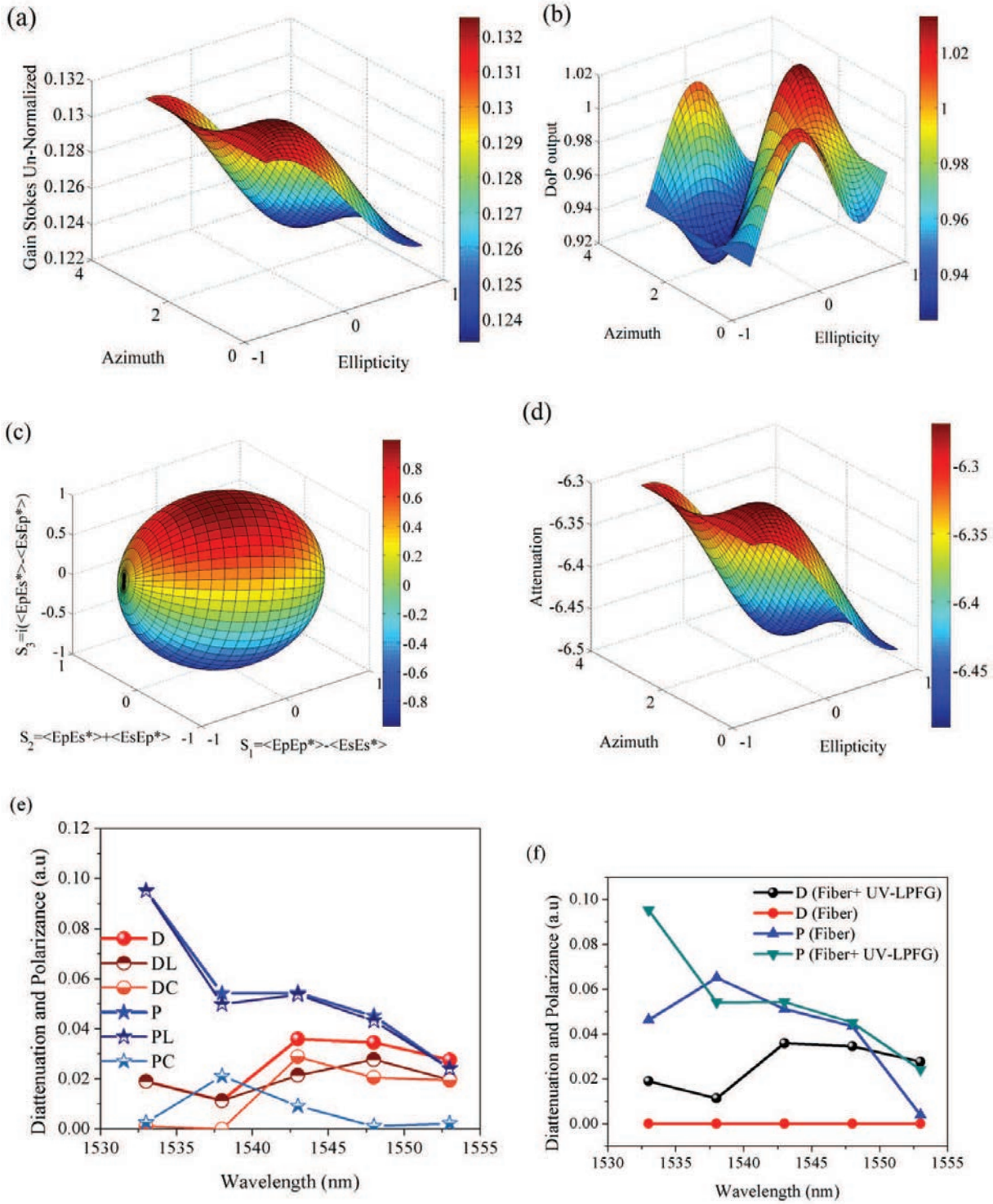
(a)
Gain Stokes Un-Normalized
0.132
0.13
0.128
0.126
0.124
0.122
Azimuth
Ellipticity
0.132
0.131
0.13
0.129
0.128
0.127
0.126
0.125
0.124
(b)
DoP output
1.02
1
0.98
0.96
0.94
0.92
Azimuth
Ellipticity
1.02
1
0.98
0.96
0.94
(c)
S3=i(<EpEs*>-<EsEp*>)
S2=<EpEs*>+<EsEp*>
S1=<EpEp*>-<EsEs*>
0.8
0.6
0.4
0.2
0
-0.2
-0.4
-0.6
-0.8
(d)
Attenuation
-6.3
-6.35
-6.4
-6.45
-6.5
Azimuth
Ellipticity
-6.3
-6.35
-6.4
-6.45
(e)
Diattenuation and Polarizance (a.u)
0.12
0.10
0.08
0.06
0.04
0.02
0.00
1530
1535
1540
1545
1550
1555
Wavelength (nm)
D
DL
DC
P
PL
PC
(f)
Diattenuation and Polarizance (a.u)
0.10
0.08
0.06
0.04
0.02
0.00
1530
1535
1540
1545
1550
1555
Wavelength (nm)
D (Fiber+ UV-LPFG)
D (Fiber)
P (Fiber)
P (Fiber+ UV-LPFG)

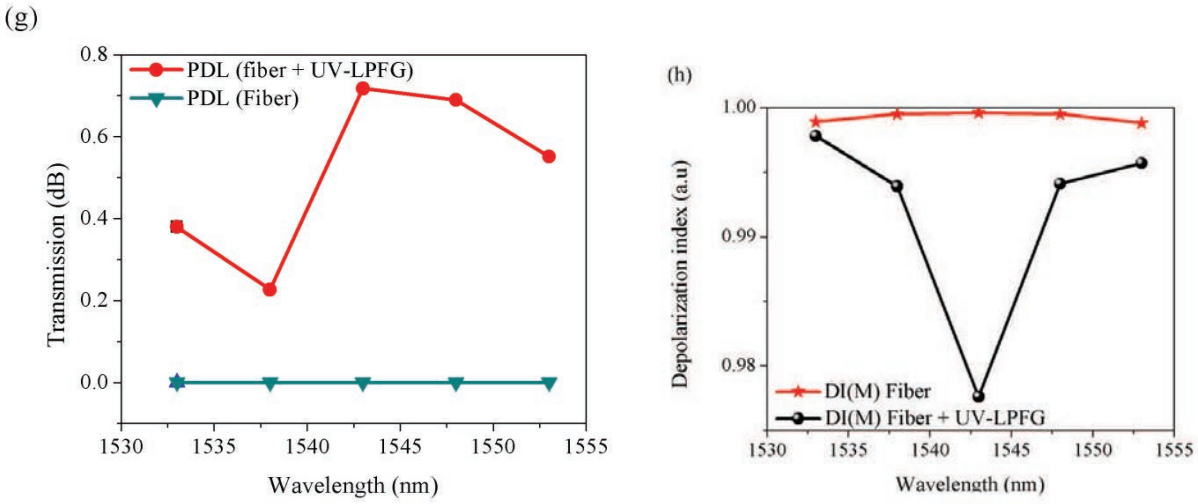


**Figure 4.13.** Mueller matrix associated with the UV-LPFG with (a) un-normalized gain, (b) the output degree of polarization, (c) the Poincaré output sphere, (d) the attenuation, (e) the total, linear, and circular diattenuation and polarizance parameters, (f) the total diattenuation and polarizance for the fiber with and without the grating, (g) PDL for the fiber with and without the UV-LPFG, and (h) the depolarization index for the fiber with and without the grating.

Figure 4.13(g) shows the PDL for the fiber with and without the grating. The PDL results as a consequence of the birefringence presented in the grating structure, and it is stronger at the principal resonance and diminishes with the wavelength at the ends of the UV-LPFG. Bearing in mind that the value of PDL was null in the fiber without LPFG (see Figure 4.13(g)), finally, we calculated the depolarization index that appears strongly with the presence of the UV-LPFG, according to Figure 4.13(h). From the calculus, one can conclude that the depolarization effect is stronger at the grating resonance wavelength, and it symmetrically decreases at detuning to both sides from the resonance wavelength (1543 nm).

Table 4.3 shows the results obtained for several scalar depolarization metrics, where all of them have physically realizable values. The depolarization index DI(M), the Q(M) depolarization scalar metric, and the theorem of Gil-Bernabeu show consistent results that prove that the UV-LPFG shows a small depolarization effect at the resonance wavelength. This means the Jones

formalism can be employed to describe it there, once the small depolarization effects are taken into account, at other wavelengths the effect of depolarization occurs in a smaller proportion.

Table 4.3. Polarimetric data obtained from the Mueller matrix associated to the UV-LPFG.

| λ (nm) | D(M) | DL(M) | DC(M) | P(M) | PL | PC | DI | Q(M) | Tr | PDL (dBm) | Add |
|---|---|---|---|---|---|---|---|---|---|---|---|
| 1553 | 0.0276 | 0.0196 | 0.0194 | 0.0242 | 0.0241 | 0.0023 | 0.9957 | 2.9714 | 0.9936 | 0.5512 | 0.0103 |
| 1548 | 0.0212 | 0.0160 | 0.0138 | 0.04351 | 0.0435 | 0.0011 | 0.9981 | 2.9869 | 0.9972 | 0.4235 | 0.174 |
| 1543 | 0.0359 | 0.0214 | 0.0288 | 0.0543 | 0.0536 | 0.0092 | 0.9776 | 2.8621 | 0.9668 | 0.7175 | 0.0339 |
| 1538 | 0.0113 | 0.0113 | 0.0000 | 0.0541 | 0.0498 | 0.0211 | 0.9939 | 2.9631 | 0.9909 | 0.2266 | 0.0153 |
| 1533 | 0.0190 | 0.0189 | 0.0011 | 0.0952 | 0.0951 | 0.0026 | 0.9978 | 2.9854 | 0.9967 | 0.3797 | 0.0555 |

Additional information about the behavior of the UV-LPFG can be obtained from the polarimetric data, through their respective Mueller matrices [9-11]. Unlike commonly reported results that are obtained by considering solely two orthogonal polarization states, s and p, which correspond somehow an approximation when the system under study does not have a simple symmetry, we are capable to provide more precise information such as the circular diattenuation, the circular polarizance, among others. All of them depend on the incident polarization state and could be used to design and control the output signal from these fibers or from potential polarization-based-devices.

## 4.3.3 Conclusions

A set of six incident Stokes vectors has been used for the determination of the Mueller matrix associated to a commercial UV-LPFG and also has been applied to the fiber without the UV-LPFG, for comparison. These depolarization scalar metrics provide consistent results that indicate an increasing in the birefringence induced in the fiber core due to the exposure of the fiber to UV radiation. The anisotropic depolarization degree, Add, indicates the polarization direction at which this behavior occurs. The obtained polarization-dependent loss (PDL) values are intrinsically low in comparison to ones in gratings produced by other fabrication techniques.

Experimentally we have been observed an important improvement by using a six incident vectors, we can observe a measurements less noisy, and more accurately [12]. The disadvantage of this method opposite a four method is more time consuming data processing.

## References

1. K. M. Salas-Alcántara, R. Espinosa-Luna, and I. Torres-Gómez, "Polarimetric Mueller-Stokes analysis of photonic crystal fibers with mechanically induced long-period gratings," Opt. Eng. **51(**085005)2012.

2. K. M. Salas-Alcántara, R. Espinosa-Luna, and I. Torres-Gómez, "Experimental polarimetric properties of long-period fiber gratings, " Recent Res. Devel. Optics, **8**, 2013

3. Edward Collett, " Polarized Light: Fundamentals and Applications, " Dekker, 1992.

4. K. Nishide, A. Wada, Y. Ishii, K. Shima, and S. Okude, "PDL suppression on long-period fiber gratings by azimuthally isotropic exposure," IEICE Trans. Electron. **85**(4)2002.

5. G. Rego, M. Melo, J. L. Santos, and H. M. Salgado, "Polarization dependent loss of arc-induced long-period fiber gratings,"Opt. Commun. **262**(2)2006.

6. K. M. Salas-Alcántara, R. Espinosa-Luna, and I. Torres-Gómez, Yuri O. Barmenkov, "Determination of the Mueller matrix of UV-inscribed long-period fiber grating, " Appl. Opt. **53**(2)2014.

7. R. Espinosa-Luna, G. Atondo-Rubio, E. Bernabeu, and S. Hinojosa-Ruíz, "Dealing depolarization of light in Mueller matrices with scalar metrics," Optik **121**(12)2010.

8. R. Espinosa-Luna, E. Bernabeu, "On the Q(M) depolarization metric," Opt. Commun., **277**(2)2007

9. R. Espinosa-Luna, E. Bernabeu, G. Atondo-Rubio, "Q(M) and the depolarization index scalar metrics, " Appl. Opt., **47**(10)2008.

10. O. Duhem and M. Douay, "Effect of UV-induced birefringence on long-period-grating coupling characteristics," Electron. Lett. **36**(5)2000.

11. T. A. Eftimov, W. J. Bock, J. Chen, and P. Mikulic, "Muller-Stokes analysis of long-period gratings part I: uniformly birefringent LPGs," J. Lightwave Technol. **27**(17)2009.

12. T. A. Eftimov, W. J. Bock, P. Mikulic, and J. Chen, "Analysis of long-period gratings part II: randomly birefringent LPGs,"J. Lightwave Technol. **27**(17)2009.

13. J. S. Tyo, "Design of optimal polarimeters: maximization of signal-to-noise ratio and minimization of systematic error," Appl. Opt. **41**(4)2002.

# Results and conclusion

In this thesis, the experimental determination of the Muller matrix and the estimation of some scalar polarimetric metrics associated with UV and mechanically induced long-period fiber gratings are presented.

This study begins with a review of the different methods that have been proposed in literature for the inscription of LPFGs and their more relevant applications in optical communications and optical fiber sensing. Furthermore, a short revision of induced birefringence during the inscription process and the induced birefringence compensation techniques are presented, to introduce the readers in the importance of the birefringence on the polarimetric response of LPFGs. Then, the background required for the understanding of principle of operation of the LPFGs and their transmission properties, based in the couple mode theory are presented. A brief review of Jones calculus and scanning method that have been used to calculate the polarization properties of the fiber devices, such as PDL and PMD is also presented.

We showed some elements to analyze the polarized light through the Stokes vectors and the Mueller matrix of an arbitrary optical system. Then, we have characterized, for the first time, both mechanically and UV induced long-period fiber gratings by using two explicit methods for the entire determination of the Mueller matrix. One method employs 4-incident polarization states (linear parallel, vertical, +45 degrees, and right-hand circular) and the other uses six-incident polarization states (where we have added the −45 degrees linear polarization and also the left-hand circular polarization state to the 4-incident polarization method) for the experimental determination of the Mueller matrix. In practice, we have found the method of 6-incident polarization states provides less noise and more stable results than the 4-incident method.

The Mueller matrix was determined through the Stokes vectors, which were measured using an incomplete, commercial, Stokes polarimeter. Some scalar polarimetric metrics were applied for the determination of the diattenuation, PDL, gain, attenuation, depolarization degree of anisotropy, among others. Experimental results obtained with these two methods were presented,

compared, and discussed. In addition, graphical elements of the Mueller matrix were presented in order to predict the behavior of the LPFG at any polarization state.

Our results offer a proof that the UV-LPFG shows a small depolarization effect at the resonance wavelength. This means; the Jones formalism can be employed to describe it, once the small depolarization effects are taken into account, and at other wavelengths, where the effect of depolarization occurs in a smaller proportion. This behavior is different to the M-LPFG, which decrease the degree of polarization. As a consequence, it can not be described by the Jones matricial formulism.

The result presented here provides more accurate information than what is usually reported, when only two orthogonal linear polarizations are considered. It seems that experimental noise decreases with an increase of measurements in the determination of the Mueller matrix. In this sense, a full polarimetric analysis could be used to design and control the output signal from these LPFGs or from potential polarization-based devices to realize the wavelength switchable fiber laser, among other applications.

# Future work

The characterization of LPFGs realized in this work can be extended to LPFGs induced by other fabrication techniques like electric arc discharges and laser $CO_2$ exposure.

Extending the analysis to measure polarization mode dispersion (PMD)

Extending the analysis to measure polarization properties in fiber devices like optical couplers, pump diode pigtails, Mach Zehnder interferometers, among many other applications.

# List of acronyms

Amplified spontaneous emission, ASE

Amplitude mask, AM

Azimuth, $\psi$

Circular Diattenuation, D(C)

Circular Polarizance, P(C)

Coarse wavelength division multiplexing, CWDM

Corrugated grooved plates, CGPs

Decibeles, dBm

Degree of polarization, DoP

Dense wavelength division multiplexing, DWDM

Ellipticity, $\chi$

Erbium doped fiber amplifiers, EDFA

Fiber Bragg gratings, FBG

Gain, (G)

Glan-Laser, GL

Grating length, L

Holey Fiber, HF

Ideal Polarimeter Arrangement, IPA

Left-hand, (l)

Linear Diattenuation, D(L)

Linear Polarizance, P(L)

Liquid Crystal Variable Retarders, LCVR

Long-period fiber grating, LPFG

Long-period holey-fiber gratings, LPHFG

Mechanically induced long-period fiber grating (M-LPFG)

Optical spectrum analyzer, OSA

Parallel state, P

Perpendicular state, S

Photonic crystal fiber, PCF

Polarization mode dispersion, PMD

Polarizer State Analyzer, PSA

Polarization State Detector, PSD

Polarizer State Generator, PSG

Refractive index, RI

Refractive index unit, RIU

Right-hand, r

Single mode fiber, SMF

State of polarization, SOP

Stokes vector, S

The anisotropic degree of depolarization, Add,

The Degree of polarization, DoP(M,S),

The Depolarization index, DI(M)

The Diattenuation, D(M),

The Mueller matrix (MM)

The Polarizance parameters, P(M),

The polarization dependent loss, PDL,

The Q metric, Q(M)

Ultraviolet light, UV

Wavelength Division Multiplexing, WDM

White Light Source, WLS

Ytterbium fiber laser, YFL

+45 degrees, (+),

-45 degrees, (-),